# Surface Modification of Bio-implantable Ti-6Al-4V Alloy for Enhanced Osseointegration and Antibacterial Capability

*By*

Ziyuan Wang

A Thesis Submitted to the Faculty of Graduate Studies of

The University of Manitoba

in partial fulfillment of the requirements of the degree of

**Master of Science**

Department of Mechanical Engineering

University of Manitoba

Winnipeg, Manitoba

# Abstract

Surface-induced osseointegration and antibacterial capability are very important criteria for the clinical success of titanium implants. To enhance these two criteria, an architectural hybrid system is constructed onto Ti-6Al-4V with a rough surface. First, thermal oxidation (TO), treatment with hydrogen peroxide ($H_2O_2$) and a mix of TO and $H_2O_2$ (Mixed) are used to modify the surface topography and chemistry of Ti-6Al-4V disks. Surface characterizations by the use of microscopes and spectroscopes indicate that TO can induce more favorable topography, roughness, wettability and hydroxyl group concentration on Ti-6Al-4V surfaces. Therefore**,** an alginate/chitosan LBL film that incorporates antibacterial nano-silver is bridged onto thermally oxidized Ti-6Al-4V alloy by mussel-inspired dopamine. The microscopies and spectrometers confirm that the hybrid system is successfully fabricated onto the Ti-6Al-4V surface while the sub-micron topography induced by TO is maintained. Bone marrow stem cell (BMSC) adhesion, proliferation and differentiation are up-regulated by the synergy of sub-micron surface produced by TO and alginate/chitosan LBL film. The incorporation of nano-silver into the hybrid system is demonstrated to inhibit the growth of *Escherichia coli* and *Staphylococcus aureus*, but not jeopardize the enhanced BMSC activities. Taken together, this thesis presents a promising strategy to fabricate novel Ti-6Al-4V implants with enhanced osseointegration and antibacterial capability.

# Acknowledgements

First, I owe my sincere gratitude to my advisor Dr. Olanrewaju Ojo and co-advisor Dr. Malcolm Xing for giving me the opportunity to work with them, and providing me with their professional and valuable instruction, encouragement and research guidance.

My special thanks also go to my thesis committee members, Dr. Norman Richards and Dr. Ann Yi for their insightful comments and expert assistance.

I would like to thank my family, especially my mother and father, for always believing in me, for their continuous love and their supports in my decisions. Without them I could not have made it here.

I also thank all members of the Materials Microstructure Lab and Tissue Engineering Lab for their technical assistance.

Last but not least, financial supports from the Natural Sciences and Engineering Research Council of Canada (NSERC), Manitoba Health Research Council (MHRC) and Manitoba Institute of Child Health (MICH) are also gratefully acknowledged.

# Table of Contents

# List of Figures

# List of Tables

# List of Copyrighted Materials for which Permission was Obtained

Figure 1: Source – Journal of Bone and Mineral Research. Reprinted from R. Lawrence, and M. Parfitt, Journal of Bone and Mineral Research, Vols. 20(2), 2005, p. 177, with permission from John Wiley and Sons (April 1, 2014).

Figure 2: Source – "Medical Physics – Artificial Knees" by P. Smith. Reprinted with permission from the author (11 March, 2014).

Figure 3: Source - "High Temperature Corrosion" by P. Kofstad, DM. Etherington and B. Boucher. Reprinted with permission from the Elsevier Applied Science (2 April, 2014).

Figure 4: Source – Science. Reprinted from G. Decher, Science, Vols. 277, 1997, p. 1232, with permission from The American Association for the Advancement of Science (1 April, 2014).

Figure 5: Source – "Basic Models of Spin Coating" by SL. Hellstrom. The author grants permission to copy, distribute and display this work in unaltered form, with attribution to the author, for noncommercial purposes only. (3 March, 2014).

Figure 6**:** Source – Reactive and Functional Polymers. Reprinted from MN. Ravi Kumar, Reactive and Functional Polymers, Vols. 46, 2000, p. 1, with permission from the Elsevier (2 April, 2014).

Figure 7: Source – Progress in Polymer Science. Reprinted from KY. Lee and DJ. Mooney, Progress in Polymer Science, Vols. 37, p. 106, with permission from the Elsevier (2 April, 2014).

Figure 8: Source – Journal of Nanoparticle Research. Reprinted from C. Marambio-Jones and E. Hoek, Journal of Nanoparticle Research, Vols. 12, 2010, p. 1531, with permission from the Springer (7 May, 2014).

Figure 9: Source - Progress in Polymer Science. Reprinted from E. Faure, C. Falentin-Daudré, C. Jérôme, J. Lyskawa, D. Fournier, P. Woisel and C. Detrembleur, Progress in Polymer Science, Vols. 38, 2013, p. 236, with permission from the Elsevier (April 2, 2014).

# List of Abbreviations

| | |
|---|---|
| TO | thermal oxidation |
| Mixed | mix of thermal oxidation and $H_2O_2$ treatment |
| LBL | layer-by-layer |
| ECM | extracellular matrix |
| RGD | Arg-Gly-Asp |
| Ra | arithmetic average surface roughness |
| EDM | electro-discharge machine |
| AFM | atomic force microscope |
| AES | Auger electron spectrometer |
| SEM | scanning electron microscope |
| EDS | energy dispersive spectrometer |
| CAG | contact angle goniometer |
| PDA | poly (dopamine) |
| DMEM | Dulbecco's modified Eagle's medium |
| BMSC | bone marrow stem cell |
| *E. coli* | *escherichia coli* |
| *S. aureus* | *staphylococcus aureus* |
| PBS | phosphate-buffered saline |
| SBF | simulated body fluid |

| | |
|---|---|
| P | polishing |
| P/$(A/C)_5$ | polishing/$(alginate/chitosan)_5$ |
| TO/$(A/C)_5$ | thermal oxidation/$(alginate/chitosan)_5$ |
| TO/$(A/C)_5$/Ag | thermal oxidation/$(alginate/chitosan)_5$/nano-silver |
| MTT | methylthiazoltetrazolium bromide |
| q-RT-PCR | quantitative real-time polymerase chain reaction |
| ALP | alkaline phosphatase |
| COL I | type I collagen |
| BSP | bone sialoprotein |
| OPN | osteopontin |
| GAPDH | glyceraldehyde-3-phosphate dehydrogenase |

# Chapter 1

# Introduction

## 1.1 General Overview

During the past three decades, it has been acknowledged that titanium and its alloys exhibit excellent biocompatibility, mechanical properties and corrosion resistance compared to some other kinds of bio-implantable alloys [1]. However, the long-term clinical success of bio-implantable titanium and its alloys is hampered by its inadequate osseointegration capability [2]. To improve this situation, various surface modification techniques have been employed to alter the surface properties of bio-implantable titanium and its alloys. These include traditional techniques, such as thermal oxidation (TO), hydrogen peroxide ($H_2O_2$) treatment, acid etching, sandblasting, hydroxyapatite coating and recently emerged techniques, such as nano-patterning, layer-by-layer (LBL) self-assembly of polyelectrolytes and biomolecules immobilization. [3-9].

Traditional surface modifications were robustly developed in the 1990s. These techniques have either induced porous or nodular topographies with different wettability, oxide layer thickness and surface composition. Studies have reached a general consensus that a surface layer with proper roughness, wettability and surface functional group content is able to enhance osseointegration through the stimulation of cell adhesion, proliferation

and differentiation [10].

Recently, the LBL self-assembly of polyelectrolytes has gained increasing interest. The films formed by electrostatic force attraction are ideal platforms to mimic the extracellular microenvironment [11]. By utilizing its advantages, such as controllable film composition and ease of attachment to various substrates, LBL self-assembly has been extensively developed during the past 5 years. In the perspective of bone tissue engineering, LBL self-assembled films made from various polyelectrolyte pairs can stimulate a specific cellular response [12], encapsulate single cells [13], and function as a carrier of bone-related chemicals [6]. Among those, alginate/chitosan pair is of particular importance. Chitosan is a positively charged linear polysaccharide. Besides its demonstrated biocompatibility, chitosan is also capable of accelerating extracellular matrix reformation and potentiate osteogenic differentiation [14]. Alginate is a negatively charged linear polysaccharide that has been widely used for drug carriers and scaffolds [15].

Studies have also focused on reducing the peri-implant infections caused by bacterial contamination, which results in the formation of a biofilm between implant and the host body, thus leading to implant failure. To inhibit bacterial contamination, nano-silver is incorporated into implants. It has been demonstrated that at a suitable dose, nano-silver bactericide exhibits a wide antibacterial spectrum, non-cytotoxicity and long-term

antibacterial effects [16].

## 1.2 Problem Definition

Robust development of various surface modification techniques substantially improved the *in vitro* and *in vivo* performance of bio-implantable titanium and its alloys. However, there is still a gap between clinical demand and the latest bio-implantable titanium and its alloys.

Although TO (500-700 °C, 1-16 h) and $H_2O_2$ treatment (30%, 1-24 h) have greatly improved the biological performance of titanium implants [17-20], the rate and quality of osseointegration in these implants are still problematic [21, 22]. LBL self-assembly of polyelectrolytes, which are advantageous in mimicking extracellular microenvironment, however, has not been employed to overcome the shortcomings of titanium implants modified by traditional treatments.

In addition, infections also largely compromise the clinical success of implant [23]. Although nano-silver particles have been employed to inhibit bacterial contamination in titanium implants, most of these studies only aimed to improve the antibacterial capability of implants.

## 1.3 Objective

The overall objective of this dissertation was to design a hybrid structure on the bio-implantable Ti-6Al-4V surface to enhance its osseointegration and antibacterial capability. To achieve this, the following tasks were performed:

1. Selection of a surface modification technique from TO, treatment with $H_2O_2$ and a mix of TO& $H_2O_2$ (Mixed) that can induce optimal surface topography, roughness, chemistry, wettability and functional groups on the Ti-6Al-4V surfaces.

2. Construction of an alginate/chitosan LBL film that incorporates antibacterial nano-silver particles on the selected Ti-6Al-4V surfaces.

## 1.4 Summary of Experimental Methods and Major Findings

### 1.4.1 Summary of Experimental Methods

In the first part of the project, Ti-6Al-4V was oxidized by TO (650°C, 8 h), $H_2O_2$ (30%, 24 h) and the Mixed treatment (TO 650°C, 4 h and $H_2O_2$ 30%, 4 h). Then, the topography and roughness of oxidized surfaces were characterized by scanning electron microscope (SEM) and atomic force microscope (AFM). Oxide layer thickness was measured by Auger electron spectrometer (AES) and energy dispersive spectrometer (EDS). Surface

wettability and chemistry were determined by contact angle goniometer (CAG) and X-ray photoelectron spectrometer (XPS).

In the second part of the project, alginate/chitosan LBL film was constructed by spin-assisted coating. Surface characterizations were performed by SEM, AFM, EDS, CAG and XPS. *In vitro* evaluation was performed on BMSCs at the Manitoba Institute of Child Health with standard protocols. In addition, agar diffusion test was carried out to test the antibacterial capability of the architectural hybrid Ti-6Al-4V sample.

### 1.4.2 Summary of Major Findings

Systematic comparison of the surface characteristics of Ti-6Al-4V modified by TO, treatment with $H_2O_2$ and the Mixed, which has not been reported in literature, is performed. Surface characterizations by the use of various microscopy and spectroscopy techniques reveal that each of these surface modification techniques can induce striking topographical and chemical features on the Ti-6Al-4V surface. Careful analysis of these results indicates that the Ti-6Al-4V modified by TO is more biologically preferred since it exhibits denser oxide layer, greater surface roughness, wettability and functional hydroxyl group density than the treatments of $H_2O_2$ and Mixed.

A hybrid architecture is constructed on the thermally oxidized Ti-6Al-4V alloy by additional alginate/chitosan LBL self-assembly and incorporation of nano-silver particles.

CAG, SEM and AFM characterizations reveal that LBLed alginate/chitosan pairs can completely cover the thermally oxidized Ti-6Al-4V surface upon deposition. Further analysis by AFM indicates that the roughness of thermally oxidized Ti-6Al-4V is altered after TO/$(A/C)_6$ sample. XPS characterization shows that the increased intensity of surface amine group is proportional to the number of alginate/chitosan layers. Based on these results, TO/$(A/C)_5$ sample was selected to further incorporate nano-silver particles to form the desired hybrid system, TO/$(A/C)_5$/Ag. Agar diffusion test reveals that the TO/$(A/C)_5$/Ag sample exhibits antibacterial capability. *In vitro* tests on BMSCs viability, morphology, proliferation and differentiation demonstrate that the synergy of alginate/chitosan LBL film and sub-micron rough topography induced by TO on the Ti-6Al-4V sample can enhance its osseointegration capability, where has never been previously reported. Further analysis on the BMSC activities indicates that additional nano-silver particles do not jeopardize the improved osseointegration capability on Ti-6Al-4V sample. Taken together, this dissertation provides a promising technique to enhance the osseointegration and antibacterial capability of Ti-6Al-4V alloy.

## 1.5 Thesis Layout

This dissertation contains six chapters. The organization is as follows,

- Chapter 1 includes a brief introduction of background, problem definition, objectives, methodology and major findings,

- Chapter 2 contains a general literature review on bone remodeling, titanium surface modification techniques and silver bactericide,
- Chapter 3 provides detailed experimental procedures and used instruments,
- Chapter 4 presents the results and discussion,
- Chapter 5 summarizes the major findings and conclusions of the research,
- Chapter 6 provides suggestions for future work.

# Chapter 2

# Literature Review

## 2.1 Bone Structure

Bones are rigid organs that provide a framework of support for the body, transfer forces for locomotion and protect internal organs. Bones can also regulate homeostasis by reserving minerals and through hematopoiesis. Bones are generally divided into compact (cortical) and spongy (cancellous) bones. Compact bones are made of osteons, mainly found in the hard outer layer of bones and solidly filled with organic ground substances and inorganic salts with minimal gaps and spaces. Spongy bones are in the inner bone structure, characterized by much higher porosity and larger surface area. These characteristics enable spongy bones to accommodate blood vessels and marrows, as well as offer supporting strength to ends of the weight-bearing bone.

As living organs, old bones are continually replaced by new bones throughout life. Bone remodeling aims to adjust the host bones to adapt to mechanical loads and strains, repair micro-damage and mobilize mineral storage upon metabolic demand. It is a homeostatic equilibrium process mainly accomplished through the resorption of old bones by osteoclast and the formation of new bones by osteoblast (Figure 1). Upon receiving a remodeling signal, mature osteoclasts are formed through a series of activities from

osteocytes. Following this process, mature osteoclasts congregate on the bone surface and start to secrete hydrogen ions to dissolve bone forming minerals and the matrix. As a result, resorption pits, which range from sub-micron to micron levels, are formed.

After bone resorption, osteoblasts are recruited around the resorption pits through the differentiation of BMSCs. Osteoids, the unmineralized, organic portion of the bone matrix, are formed through a series of osteoblast activities. The first activity is the synthesis of type I collagen, which is the most important structural protein of the bone extracellular matrix (ECM). The second activity is marked by the production of alkaline phosphatase (ALP), an early marker of osteoblast differentiation. Third, bone sialoproteins (BSPs), a significant component of the bone ECM, constitute approximately 8% of all non-collagenous proteins [24]. Lastly, osteocalcins (OCN), the most abundant non-collagenous protein in the organic matrix of bone and dentin, act as a late marker of the bone formation process. When the thickness of osteoids reaches a critical value, they begin to mineralize under the regulation of osteocytes, which secretes matrix vesicles like ALP. The resorption pits are fully filled with bone and the mineralized chemicals are gradually packed, becoming denser and finally form new bones in a couple of months.

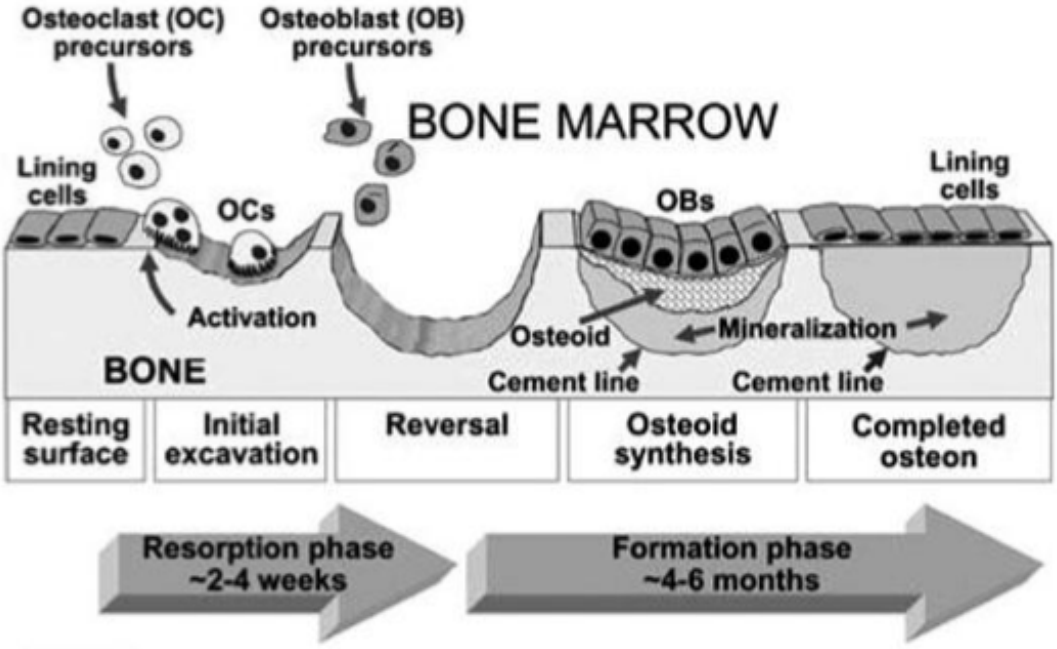


Figure 1. Illustration of bone remodeling process[25]

## 2.2 Osseointegration

In the 1950s, Branemark, for the first time, defined the term osseointegration as "the formation of a direct interface between an implant and bone, without intervening soft tissue" [26]. In his study, it was showed that titanium implants could be permanently fused with host bones without soft tissues, like scar tissues, cartilage or ligament fibers. Since then, osseointegration has been widely accepted as the basis for clinical implant success with the advantage of predictable and reproducible surgical results on the interface between load bearing implants and natural bone [27]. A successful osseointegration process consists of a series of discrete but overlapping events. Although not fully interpreted, Schwartz and Boyan briefly summarized this process into several steps: upon implantation, serum proteins immediately attach to the implant surface; then the BMSCs are transferred to the implant site and start the adhesion and proliferation [28]. The third stage is marked by the formation of osteoids; when the osteoids reach a critical thickness, the bone matrix starts the calcification, which is completed in about 3 weeks after implantation. This stage is followed by bone remodeling as described in Section 2.1. Therefore, a successful implant requires three prerequisites: 1) precise fitting, 2) primary stability, and 3) adequate loading during the healing process [29]. However, the long-term success of bio-implants, which is anticipated as having a stable interface between bone and implant, has not been fully supported by subsequent studies. Local

anatomic, local biologic, systemic or functional factors give rise to a high rate of micromotions between the implant and host body, thus leading to osseointegration failure [30-33]. To improve this situation from bone-tissue engineering perspective, researchers have exerted many efforts on improving the primary stability of implants by surface modification of titanium and its alloys.

## 2.3 Cell-implant Interactions

### 2.3.1 Cell-implant Interaction Process

The bone-implant interface is formed upon implantation. Then a series of events occur at the interface. The first event is believed to the dynamically selective adsorption of biological proteins (albumin, fibronectin, and vitronectin) from blood, tissue fluids and the peri-prosthetic region to form a thin proteinacious film. The adsorption of proteins is affected by the implant topography, surface chemistry, etc. The second event is the characterized by the appearance of macrophages, which phagocytize bacteria and damaged tissue. The event is followed by the resorption of ECM, cell membrane and cytoskeleton proteins. These proteins can interact together to function as a signal transducer to regulate the subsequent cell activities. Specifically, cell membrane are heterodimeric transmembrane glycoproteins that mediate cell attachment [34]. ECM proteins can either link cells to host tissues or dictate cell migration during the healing

process. Cytoskeletal proteins work through microfilaments, intermediate filaments, and microtubules to adjust cells in shape, support, and movement. The fourth event is the rapid attachment osteogenic cells onto implant surface. Then the adhesion of osteogenic cells is taken place over a long period of time. Finally, osteogenic cells are activated to proliferate, differentiate and ultimately form new bones as described in Section 2.1.

Although there is little information on how surface chemistry and topography of implant regulate the aforementioned events at the cellular level, it is widely accepted that the implant surface properties do have important influences on the cell-implant interactions [35]. The following paragraphs will review the most current interpretations on the role of surface properties on cell-implant interactions process.

### 2.3.2 Roles of Implant Surface Properties on Cell-implant Interactions

The role of implant surface properties on cell-implant interactions was initially examined on the basis of micron-scale topography and surface chemistry. With the development of nanotechnology, recent investigations have further looked into the implant-cellular interactions on a nano-scale topography. Taken together, these form a preliminary explanation of the profound bone healing process.

#### 3.3.3.3 Micron-scale Topography

Topographies with a micron-rough surface can be used to explore improvement in

osseointegration from the biomechanical and bio-signal perspectives. The first theoretical explanation of the function of micron-scale topographies focused on the physical association of implants with bones. In 1991, Buser et al. conducted an *in vivo* study on miniature pigs and demonstrated that bone-implant contact is proportional to the surface roughness [36]. In 1999, Hansson and Norton proposed a mathematical model to categorize surface characteristics by introducing the pit effectivity and pit density factors to describe the characteristics of individual and overall pits [37]. It is postulated that micron-rough titanium can be sensed by osteocytes, thus stimulating the secretion of bone-formation proteins and minerals, which results in increased bone volume around implant sites with a micron-rough surface, and therefore forms a stronger mechanical interlocking between implant and bone [38, 39]. Further studies have summarized that pits with a depth of 1.5 μm and diameter of 3-5 μm can achieve a higher percentage of bone-implant contact [40, 41]. However, more convincing evidence has not been obtained to elucidate the specific function of mechanical signals to host tissues. For example, the way of osteocytes sense signals derived from micron-scale topography and the difference between the signals produced by a nodular surface versus that of a porous surface, have not been revealed.

The second theoretical interpretation on the role of micron-scale topography is addressed at a bio-signal level. Upon implantation, it is known that the wound site would be

covered by blood clots, followed by cell migration to the site. Therefore, the activation of platelets is extremely important. The commercially pure titanium (cpTi) surface is proposed to activate platelets as a function of surface micro-texture through a larger surface area to enhance plasma protein adsorption, followed by platelet adhesion and activation [42]. Although the cause of enhanced osteoblast lineage differentiation is not fully understood, it is suspected that a micron-rough surface has a compulsory effect on cellular shape, or accelerates ECM formation to evoke osteoblast lineage differentiation and finally promote osseointegration [43-45].

#### 3.3.3.4 Nano-scale Topography

As nanotechnology develops, a growing number of studies have explored the effect of nano-scale topography on cell-implant interactions. In spite of the research gaps, pioneering investigations have achieved some breakthroughs during the past years. The nano-scale topography alters cell activities, directly or indirectly, through initial cell adhesion to further influence cell proliferation and differentiation.

The indirect role of a nano-scale topography on cell-implant interactions stem from their impacts on protein adsorption. Nano-scale topography can influence the conformation of the Arg-Gly-Asp (RGD) sequence containing proteins like fibronectin and vitronectin, therefore impacting integrin binding, which is essential for the regulation of the cell adhesion. Higher protein absorption and cell adhesion on nano-scaled surfaces as

opposed to those conventional surfaces have been observed by several studies [46-48].

Nano-scale topography can also directly regulate cell adhesion. It is widely accepted that the integrins are within the focal adhesion architecture (300 nm) and serve as important membrane receptors on mediating cell attachment and adhesion through signal transduction between cells and the ECM. Nano-topography-induced geometrical constraints spatially segregate integrin occupancy, trigger ligand binding, and consequently result in cell adhesion [49, 50]. In contrast, the micron-scale topography is unable to provide this kind of binding structure. As summarized by Klymov et al., nano-islands can stimulate stronger cell adhesion than smooth surfaces. In particular, the focal adhesion of fibroblasts and endothelial cells on shorter islands (13 nm) was greater than on higher islands (33-45 nm) [51]. However, when the island height reached 160 nm, the fibroblast and osteoblast adhesion were reduced when compared to those on a flat surface [51].

The impact of nano-scale topography on cell proliferation and differentiation has not been well understood, yet studies have proven its ability to promote these two activities. A prevalent speculation on cell proliferation is that the activation of cell adhesion by integrins initiates a cascade signaling pathway, which simultaneously enhances cell proliferation [52]. Cell differentiation is a key factor for the success of osseointegration. Although differentiation is a more advanced and complicated stage of specific cell

activity, pioneering investigations have suggested evidence of a mechanotransduction mechanism. Mechanical stresses are induced when cells adhere onto nano-scale topographies such as pits, grooves and islands. Cells are able to sense these loadings and convert them into biological signals and alter the gene expressions of ECM components [53].

#### 3.3.3.5 Surface Wettability

Surface wettability is also very influential on cell-implant interactions. Hydrophilic surfaces can alter extracellular protein adsorption by inducing functional groups, such as hydroxyl, carbonyl, carboxyl and amino groups. Studies have observed increased biological protein adsorption on hydrophilic surfaces while the opposite is true for hydrophobic surfaces [54]. Increases in the amount of adsorbed proteins can subsequently contribute to cell adhesion, proliferation and differentiation. In addition, studies have also found that these surface functional groups can also improve osseointegration by directly releasing signals to stimulate integrin binding or osteogenic differentiation [55, 56].

To summarize, the effect of topography and surface wettability on cell-implant interactions are only partially understood. More efforts should be made to interpret the complicated relationships between implant surface properties and host tissues.

## 2.4 Bone Marrow Stem Cell

BMSCs were first identified by Friedenstein et al. in 1966, who extracted bone-forming progenitor cells from rat marrow [57]. Thereafter, studies have identified other encouraging properties of BMSCs, such as ease of isolation and expansion, strong and diverse differentiation ability, and transplantability. In this context, BMSCs have become one of the most promising cell sources for regenerative medicine and tissue engineering.

BMSCs are mostly isolated and harvested from bone marrow [58]. Although these BMSCs just represent 0.001-0.01% of the overall population of nucleated cells in marrow, they can be easily enriched by culturing them with colony-forming unit-fibroblasts to reach a high cell density up to $4\times10^5$ cells/$cm^2$ [59].

A proper induction medium during the culturing of BMSCs can lead to their selective expression of BMSCs to the desired phenotype. For example, the presence of β-glycerol-phosphate, ascorbic acid-2-phosphate, dexamethasone and fetal bovine serum has been reported to activate the osteogenic potential of human BMSCs [60]. The ability of BMSCs to differentiate in many ways has attracted great interests for its use in the reconstruction of defective tissues through transplantation. Autologous and allogeneic BMSCs have been successfully transplanted not only in animal models but also in clinical patients for bone and cardiovascular repair, treatment of lung fibrosis, etc. [61-63].

Many studies have employed BMSCs to investigate the effects of surface modification on titanium and its alloys. Liu et al. fabricated BMSC-sheet 3D scaffold to promote bone regeneration *in vitro* and *in vivo* [64]. Costa-Pinto et al. seeded human BMSCs onto chitosan/polyester scaffolds to induce osteogenic differentiation [65]. Other studies have employed BMSCs to evaluate the *in vitro* performance of modified titanium-based implants [5, 6].

## 2.5 Biomedical Applications of Titanium and Its Alloys

### 2.5.1. Hard Tissue Replacements

Hard tissues are one of the most vulnerable parts of the human body due to accidents, aging and other causes. The first common use of titanium and its alloys in hard tissue replacements are artificial hips and knee joints. Figure 2 is an illustration of titanium artificial knee joints. When used as artificial organs, titanium and its alloys are favored over conventional stainless steel and cobalt alloys because of their moderate Young's modulus, high biocompatibility, superior tribology properties and excellent corrosion resistance. Therefore, artificial knees and hips have been made of titanium and its alloys have been permanently anchored to the intramedullary canal to reproduce natural movement [66].

The second common use of titanium and its alloys in hard tissue replacements is in dental

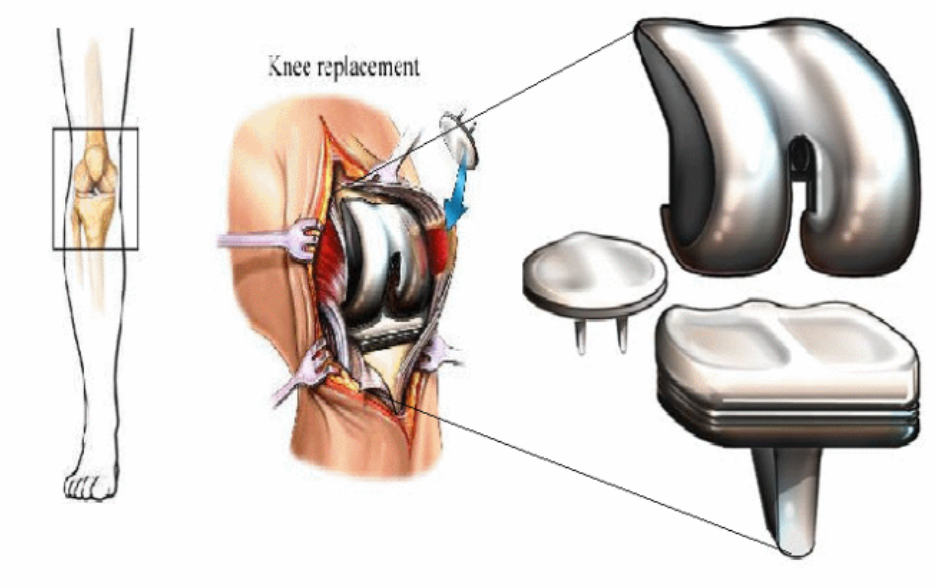


Figure 2. Artificial knee joint made of titanium and its alloys [67].

implants, which serve as anchors for prosthetic replacement of missing teeth. Dental implants are mainly classified into subperiosteal, transosteal and endosseous implants, based on their shape and position to the jawbone. Subperiosteal implants are placed on top of the jawbone. They are metal frameworks that are attached onto the jawbone top but beneath the gum tissue. Transosteal implants penetrate the jawbone and gum tissue with a pin-like or U-shaped framework. Endosseous implants are placed within the bone and usually processed into screw- or cylinder- like shapes. It is universally acknowledged that titanium and its alloys have better clinical performance in osseointegration than other types of materials in dental applications [68]. Contemporary clinical demands toward titanium and its alloys have gradually gravitated towards a faster and more compact integration process with natural bone.

### 2.5.2. Cardiovascular Implants

Titanium and its alloys are also used in cardiovascular implants such as heart valves, artificial hearts and circulatory devices because they are mechanically strong, chemically inert and non-magnetic. However, pure titanium is seldom used in the cardiovascular field due to the high rate of blood-clotting and insufficient radiopacity in finer structures [69]. By alloying titanium with nickel, these shortcomings have been partly overcome and more importantly, the resultant shape-memory property has attracted significant attention in its application in vascular stents. A collapsed stent can be implanted into

veins or arteries and later when body temperature warms the stent, it will return to its original shape to support blood flow within the veins or arteries.

## 2.6 Bio-implantable Titanium and Its Alloys

CpTi has been developed as surgical implant material since the 1940s [70]. In its elemental form, cpTi possesses a hexagonal close packed (hcp) crystal structure with an α phase. Its mechanical properties, such as tensile strength and Young's modulus, are closer to those of natural bone than other metals like stainless steel. Meanwhile, the formation of an ultra-thin oxide layer (less than 10 nm), when exposed to air, provides titanium with excellent corrosion resistance and biocompatibility. However, even though the strength, fatigue properties and wear resistance are better than other kinds of metals, titanium is not ideal. This led to the early investigation of alloying pure titanium with other elements. Later, annealed Ti-6Al-4V started to gain widespread use in biomedical applications, especially for dental, hip and knee prostheses [71]. Annealing above 882.5 °C enables the transformation of the α phase into a body centered cubic (bcc) structure (β phase). By alloying with an α phase stabilizer (Al) and a β phase stabilizer (V), Ti-6Al-4V is stabilized as an (α+β) alloy and exhibits higher strength and better fatigue properties [71]. Although some of the other titanium alloys such as Ti-6Al-7Nb and Ti-13Nb-13Zr have been subsequently developed to further mimic natural bone properties, Ti-6Al-4V is still widely used in biomedical devices as a mature material [71].

## 2.7 Surface Modification of Titanium and Its Alloys

Although the clinical performance of titanium and its alloys is superior to other bone substitute materials, there is still a high rate of implants failure due to the inadequate osseointegration. To improve the osseointegration capability of titanium and its alloys, various surface modification techniques have been introduced over the past three decades. Table 1 is a summary of commonly used surface modification techniques. Due to limited space, only the most popular techniques will be reviewed in Section 2.7.1- 2.7.8.

### 2.7.1 Calcium Phosphate Coating

The coating of the titanium surface with calcium phosphate, particularly hydroxyapatite $Ca_{10}(PO_4)_6(OH)_2$, has been extensively studied since it was found to comprise part of inorganic components of human bone. Upon implantation, calcium phosphate is released into the peri-implant regions and precipitates biological apatite to stabilize the implant. This biological apatite also allows the permeation of bone organic matrix components, which are relevant to processes such as protein adsorption and type I collagen fiber formation. As a consequence, the bone healing process is accelerated, particularly in the initial stage of osseointegration [72]. As such, many researchers have attempted to coat hydroxyapatite onto titanium implant surfaces and scaffolds, such as through the use of plasma spraying, ion sputter deposition, sol-gel coating, etc. [73]. Among these,

Table 1. Summary of surface modification techniques for titanium and its alloys

| Technique | Principle | Characteristic |
|---|---|---|
| ***Mechanical modification*** | | |
| Polishing | | Clean surface; flat topography. |
| Machining | Mechanical friction | Micron-rough surface. |
| Grinding | | |
| Sandblasting | Projection micro-particles ($Al_2O_3$, $TiO_2$) onto substrate. | Produces micron-rough surface; high potential of detachment and release into host body. |
| ***Chemical modification*** | | |
| Acid etching | | Forms porous structure with roughness that range from micron- to nano- level. |
| Alkaline treatment | Chemical corrosion. | Forms sodium titanate gel layer that potentiates HA deposition when processed with subsequent SBF immersion. |
| Peroxidation | | Forms titania gel layer with micro- or nano-topography. |
| Sol-gel | | 3D architectural micron level thin films composed of versatile compounds such as calcium phosphate, $TiO_2$ and silica. |
| Chemical Vapor Deposition(CVD) | Deposits non-volatile compounds onto substrate through gas phase reaction. | Uniform films with controllable density and thickness. |

| | | |
|---|---|---|
| ***Oxidation*** | | |
| Anodic oxidation | Electrochemical oxidation. | Induces nanotube matrix. Incorporates additional elements from electrolytes. |
| Thermal oxidation | High temperature oxidation. | Exhibits both micron- and nano-scale roughness by formation of compact and dense oxide films with agglomeration of $TiO_2$. |
| ***Physical modification*** | | |
| Thermal spray<br>Flame spray<br>Plasma spray | Produces very high temperature to melt desired particles, then sticks and condenses liquid droplets onto substrate. | Imparts thick coatings (up to 200 μm) such as $TiO_2$, $Al_2O_3$, calcium silicate, HA. |
| Physical vapor Deposition (PVD) | Deposits films by condensation of vaporized forms of desired materials onto substrate surface. | Uniform films with controllable density and thickness. |
| Ion implantation and deposition | Energetic ions are bombarded onto solid substrates. | Forms a distinct surface layer with graded composition. |
| Glow discharge plasma treatment | Bombards surface layers by electrons and ions produced from glow discharge plasma. | Removes passive layer and creates a clean, sterilized surface layer. Ion bombardment influences molecules adsorption. |

| | | |
|---|---|---|
| Laser ablation | Irradiating and heating result in melting and evaporation of surface atoms. | Produces ordered micron-level grooves or pillars on substrate surface. |
| Lithography | Patterns surface through high-energy electrons or wave-specific light. | Creates highly ordered nanopatterns (pits, pillars, grooves) on substrate. |
| ***Bio-chemical modification*** | | |
| Layer-by-layer self-assembly | Electrostatic attraction between polycations and polyanions. | 3D architecture with drug-carrier capability. Can be fabricated onto substrates with various morphology and induce surface functional groups. |
| Immobilization of proteins<br>Hormones<br>Incorporation DNA and enzymes | Immobilizes biomolecules through polymerization, plasma pre-treatment, scaffolds, LBL etc. | Induces bio-inspiring materials in accordance with targeting bioactivities. |

plasma-spraying is the only hydroxyapatite coating technique that has been used in clinical practice [10]. The plasma torch can reach a critical temperature to project semi-molten hydroxyapatite powders carried by an argon and hydrogen mixture onto titanium surface, where the hydroxyapatite is condensed and fused. This process results in a compact hydroxyapatite layer on the titanium surface with a thickness that ranges from micrometers to millimeters.

Although hydroxyapatite coatings have been reported to enhance the osseointegration capability of titanium and its alloys, they are still problematic. The first disadvantage of plasma sprayed hydroxyapatite coatings is the varying percent composition of crystalline hydroxyapatite, tricalcium phosphate and amorphous CaP [74]. The second disadvantage is the detachment of the coating from titanium substrate despite that the hydroxyapatite-bone tissue interface remains intact [75]. To minimize these drawbacks of plasma-sprayed hydroxyapatite coatings, researchers have further developed related methods by combining the use of anodic oxidation or alkali treatment. A detailed discussion of these techniques will be presented in Section 2.7.5 and 2.7.6.

### 2.7.2 Thermal Oxidation

TO is a high temperature oxidation process. Thermal energy produces atoms that are excited to a higher energy level and when combined with oxygen, form oxides. The

oxidation process of a metal can be written as:

$$\mathrm{aM} + (b/2)O_2 = M_aO_b$$

This process can be further divided into several steps (Figure 3). With the start of metal-oxygen contact, the absorption of oxygen on a bare metal surface takes place, thus forming a monolayer of oxide. Then oxygen starts to dissolve into the metal, and continues to form oxides, thus enhancing the thickness of the oxide layer. Actually, this is the same process that a metal undergoes when exposed to air conditions. The only difference is attributed to the reaction rate. At room temperature, this reaction is quite slow and reaches equilibrium after the formation of a very thin oxide layer. In contrast, the reaction proceeds at a much faster rate under high temperature, and therefore produces a denser and thicker oxide layer. The resultant ceramic oxide layer, especially in presence of rutile titanium dioxide, can greatly enhance hardness, wear and corrosion resistance of titanium and its alloys [76, 77].

*In vitro* experiments have demonstrated that thermally oxidized titanium and its alloys exhibit several advantages. MacDonald et al. showed that the TO of Ti-6Al-4V can enhance osteoblast lineage cell attachment, regardless of the oxidation atmosphere [78]. Saldana et al. demonstrated that a thermally oxidized Ti-6Al-4V surface is able to promote cell attachment by enhancing β1 integrins and FAK-Y397 expression when

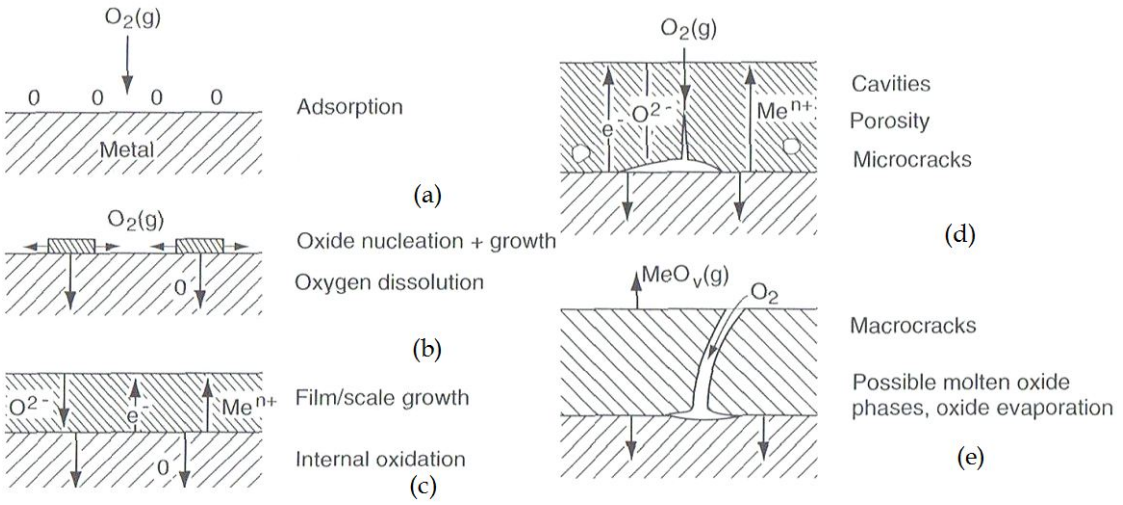


Figure 3. Formation process of $TiO_2$ oxide layer: (a) Oxygen adsorption. (b) Oxygen dissolution and oxide nucleation. (c) Oxide film growth. (d) Formation of cavities, porosity and microcracks. (e) Formation of thick oxide layer [79].

compared to a polished Ti-6Al-4V [17]. Alonso et al. compared the effect oxidation temperature on osteoblast behavior and indicated that oxidation at 750°C results in higher levels of osteoblast proliferation than at 500 °C, without affecting osteoblast adhesion [80].

The combination of TO with other surface modification techniques is a powerful strategy to enhance osseointegration. Nishiguchi et al. speculated that a subsequent TO after NaOH treatment may enhance the osseointegration capability of titanium and its alloys by reducing intervening of soft tissues [81]. Ueno et al. indicated that a subsequent NaOH treatment and TO of sandblasted Ti-6Al-4V can significantly increase the bone bonding ability of polished Ti-6Al-4V *in vivo* [18]. Taken together, these studies imply that the thick and rough oxide layer formed by TO can influence osseointegration capability of titanium and its alloys.

### 2.7.3 Sandblasting

Sandblasting is the process of propelling fine bits at high-velocity from a blasting nozzle onto the material surface by compressed air. Alumina, corundum, rutile and hydroxyapatite are common particles used in sandblasting, with a typical diameter that ranges from of 25 to 900 μm [82]. These resultant titanium surfaces are embedded with these particles and exhibit sub-micron to micron scale roughness.

Many studies have demonstrated that sandblasting can improve the biological performance of titanium and its alloys. Mustafa et al. roughened cpTi surfaces by blasting $TiO_2$ particles and found the levels of human mandibular alveolar cell proliferation and differentiation are proportional to the surface roughness of modified cpTi [83]. Schneider et al. indicated that sandblasted cpTi can improve the expression levels of Cbfa 1 gene, which is an essential transcription factor for bone formation [84]. Ronold and Ellingsen found that cpTi blasted by $TiO_2$ particles with a diameter between 180-220 μm exhibit the best bone bonding ability among the cpTi blasted by $TiO_2$ particles that with diameter range from 7.5 to 330 μm [85]. An *In vivo* study conducted by Wennerberg et al. indicated that titanium screws blasted with 75 μm $Al_2O_3$ particles exhibit a significant higher bone-to-metal contact [86]. To sum up, these encouraging biological effects of sandblasting have been mostly attributed to its ability to roughen the surface of titanium and its alloys.

### 2.7.4 Immobilization of Bio-functional Molecules

The immobilization of biomolecules on an implant surface has created bioactive titanium surfaces to control cell and tissue responses. Common biomolecules employed include collagens and bone growth factors, etc.

Collagen is the most abundant protein within ECMs, acts as structural support and plays a

critical role in the regulation of cell adhesion through its RGD fragments. *In vitro* studies have covalently linked type I collagen to titanium surfaces and found that type I collagen influences the initial stages of cell activities by reducing initial detrimental protein interactions at the implant surface [87]. *In vivo* studies have also demonstrated that type I collagen induces bone growth and bone-implant contact [88]. Other types of collagen have also been explored. These studies indicated that type III collagen can decrease heterotypic fibril diameter and increase matrix production in the initial bone-healing process and later replaced by type I collagen [89, 90], while type I collagen enhances cell adhesion through a faster focal adhesion formation process [91].

Other proteins, such as bone morphogenic proteins (BMPs) and transforming growth factor- β1 proteins, have also been used to improve bone regeneration. They are members of the transforming growth factor beta superfamily proteins that exhibit promising bone reformation ability [92, 93]. By grafting these proteins onto titanium surfaces, studies have demonstrated the resultant titanium surface can stimulate osteoblast adhesion, proliferation and differentiation *in vitro* and promote bone bonding *in vivo* [94-97].

The most challenging issue in the immobilization of biomolecules is the uncontrollable release rate. Insufficient evidence of a stable release rate, to some extent, has discounted the efficiency of these biomolecules. Although some studies have attempted to control the release rate by the use of different models, further improvements are still needed [98,

99].

### 2.7.5 Anodic Oxidation

Anodic oxidation is an electrochemical oxidation technique used to produce nano- to micron-scale topography on titanium and its alloys. During the electrochemical oxidation process, titanium and its alloys are placed in the anode and the cathode is usually made of Pt. Strong but diluted acids such as $H_2SO_4$, $H_3PO_4$, $HNO_3$, are used as electrolytes. The fundamental reactions can be expressed as [68]:

Ti/Ti oxide interface:

$Ti \leftrightarrow Ti^{2+} + 2e^-$

Ti oxide/ electrolyte interface:

$2H_2O \leftrightarrow 2O^{2-} + 4H^+$

$2H_2O \leftrightarrow O_2 + 4H^+ + 4e^-$ ($O_2$ gas formation)

At both interfaces:

$Ti^{2+} + 2O_2\text{-} \leftrightarrow TiO_2 + 2e^-$

The properties of the $TiO_2$ oxide formed in this process can be altered by adjusting experimental parameters, such as applied voltage, oxidation time, current density,

electrolyte temperature and concentration. If the applied voltage is high enough to breakdown the oxide layer, then there is an increasing rate of gas evolution and frequent sparking. The dissolved $Ti^{4+}$ and oxygen ions from the electrolytes would promptly combine with each other to form $TiO_2$ oxides again. This process is called micro-arc oxidation (MAO). The first advantage of MAO is that the newly formed $TiO_2$ layer can firmly attach onto the substrate. Second, the resultant porous $TiO_2$ oxide structure has been demonstrated to be necessary for the formation of apatite [100]. Meanwhile, the chemical composition of the oxide layer can be altered through the incorporation of magnesium, calcium, sulfur or phosphorus [101].

By adjusting the aforementioned experimental parameters, porous surface oxide layer with various compositions has been produced by anodic oxidation and MAO. *In vitro* and *in vivo* evaluation of these titanium-based implants demonstrated they have excellent biological performance [102, 103].

### 2.7.6 Chemical Etching

Chemical etching is an alternative way to induce nano-scale features on the surface of titanium and its alloys. Commonly used methods include NaOH treatment, acid etching and peroxidation.

NaOH treatment of titanium results in a porous sodium titanate gel layer. During the

treatment, hydroxyl groups from NaOH preferentially attack the $TiO_2$ passive layer and then penetrate into the titanium substrate to hydrate titanium. This process can be described by the following reactions [68]:

$TiO_2+NaOH \rightarrow HTiO_3^-+Na^+$

$Ti+3OH^- \rightarrow Ti(OH)_3^+ +4e^-$

$Ti(OH)_3^+ +e^- \rightarrow TiO_2.H_2O+1/2H_2\uparrow$

$Ti(OH)_3^+ +OH^- \leftrightarrow Ti(OH)_4$

$TiO_2.H_2O+OH^- \leftrightarrow HTiO_3^- +nH_2O$

As a consequence, a titanate hydrogel layer is produced by these negatively charged species with alkali ions in an aqueous solution. Later, this method was further modified by a subsequent heat treatment to dehydrate the hydrogel layer to form a crystalline alkali titanate layer [104].

When alkali- and heat- treated titanium are immersed into a simulated body fluid (SBF), a bioactive bone-like apatite layer is formed. Study has shown that the sodium titanate is highly charged when immersed into SBF [105]. As a result, it selectively combines with $Ca^{2+}$ ions to balance its electrical potential and simultaneously form calcium phosphate, which finally transforms into apatite [106]. An *in vitro* investigation indicated that apatite

formation can promote BMSC differentiation, possibly due to the formation of a calcium phosphate layer [107]. Nishiguchi et al. revealed that alkali- and heat- treatment can enhance the bonding ability of titanium *in vivo* [108]. Oh et al. revealed the extremely fine nanostructure of sodium titanate nanofibers (~ 8 nm) and demonstrated their ability to enhance osteoblast adhesion [109, 110].

Acid etching and peroxidation, especially when combined with other surface modification techniques, are alternative methods that induce a nano- to micron- scale topography on titanium implants. Chemicals like $H_2O_2$, $HNO_3$ and HCL can dissolute and oxidize titanium to produce discrete pits on the surfaces. Dual acid etching has been shown to cause profound effects on bone healing due to the nano-scale topography, which is able to enhance cell activities *in vitro* and improve bone-implant contact *in vivo* [111-113]. A further study was conducted by using a subsequent heat treatment after dual acid etching and found that the adsorption of RGD peptides and mineralization were increased [114]. Meanwhile, acid etching is also used with sandblasting to improve the initial cell anchorage *in vitro* and bone-implant contact *in vivo* [115, 116]. Recently, Yang et al. found that titanium implants treated by $H_2O_2$, HCl and heat can enhance the new bone area [117]. However, acid etching and $H_2O_2$ treatment impairs the corrosion resistance of titanium implants in the form of hydrogen embrittlement and creation of micro cracks, thus reducing the ductility of titanium implants [118].

### 2.7.7 Nano-patterning

Nano-patterning is able to produce highly ordered nano-scale patterns, such as grooves, holes and pillars. This technique has improved the accuracy of surface science from a micron-scale to nano-scale. A typical method used in nano-patterning is lithography, which employs specific wavelengths to form desired nano-scale topographies. Lithography has a higher accuracy in controlling the implant topography than traditional modification techniques. For example, the highest accuracy can be achieved prior to the use of nano-patterning is still limited to the micron-level by laser treatment.

Controlled nano-scale structures on implant surfaces have been deemed to be very promising in mimicking bone tissues. For example, Weiner and Wagner revealed that the natural bone surface has a roughness of 32 nm and the hydroxyapatite crystals embedded in fibrils formed by type I collagen have an average size of 50 x 25 x 4 $nm^3$ [119]. *In vitro* studies have mimicked the natural bone surface and type I collagen structure by using nanophase polymers [120-122].

The geometry of nano-patterns has been thought to affect cell responses. Lamers et al. elucidated osteoblast alignment to nanopatterns with minimal widths of 75 nm and depth of 33 nm, and the aligned mineralization was even found on nanopatterns of 50 nm in width and 17 nm in depth [123]. Fiedler et al. indicated that local cellular adhesion occurs on the exact top of nanopillars down to 10 nm in diameter and 50 nm in pillar distance

[124]. Cell proliferation is also affected by nano-scale patterns. Lim et al. indicated that osteoblast proliferation and differentiation increase on nano-islands that are 11 nm in height as opposed to higher levels of 38-85 nm [125]. Very recently, Fiedler et al. demonstrated that BMSC proliferation is independent of nanopillar dimensions, while osteoblast proliferation is significantly sensitive to pillar height [124]. The different levels of proliferation between osteoblasts and BMSCs were attributed the difference in the elasticity of cell membranes between these two cell types. In addition, a nano-patterned surface is also beneficial for osteogenic differentiation of cells [48, 123, 126]. To summarize, it is generally acceptable to say that nano-scale patterning is a bio-mimetic technology not only used to reveal the molecular biology principles of the bone healing process but also to accurately control specific cell activities.

### 2.7.8 Layer by Layer Self-assembly Technique

LBL self-assembly is a simple and versatile technique used to control the bulk and surface properties of materials. Since the 1990s, LBL self-assembly has been considerably developed in the production of hybrid carrier systems for dyes, sensors, enzymes, drugs and cells [127]. Recent investigations have employed these macroscopic or microscopic coatings as ideal platforms for functionalizing surfaces, targeting cells and molecules, etc. [128]. LBL membranes have advantages such as a vast variety of protocols, ability to achieve the desired surface chemistry, adaptation to both regular and

irregular substrates, and controllable thickness.

The principle of LBL construction varies according to its driving force. Mostly, LBL construction is based on the electrostatic attraction of oppositely charged polyelectrolytes. Meanwhile, hydrogen bonding, hydrophobic interactions and van der Waals force have also been used as driving forces to build-up LBL films [129-131]. These driving forces greatly expand the available materials from charged polyelectrolytes to uncharged materials like carbon nanotubes, pH and sugar- sensitive drugs [132]. However, the application of LBL in bone-tissue engineering is mainly focused on electrostatic attraction due to its simplicity and stability.

The constructing of LBL films is quite straightforward in which dip coating is used. As shown in Figure 4, this is a four step process: 1) pre-charged substrate is immersed into a polyanion solution to form a negatively charged monolayer, 2) the substrate is washed with water to remove weak and unbound polyanions, 3) the coated substrate is submerged to a polycation solution to obtain a positively charged second layer, 4) the washing step is repeated to remove extra polycations. As such, a bi-layer LBL film, $(A/B)_1$, is formed. Finally, this process is repeated until the desired layer numbers are achieved. Although this process is straightforward, it is time-consuming and more importantly, the uniformity of the resultant LBL film is not guaranteed due to the strong dependency of operator. In this context, spin-assisted layer-by-layer assembly (SA-LBL) is suggested. This emerging

method is found to be a time-efficient technology for the LBL fabrication (Figure 5). Under shear forces applied by a spin-coater, the resultant LBL films can be fabricated with a higher uniformity and a well-ordered structure, accompanied by much higher efficiency than dip coating [133, 134]. For example, Jiang et al. fabricated LBL nanofilms that contain gold nanoparticles by SA-LBL and demonstrated that the LBL films have a well-organized microstructure and high optical quality as opposed to those fabricated by dip coating [133]. From the perspective of bone-tissue engineering, LBL films can regulate osteoblast lineage activities through the selection of polyelectrolytes.

Depending on the origin, polyelectrolytes can be divided into synthetic and natural polymers. Commonly used synthetic polymers include styrene sulfonate (PSS), poly(acrylic acid) (PAA), poly(allylamine hydrochloride) (PAH), poly(ethylenimine) (PEI), etc. Natural polymers include chitosan, alginate, proteins, nucleic acids and DNA. Among these, chitosan/alginate are one of the most popular pairs used to fabricate LBL films.

Chitosan is a positively charged linear polysaccharide with deacetylated unit β(1,4)-D-glucosamine and acetylated unit N-acetyl-D-glucosamine. It is a natural polymer produced by the deacetylation of chitin, which is widely distributed in shrimp and other crustacean shells (Figure 6). In an aqueous environment with acidic pH, the 2-amino group can be protonated to render positive charge units. These cationic

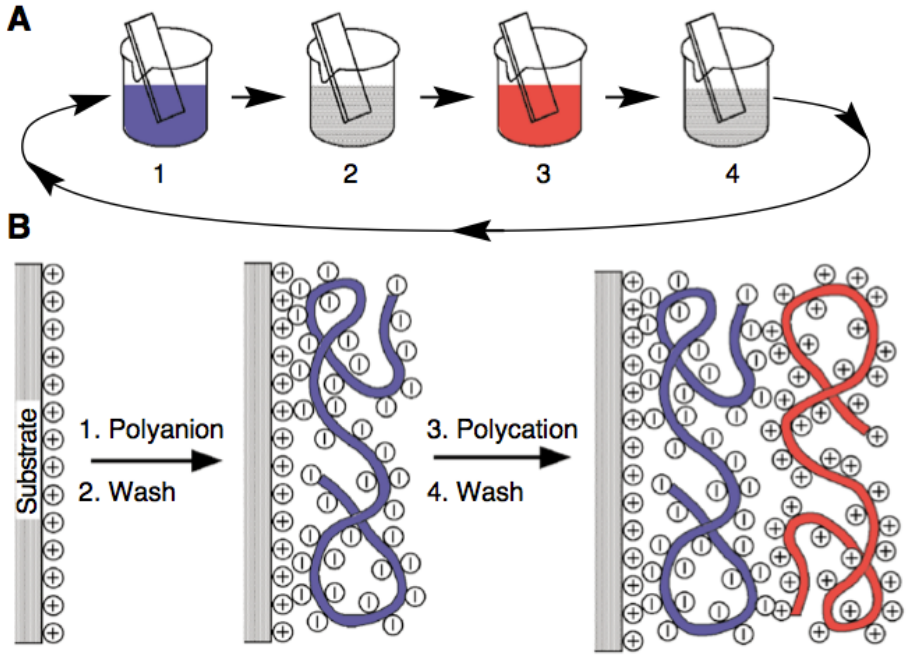


Figure 4. (A) Deposition process of LBL pairs using beakers and slides. (B) Schematic illustration of polyelectrolytes assembly process [135].

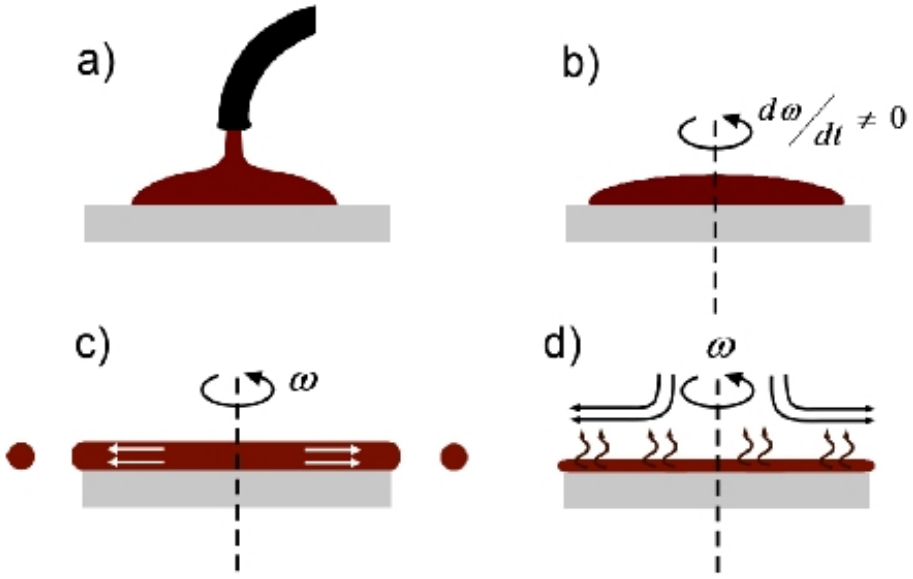


Figure 5. Schematic illustration of spin-coating: (A) Pipetting polyelectrolytes. (B) Spin acceleration. (C) Constant spinning process. (D) Evaporation process[136].

characteristics enable chitosan to interact with anionic charged glycosaminoglycan (GAGs), proteoglycans and other molecules, which are linked to a large number of cytokines and growth factors in ECMs [137, 138]. Chitosan has gained considerable applications in bones, nerves, skin, wound healing, drug delivery, and artificial human organs due to its excellent bio-compatibility, low toxicity, predictable degradation rate and potential antibacterial ability [138]. Furthermore, in the perspective of bone tissue engineering, chitosan has been found to have a positive influence on cell attachment, proliferation and osteogenic differentiation, regardless of the material shape [8, 139].

Alginate is a negatively charged polysaccharide that comprises varying amounts of 1,4'-linked β-D-mannuronic acid (M units) and 1,4'-linked α-L-guluronic acid (G units) residues (Figure 7). It is also a natural polymer mainly extracted from brown algae including *Laminaria hyperborean, Ascophyllum and Macrocystis pyrifera* [140]. The dissolution properties, in contrast with chitosan, proceed in an alkaline pH environment from the carboxyl functional group of G units. Alginate has more applications than chitosan, including in the food and beverage industry, drugs, wine technology and tissue engineering due to its high bio-compatibility, low cost and chemical versatility [15]. For tissue engineering, pure alginate hydrogels, scaffolds and beads have been applied to DNA and cell encapsulation, protein release, etc. [141, 142].

The pairing of chitosan and alginate is widely accepted in the formation of LBL

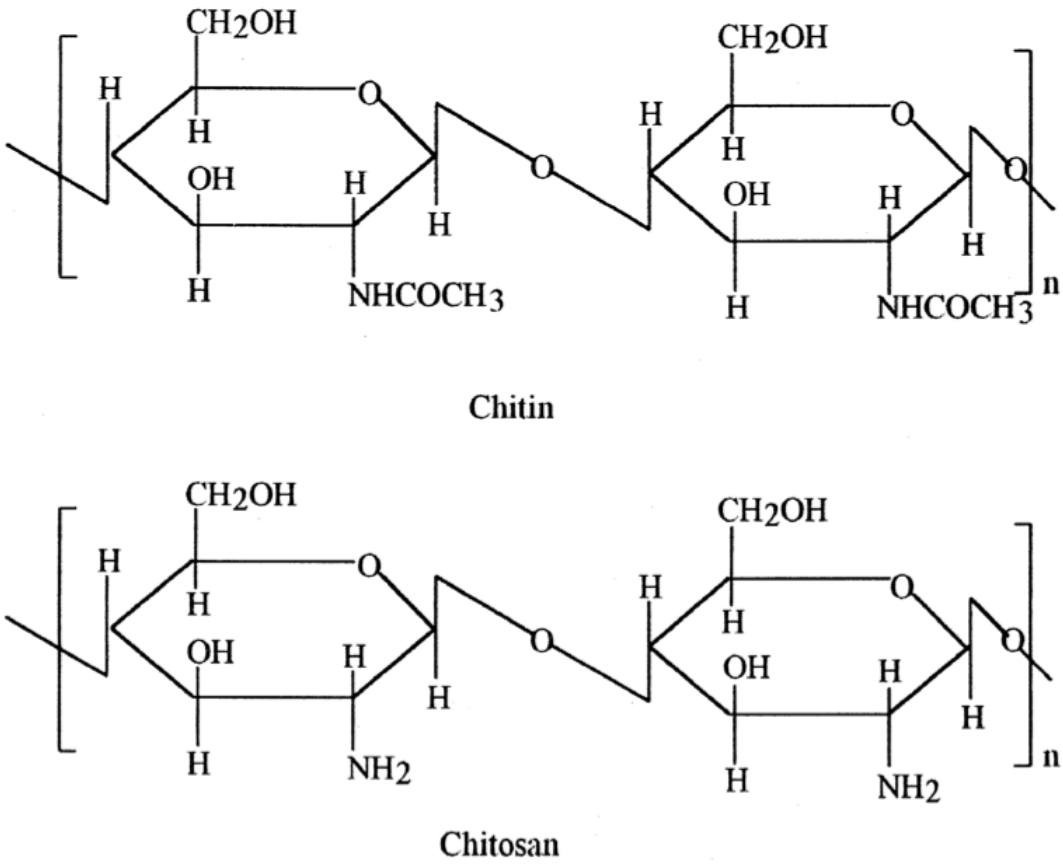


Figure 6. Molecular structures of chitin and chitosan[143].

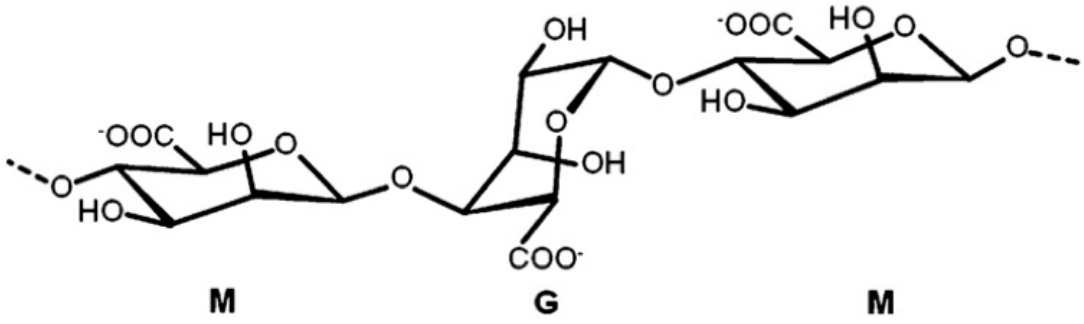


Figure 7. Molecular structure of alginate[15].

architectures, such as ultra-thin/freestanding films, scaffolds [144, 145], hydrogels and the encapsulation of cells or nanotubes [146]. These studies have indicated that chitosan/alginate pairs exhibit mechanical stability, controllable porosity, permeability, etc. [144-146]. *In vitro* studies have also shown the chitosan/alginate scaffold excellent biocompatibility [147].

## 2.8 Nano-silver and Anti-infectiveness

Implant-centered infections are the second most common complication besides osseointegration failure. An 8-year follow up of 3609 implants reported that infection-related bone failure accounts for 52.5% of the total failure rate in dental implants [148]. Implant infections occur at all stages of bone healing process since bacteria exist almost everywhere. Rubin et al. have confirmed that most infections are caused by *Staphylococcus aureus* and *Staphylococcus epidermidis* [149].

Silver ions ($Ag^+$) have been extensively used as bactericidal and inhibitory agent. In a nitrate solution, $Ag^+$ has the ability to kill a wide range of microorganisms at submicromolar concentrations. Since the last century, $Ag^+$ containing compounds have been applied in the food industry, storage, clinical treatment of burns, wound dressings, etc. However, $Ag^+$ exhibits cytotoxicity at even submicromolar concentrations due to the excessive release of reactive oxygen species [150]. In this context, nano-silver particles were developed to overcome this challenge.

Nano-silver particles are known as a cluster of metallically bonded silver atoms with a size range from 1-100 nm. The presence of high-atom-density facets enable nano-silver to exhibit a stronger antibacterial ability than silver ions [151]. The mechanism, although not fully understood, is generally attributed to the contribution of both silver ions and metallic silver which interact through three means to with bacterial: 1) interference withthe permeability of the peptidoglycan cell wall and plasma membrane, 2) interaction with sulfur and phosphorus-containing bio-structures to generate reactive oxygen species, which will destroy DNA, proteins, specific enzymes, etc. and 3) inhibition of respiratory chain enzymes in bacterial proteins (Figure 8).

The fabrication nano-silver is quite straightforward. Nano-silver can be obtained by the chemical reduction of silver nitrate by using $NaBH_4$, citrate, hydrazine, etc. However, these reduction methods require stabilizers to control the potential agglomeration of colloids and the reducing agents are considered hazardous. As a consequence, green syntheses of Nano-silver particles have attracted increased research interests. These approaches include the use of irradiation, polysaccharides, polyphenols, Tollens' reagent and biological reduction. Among these, biological reduction is particular attracting. Biomolecules, such as enzymes, proteins, amino acids, vitamins are physiologically-friendly to host tissues [152, 153]. Biomolecules can also be simultaneously employed as capping and reducing agents in the reduction process of

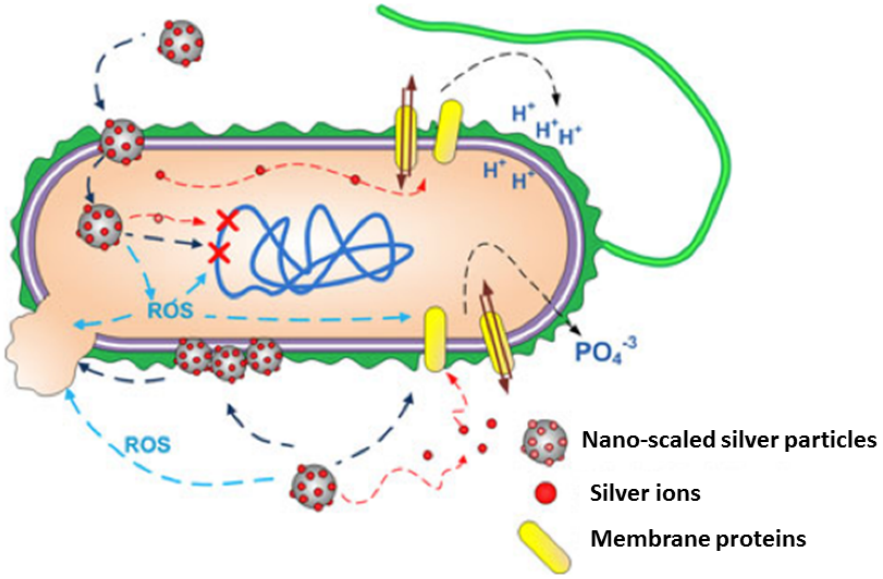


Figure 8. Schematic illustration of nanosilver-bacterial interactions[150].

silver ions. Consequently, biomolecules have been extensively used as reducing agents for silver ions, such as Vitamin E, tripeptide (Asp-Asp-Tyr-OMe), glutathione, dopamine, etc. [154].

Dopamine (3,4-dihydroxyphenethylamine) is a mussel-inspired biomaterial. Under alkaline conditions, dopamine can self-polymerize to generate poly-dopamine (PDA), which exhibits strong adhesive properties (Figure 9). When used as a reducing agent, its additional adhesive properties can result in the adhering of reduced Ag atoms on the material surface, thus allowing the controlled release of nano-silver particles.

In bone tissue engineering, researchers have attempted to incorporate nano-silver particles onto implant surface. Yuan et al. incorporated nano-silver particles into a $TiO_2$-chitosan-heparin hybrid system and found that the system exhibits a short-term antibacterial effect [155]. Qu et al. loaded nano-silver particles onto hydroxyapatites on porous titanium substrates and showed that the nano-silver particles can enhance the antibacterial ability of the titanium-based system [156]. Saravanan et al. presented a chitosan/nano-hydroxyapatite/nano-silver composite scaffold and found that this composite scaffold exhibits antibacterial capability [157]. However, these studies have only addressed the antibacterial aspect of implant materials while the sustained release of nano-silver particles was neglected. More importantly, whether nano-silver particles jeopardize the enhanced cell adhesion, proliferation and differentiation that induced by

the surface modification of titanium implants have not been systematically reported.

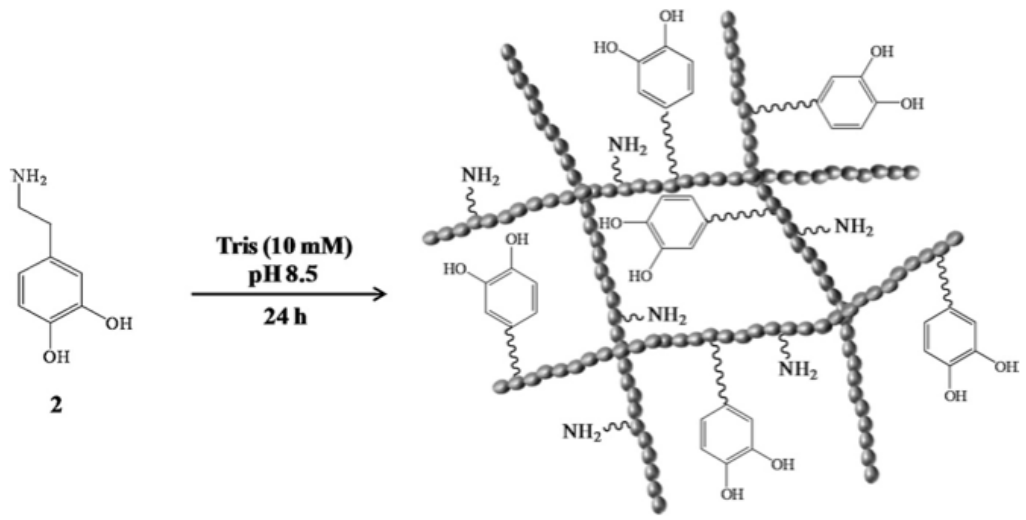


Figure 9. Schematic transformation of dopamine to poly (dopamine) under 10mM Tris-HCl buffer [158].

# Chapter 3

# Experimental Procedures

## 3.1 Introduction

This chapter contains detailed experimental procedures for the two projects involved in this dissertation. In Section 3.2, three surface modification techniques on Ti-6Al-4V and related characterization procedures by AFM, SEM, AES, XPS and CAG are described. In Section 3.3, the construction of LBL hybrid system on thermally oxidized Ti-6Al-4V substrates and related characterization by AFM, SEM, CAG and XPS are thoroughly presented. This section also includes the protocols of *in vitro* evaluation on BMSCs adhesion, proliferation and differentiation, as well as antibacterial test on the modified Ti-6Al-4V substrates.

## 3.2 Characterization of Surface Oxide Films on Bio-implantable Ti-6Al-4V

### 3.2.1 Sample Preparation

A Ti–6Al–4V (ASTM F-1472) bar that was 1.27 cm in diameter and 76.2 cm in length was purchased from Titanium Industries, Inc. (Montreal, Canada). This bar was cut into circles that were 12.7 mm in diameter and 1 mm in thickness with a numerically controlled wire electro-discharge machine (EDM). The substrates were polished to 1 μm

to form mirror-like surfaces and ultrasonically washed for 15 mins with acetone and ultrapure water, then dried by using a stream of compressed air. The thermally oxidized samples were treated in a laboratory furnace at 650°C for 8 h and hereafter termed as TO samples. In terms of $H_2O_2$ treatment, the samples were immersed into a 30% $H_2O_2$ solution for 24 h and hereafter termed as the $H_2O_2$ samples. Finally, a mixed treatment was conducted by oxidizing the samples in a laboratory furnace at 650°C for 4 h, followed by immersing into a 30% $H_2O_2$ solution for 4 h and hereafter termed as the Mixed samples.

### 3.2.2 Surface Characterization

#### 3.2.2.1 Surface Topography and Oxide Layer Thickness

The samples topography and oxide layer thickness were examined and analyzed by using a JEOL-5900 scanning electron microscope (SEM) equipped with an Oxford energy dispersive spectrometer (EDS) and JEOL JAMP-9500F field emission Auger electron spectrometer (AES). The EDS was employed to measure the thickness of TO and Mixed samples and the AES depth profiling was carried out to measure the oxide layer thickness of the polished and $H_2O_2$ samples.

#### 3.2.2.2 Surface Roughness

Atomic force microscopy (AFM) was employed to measure the average surface roughness (Ra) induced by different surface modification techniques. In brief, a Nanosurf easyScan 2 atomic force microscope was operated under contact mode by using a SiN tip to scan over a surface area of 10 x 10 $\mu m^2$. Raw data was processed by using Scanning Probe Image Processor software (Image Metrology, version 6.2.6).

#### 3.2.2.3 Surface Chemistry

An Axis DLD Ultra X-ray photoelectron spectrometer (XPS) was employed to determine the surface chemistry of the modified Ti-6Al-4V samples. The X-ray photoelectron spectroscopy analysis was carried out with an Al Kα (1486.6 eV) monochromatic source at base pressures less than $10^{-8}$ Torr with a perpendicular take-off angle. For the survey spectra, a hybrid lens mode was used with a slot aperture at 160 eV pass energy. The survey scan was executed between a binding energy of 0 and 1200 eV binding energy. For the high-resolution scanning, a hybrid lens mode with a slot aperture was used at a pass energy of 20 eV. High resolution scans were recorded for C 1s, O1s, N 1s, Ti 2p, Al 2p and V 2p. The energy shift due the surface charges was corrected with C 1s with a binding energy of 285 eV. Peaks were fitted (Gaussian/Lorentzian curves) after background subtraction with CasaXPS® software.

#### 3.2.2.4 Surface Wettability

Measurement of the water contact angle measurement was conducted to determine the surface wettability of polished and oxidized Ti-6Al-4V samples. The measurement was conducted at room temperature (20°C) on an NRL-100-00-115-S contact angle goniometer (Rame-Hart, USA) with automatic image analysis software. Triplicate samples were prepared for each group, and each sample was tested three times by controlling identical sized droplets to ensure the reproducibility of measurement. The results were presented as a mean ± standard deviation.

## 3.3 Construction of Ultrathin Film on Rough Ti-6Al-4V Surface for Enhanced Osseointegration and Antibacterial Capability

### 3.3.1 Construction of Alginate/Chitosan LBL Film

#### 3.3.1.1 Materials

Ti–6Al–4V (ASTM F-1472) bar, 1.27 cm in diameter and 76.2 cm in length, was purchased from Titanium Industries, Inc. (QB, Canada). Medium molecular weight chitosan and alginic acid were purchased from Sigma-Aldrich Chemical Co. (MO, USA). Dopamine hydrochloride was obtained from Alfa Aesar (MA, USA). Other chemicals were purchased from Fisher Scientific (ON, Canada). Mouse BMSCs were purchased from American Type Culture Collection (MD, USA). As received Dulbecco's modified

Eagle's medium (DMEM), fetal bovine serum (FBS) and related cell culture reagents were purchased from Gibco (ON, Canada) and used without further treatment. Live/Dead® viability assay kit, TRIzol and Oligo dT was obtained from Invitrogen (CA, USA). methylthiazoltetrazolium bromide (MTT) cell proliferation assay kits were purchased from Biotium Inc. (CA, USA).

#### 3.3.1.2 Thermal Oxidation of Ti-6Al-4V Samples

The Ti-6Al-4V bar was cut into circular shapes that were 12.7 mm in diameter and 1 mm in thickness with a numerically controlled wire EDM. These samples were polished to 1μm to form mirror-like surfaces and ultrasonically washed for 15 mins with acetone and ultrapure water, followed by drying using a stream of compressed air. To fabricate thermally oxidized Ti-6Al-4V, the samples were placed into a laboratory furnace under an atmospheric condition at 650°C for 8 h. After oxidation treatment, all of the samples were ultrasonically washed with ethanol, acetone and ultrapure water for 15 mins, then dried and stored under a nitrogen gas atmosphere. Thereafter, the polished Ti-6Al-4V samples were denoted as P samples, and the thermally oxidized Ti-6Al-4V samples were denoted as TO samples.

#### 3.3.1.3 Preparation of Polyelectrolytes

A chitosan solution (5 mg/ml), used to fabricate the positively charged layer, was obtained by dissolving chitosan into 0.1 M HCl that contained 0.14 M NaCl. An alginate

solution (5mg/ml), used to fabricate the negatively charged layer, was prepared by dissolving alginic acid into 0.1 M NaOH that contained 0.14 M NaCl. After dissolution, the chitosan solution was adjusted to pH=5 and alginate solution was adjusted to pH=8 by using either NaOH or HCl. In addition, poly(dopamine) (PDA), used to obtain an adhesive layer to initiate the alginate/chitosan LBL self-assembly process, was prepared by dissolving dopamine into Tris-HCl (0.1 mM, pH=8.5) buffer at a concentration of 2 mg/ml.

#### 3.3.1.4 Build-up of with Alginate/chitosan LBL Self-assembly Film

The samples were first immersed into the PDA solution overnight to obtain the precursor layer to initiate the LBL self-assembly process. A spin-coater (Headyway, USA) was employed to fabricate the alginate/chitosan LBL pairs. Briefly, 1 mL of the alginate solution was pipetted to cover the surface followed by spinning at 2500 rpm for 90 secs. Then, the samples were washed with ultrapure water twice at a rate of 1000 rpm for 60 secs. Thus a negatively charged alginate layer was obtained. The construction of the chitosan layer was carried out by using the same procedure. Finally, this procedure was repeated until the desired pairs of alginate/chitosan were attained. The resultant samples fabrication on polished and thermally oxidized Ti-6Al-4V samples were denoted as $P/(A/C)_X$ and $TO/(A/C)_X$ samples, where x represented the number of alginate/chitosan pairs.

#### 3.3.1.5 Incorporation of Nano-silver

To incorporate nano-silver into the LBLed films, the TO/$(A/C)_X$ samples were immersed into 2 mg/ml of the PDA solution for 3 h, and then washed with ultrapure water twice for 2 mins, and dried in air. The samples were then immersed into 10 mM $AgNO_3$ solution for 3 h to reduce the silver ions into nano-silver particles, subsequently rinsed twice with ultrapure water and then dried in air. The resultant fabrication was denoted as TO/$(A/C)_X$ /Ag sample, where x represented the number of alginate/chitosan pairs..

### 3.3.2 Surface Characterization

The contact angle measurements were conducted on an NRL-100-00-115-S contact angle goniometer to measure the wettability changes during the LBL fabrication process and the stability (Rame-Hart, USA). The droplets were controlled so that they were all identical in size during testing. Each sample was tested three times to ensure the repeatability of the experiment. An atomic force microscope (Vecco D3100, USA) was used to examine the surface topography and roughness of the Ti-6Al-4V samples. A surface area of $10\times10$ $\mu m^2$ was scanned under a tapping mode at room temperature.

A JEOL 5900 SEM was employed to characterize the surface topographies of Ti-6Al-4V samples. Additionally, an X-ray photoelectron spectroscopy analysis was carried out with an Axis DLD Ultra X-ray photoelectron spectrometer with an Al Kα (1486.6 eV)

monochromatic source at base pressures less than $10^{-8}$ Torr and a perpendicular take-off angle. The energy shift due to the surface charge was corrected with C 1s that had a binding energy of 285 eV.

### 3.3.3 *In vitro* Evaluation

#### 3.3.3.1 Antibacterial Test

Gram-negative bacteria *Escherichia coli (E. coli)* and gram-positive bacteria *Staphylococcus aureus* (*S. aureus*) were used to evaluate the antibacterial capability of all the Ti-6Al-4V samples. All disks and materials were sterilized by using autoclave or 75% alcohol before experiment. The broth containing *E. coli* and *S. aureus* were centrifuged at 3000 rpm for 10 mins. After the removal of the supernatant, the *E. coli* and *S. aureus* were washed twice with phosphate-buffered saline (PBS) and re-suspended at a concentration of $10^7$ cells/ml. The dishes were sprayed with the bacterial suspension and then all of the modified Ti-6Al-4V samples were placed in these dishes. The zone of inhibition was observed after these petri dishes were sealed with growth agar and incubated at 37°C for 24 h.

#### 3.3.3.2 Cell Culture

Passages 5-6 mouse BMSCs were cultured in DMEM with low glucose supplemented with 10% FBS and 1% penicillin-streptomycin at 37°C under a 5% $CO_2$ atmosphere. The

medium was changed every 2 days. The cells were then detached with 0.25% trypsin in 1 mM ethylenediaminetetraacetic acid (EDTA), centrifuged and re-suspended in a completely new medium for re-seeding in three new culture flasks.

#### 3.3.3.6 Live & Dead Assay and Cell Morphology

Live & Dead assays were performed to study the viability and morphology of BMSCs. The modified Ti-6Al-4V samples were placed in a 24 well-plate and then BMSCs were seeded on the samples with a density of 10,000 cells/cm$^2$. After 1 day of culturing, samples were washed twice with PBS. Then 100 µl Live & Dead assay reagents were pipetted on each sample and incubated for 30 min at room temperature, followed by washing samples twice with PBS. Visual examinations were conducted on an Olympus X51 fluorescence microscopy.

For cell morphology observation, Ti-6Al-4V samples were immersed in the mixture of 2.5% glutaraldehyde and 4% paraformaldehyde solution for 4 h at 4°C. This step was followed by washing twice with PBS for 10 mins. To dehydrate BMSCs, the Ti-6Al-4V samples were alternatively treated twice with 50%, 75%, 95%, and 100% ethanol for 15 mins. Finally, the samples were coated with platinum by using a technosyn cold cathode luminescence system and examined by a JEOL 5900 SEM.

#### 3.3.3.7 Cell Proliferation

A MTT assay was performed to determine the level of cell proliferation. The modified

Ti-6Al-4V samples were first placed in a 24 well-plate and BMSCs with a density of 10,000 cells/cm$^2$ were seeded on each of the sample. Then 1 mL DMEM medium was added to each well. After 1, 3 and 7 days of culturing, 100 μl MTT (5 mg/ml) was added to each well and the samples were incubated at 37°C for 4 h. Then the Ti-6Al-4V samples were transferred to a new 24-well plate and 0.5 ml dimethyl sulfoxide (DMSO) was added to dissolve the formazan crystals. After 15 mins, 200 μl DMSO was extracted to a new 96 well-plate. Finally, the absorbance was recorded at a wavelength of 570 nm.

#### 3.3.3.8 Cell Differentiation

A quantitative real-time polymerase chain reaction (q-RT-PCR) test was performed to determine the level of representative gene expressions. BMSCs were cultured with a density of 30,000 cells/ cm$^2$ and collected after 2 and 7 days of osteogenic induction. The control was day 0 BMSCs. The Total ribonucleic acid (RNA) was extracted by using TRIzol in accordance with the supplier instructions. Then 1 μg RNA sample was reversely transcribed for standard cDNA synthesis. The q-RT-PCR was conducted by an SYBER Green assay (Applied Biosystems, USA). An amplification program was started with an initial denaturation at 95°C for 10 mins, followed by 40 cycles at 95°C for 15 secs and 60°C for 1 min. The five gene premiers used in this study were (form 5'-3'): **ALP-F**: CTC CAA AAG CTC AAC ACC AAT G, **ALP-R**: ATT TGT CCA TCT CCA GCC G; **BSP-F**: CCA CAC TTT CCA CAC TCT CG, **BSP-R**: CGT CGC TTT CCT

TCA CTT TTG; **COL I-F**: AAC AGT CGC TTC ACC TAC AG, **COL I-R**: AAT GTC CAA GGG AGC CAC; **OPN-F**: CTA CGA CCA TGA GAT TGG CAG, **OPN-R**: CAT GTG GCT ATA GGA TCT GGG; **GAPDH-F**: AGG TCG GTG TGA ACG GAT TTG, **GAPDH-R**: TGT AGA CCA TGT AGT TGA GGT CA. The relative expressions of genes were determined by the $2^{-\Delta\Delta Ct}$ method. GAPDH was selected as a housekeeping gene to normalize the expression levels of the target genes.

### 3.3.4 Statistical Analysis

All of the results are presented in mean ± standard deviation (SD). One-way analysis of variance (ANOVA) was used to calculate the significance level. Significant difference was considered when $p<0.05$.

# Chapter 4

# Results and Discussion

## 4.1 Introduction

This chapter presents the results and discussions of the experimental work. Section 4.2 shows the characterization results from SEM, AFM, EDS, AES, CAG and XPS. The surface topography, roughness, oxide film thickness, wettability, composition and functional hydroxyl group density on the Ti-6Al-4V samples induced by TO, treatment of $H_2O_2$ and Mixed are also presented and discussed. In Section 4.3, the build-up process and *in vitro* performance of the alginate/chitosan LBL film that incorporates nano-silver on thermally oxidized Ti-6Al-4V are reported and discussed. Delete

## 4.2 Characterization of Surface Oxide Films on Bio-implantable Ti-6Al-4V

### 4.2.1 Topography and Roughness Characterization

Scanning electron and atomic force microscopy techniques revealed differences in the surface topography and roughness induced by different treatments (Figure 10&12). The polished Ti-6Al-4V surface was smooth (Ra=2.0 ± 0.56 nm) (Figure 10A). The TO sample exhibited the greatest average roughness (81 ± 4.78 nm) and a topography that consists of numerous nano-scale and micron-scale oxide particles (Figure 10B). Careful

observation shows that the micron-scale oxide particles are derived from the agglomeration of these nano-scale oxide particles. $H_2O_2$ treatment induced non-uniform cavities on the surface, with a roughness value of 17.3 ± 2.83 nm (Figure 10C). Sharp crests and pits were observed on the Mixed sample, which showed a moderate roughness of 45.8 ± 8.54 nm (Figure 10D).

The surface treatment also induced significant changes in the oxide layer thickness (Table 2). P and $H_2O_2$ group of samples exhibited oxide layer thickness of 10 and 450 nm. Mixed and TO samples had values of 6 and 9 μm, which are considered to be micron-level thickness.

The surface topography, roughness and oxide layer thickness are considered to be important parameters when evaluating the properties of bio-implants. Although each of the TO, $H_2O_2$ and Mixed treatment has greatly altered the surface topography, roughness and oxide layer thickness of polished Ti-6Al-4V, not all of these treatments are desirable. The $H_2O_2$ sample showed a relative flat surface with an average roughness of 17.3 ± 2.83 nm, while the TO and Mixed samples exhibited surfaces that were fully covered by oxide particles with larger roughness values of 81 ± 4.78 and 45.8 ± 8.54 nm. Meanwhile, the $H_2O_2$ treatment only produced an oxide layer with 450 nm in thickness, which is significantly thinner than the oxide layer induced by TO (9 μm) and Mixed (6 μm). When used as clinical implant, it is widely accepted that rough implant surfaces like those

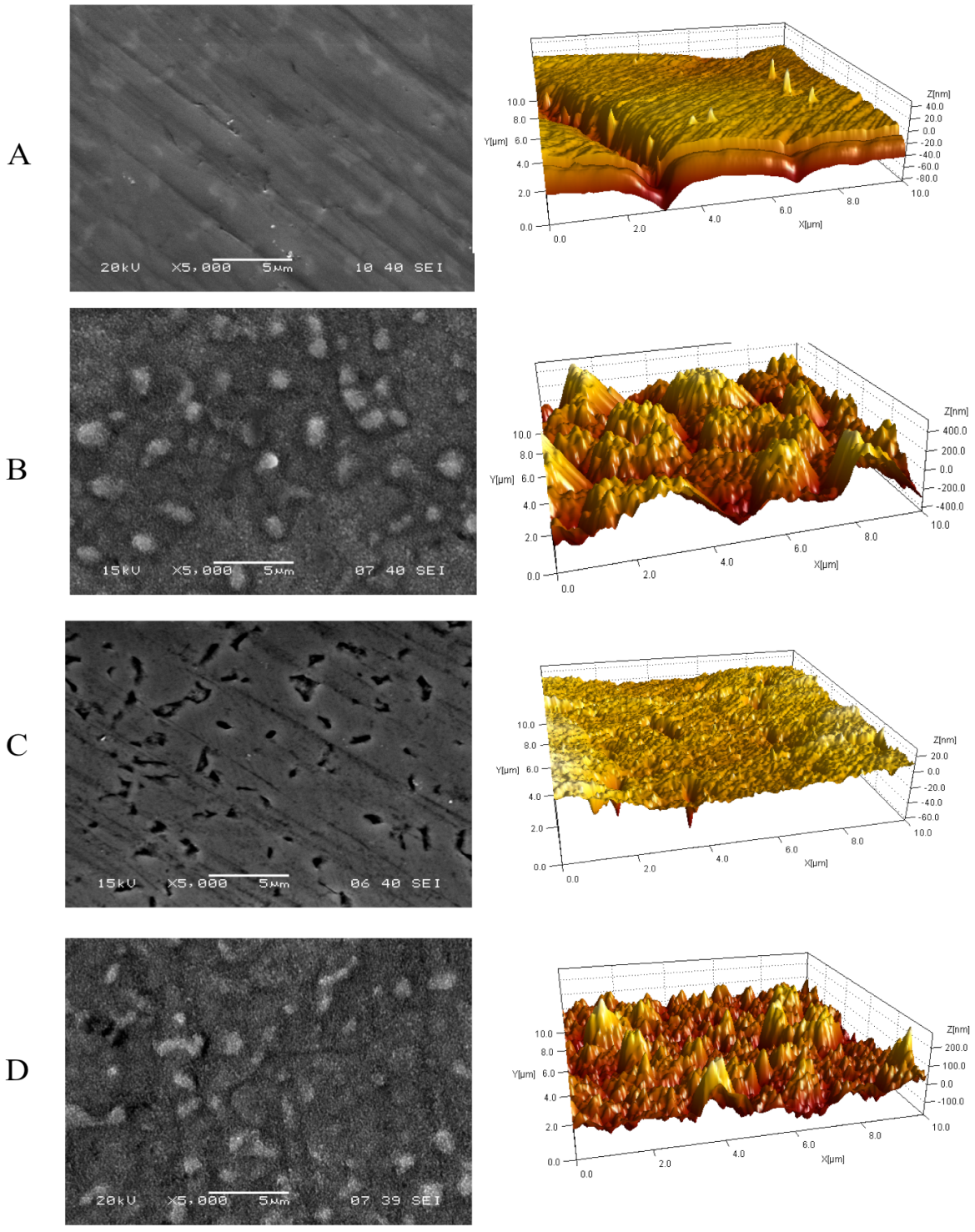


Figure 10. Surface topography of Ti-6Al-4V samples treated by: (A) P, (B) TO, (C) $H_2O_2$ and (D) Mixed.

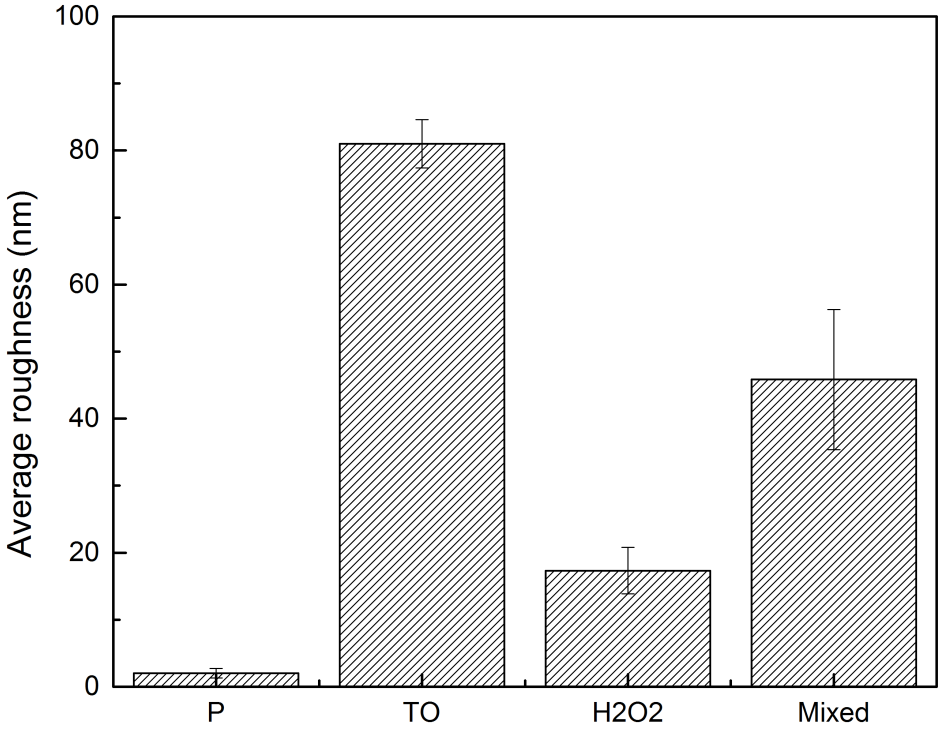


Figure 11. Surface roughness of Ti-6Al-4V samples after different treatments.

Table 2. Oxide layer thickness of Ti-6Al-4V samples after different treatments.

| Treatment | P | TO | $H_2O_2$ | Mixed |
|---|---|---|---|---|
| Thickness | 10 nm | 9 μm | 450 nm | 6 μm |

produced by TO and Mixed treatments are more favorable for cell activities than smooth surface. In addition, the ultrathin oxide layer on the $H_2O_2$ sample may be penetrated by wear and fretting. In contrast, the samples treated by TO and Mixed are more desirable. Therefore, the TO sample is favored over Mixed sample when comparing the surface roughness, topography and oxide layer, followed by the $H_2O_2$ sample.

### 4.2.2 Surface Wettability

A hydrophilic implant surface is capable of enhancing protein adsorption and cell adhesion by inducing functional groups such as $–CH_3$ and -OH [54]. The surface wettability of polished and oxidized samples was measured by water contact angle. As shown in Figure 12, the polished samples exhibit the largest water contact angle of 56.9 ± 1.26°, followed by the Mixed (33.0 ± 4.86°) and $H_2O_2$ (32.4 ± 2.64°) samples, respectively. The sample treated by TO showed the lowest contact angle of 26.5 ± 7.87°.

### 4.2.3 Surface Composition

Figure 13 shows the survey spectra of the polished, TO, $H_2O_2$ and Mixed samples. All of the spectra indicate the major elements of Ti, Al, V, O, C and N. Meanwhile, the sample treated by $H_2O_2$ also shows the presence of Sn. Herein, this element is regarded as a contaminant during sample preparation and will not be further discussed. High resolution scans were conducted on C 1s, O 1s, Ti 2p, Al 2p and V 2p. The C 1s spectra were

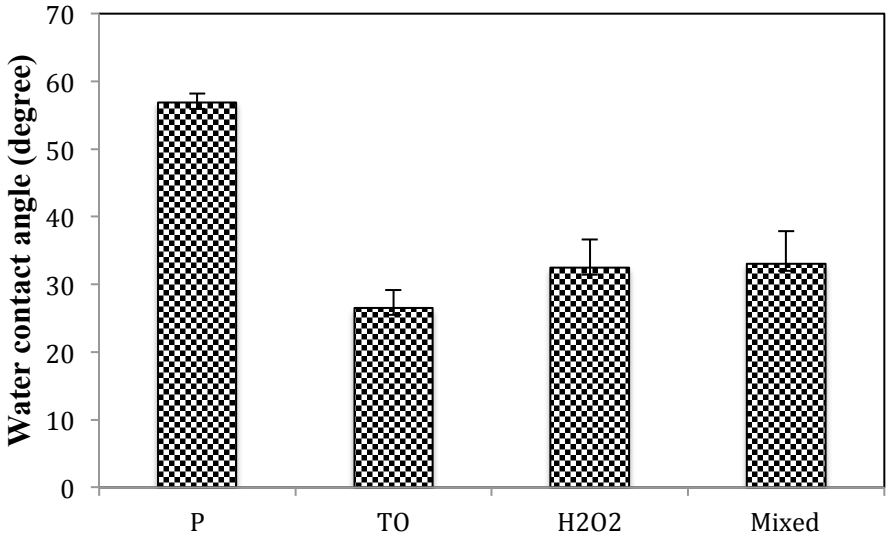


Figure 12. Water contact angle of Ti-6Al-4V samples after different treatments.

deconvoluted into three parts: C-H at 284.3-285.0 eV, C-O at 285.8-286.4 eV and C=O at 288.1-288.2 eV (Figure 14). The carbon peaks that appeared on inorganic materials are generally considered to be the atmospheric contaminant [159]. A previous study has reported absorbed carbon exerts negative effects on the wettability of modified Ti-6Al-4V surfaces [160].

The Ti 2p spectra provide information on the chemical state of titanium (Figure 15). Typically, the electron binding energies observed for Ti 2p3 peak are 458.1-459.2 eV ($TiO_2$ with chemical state 4+), 457.2-457.6 eV ($Ti_2O_3$ with chemical state 3+), 455.1-455.7 eV (TiO with chemical state 2+), 453.6-454.2 eV (metallic Ti with chemical state 0) [161, 162]. For these four groups, titanium peaks were only observed between 464.0-464.4 eV for Ti $2p_{1/2}$ and 458.1-458.5 Ti $2p_{3/2}$, which demonstrate that titanium mostly existed in the form of $TiO_2$.

The O 1s high resolution spectra featured asymmetric peak structures (Figure 16). The spectra could be peak-fitted into three subpeaks. The first one can be attributed to the O atoms in metallic oxide ($O^{2-}$) with a binding energy range of 529.9-530.8 eV. The second peak at a higher binding energy (531.9-532.1 eV) was assigned to bridging hydroxyl groups (acidic –OH). The last peak at the highest binding energy (533.3-533.7 eV) originated from hydrate and chemisorbed $H_2O$.

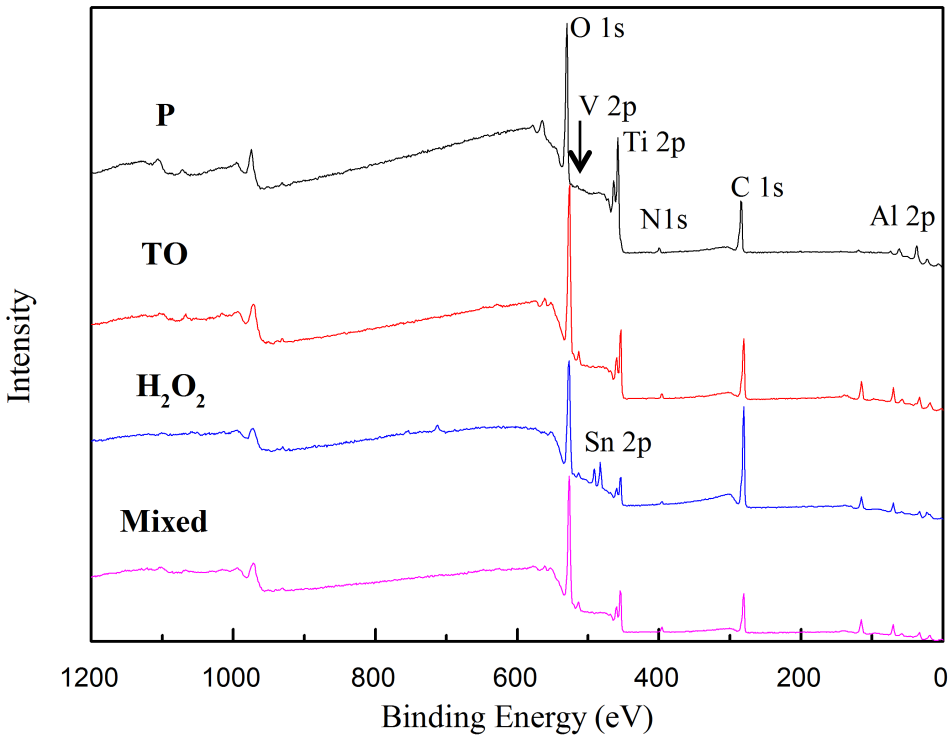


Figure 13. XPS survey spectra of Ti-6Al-4V samples after different treatments.

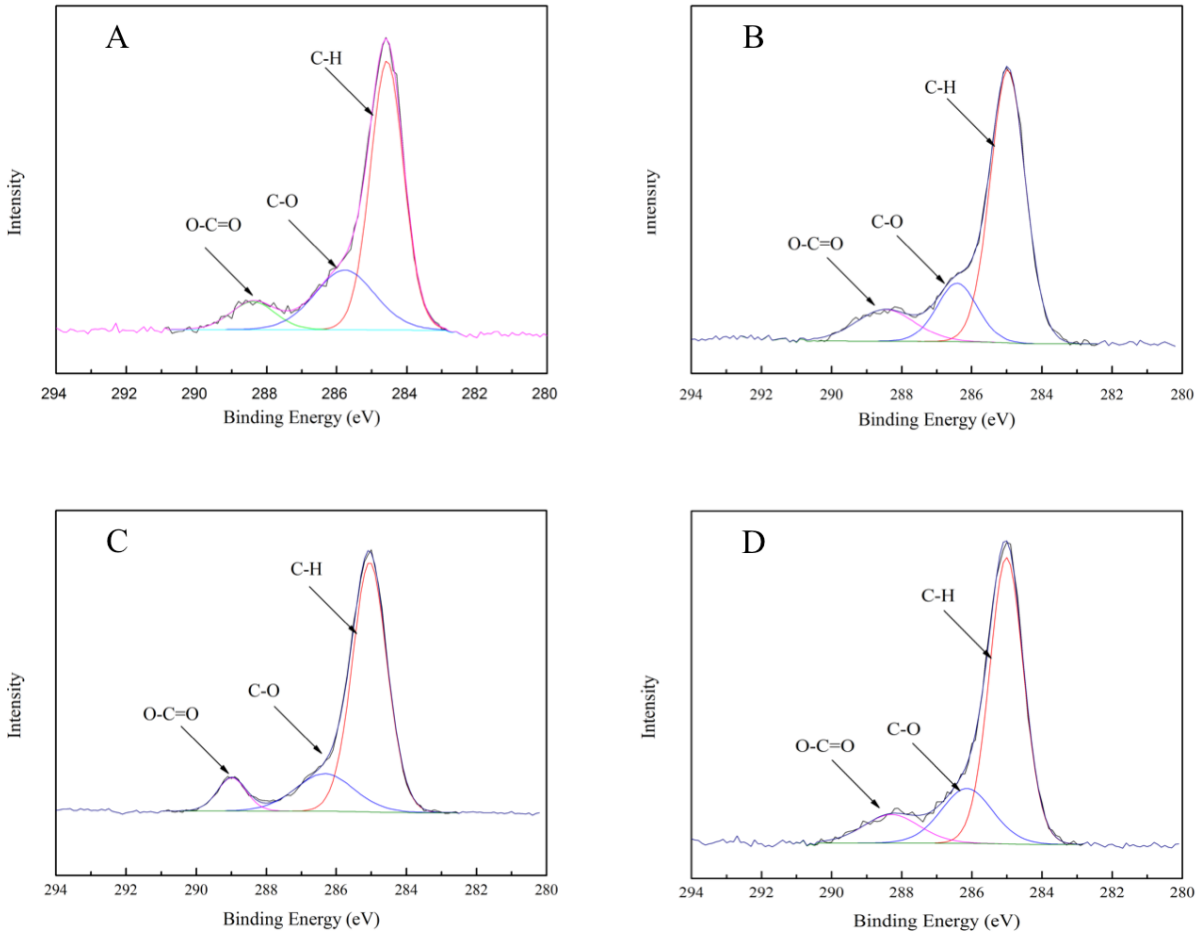


Figure 14. High resolution C 1s spectra of: (A) Polished, (B) TO, (C) $H_2O_2$ and (D) Mixed samples.

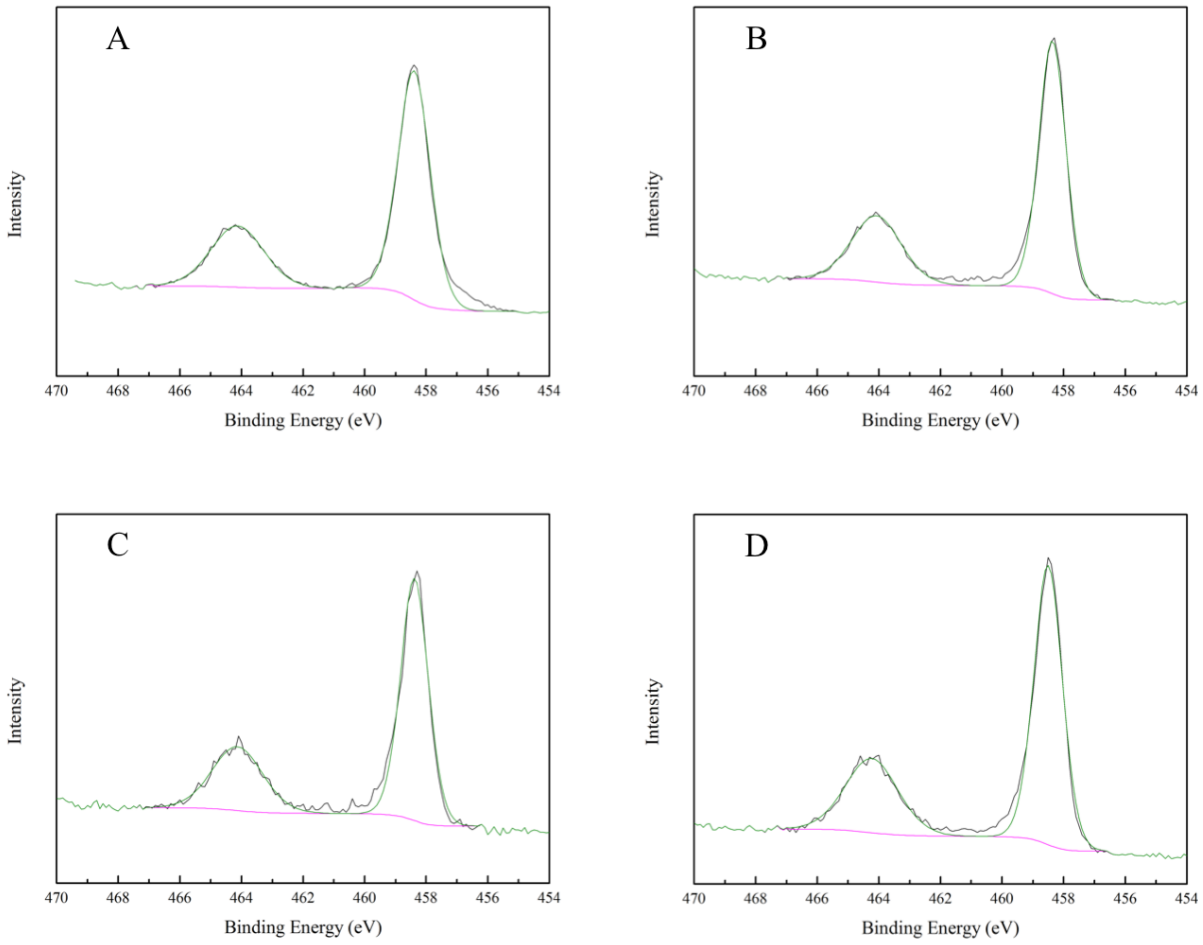


Figure 15. High resolution Ti 2p spectra of: (A) Polished, (B) TO, (C) $H_2O_2$ and (D) Mixed samples.

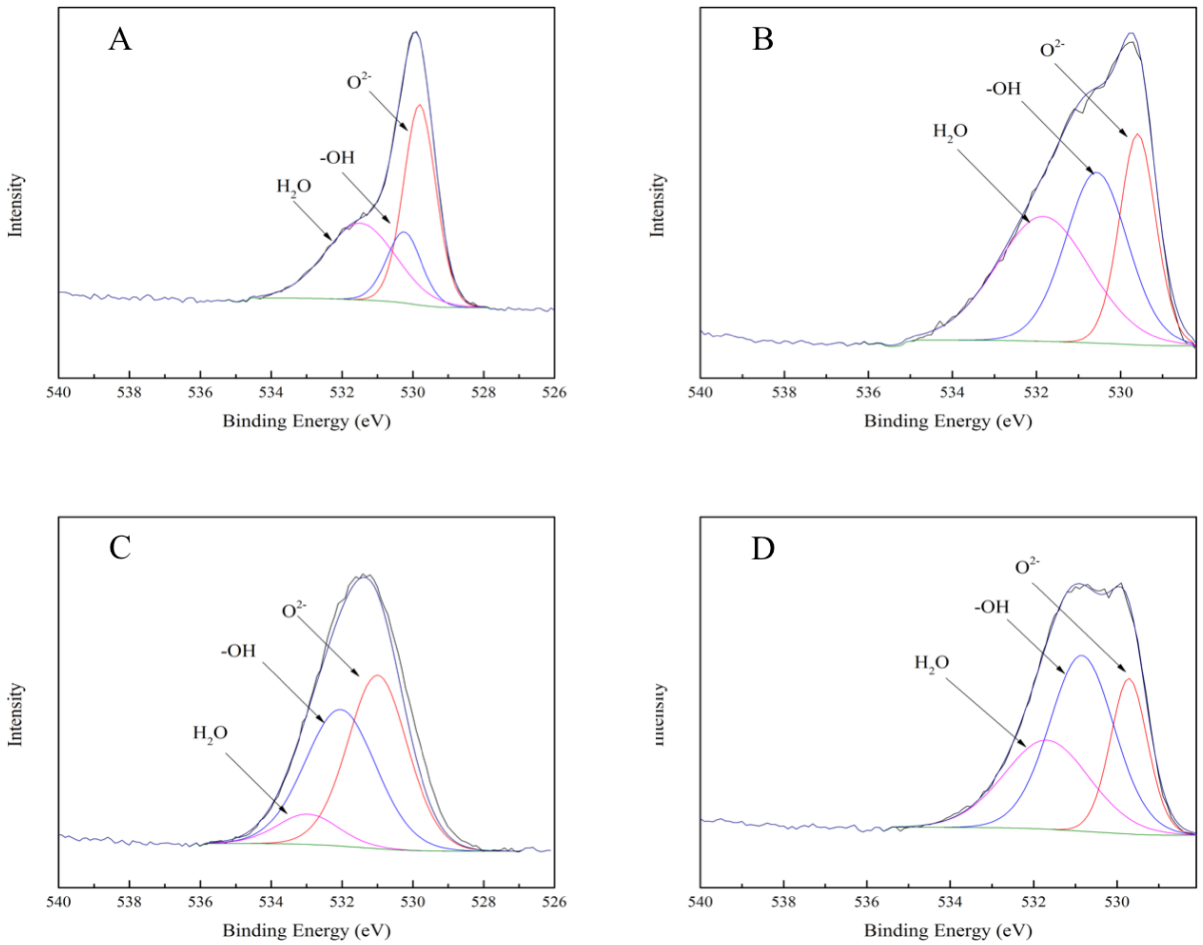


Figure 16. High resolution O 1s spectra of: (A) Polished, (B) TO, (C) $H_2O_2$ and (D) Mixed samples.

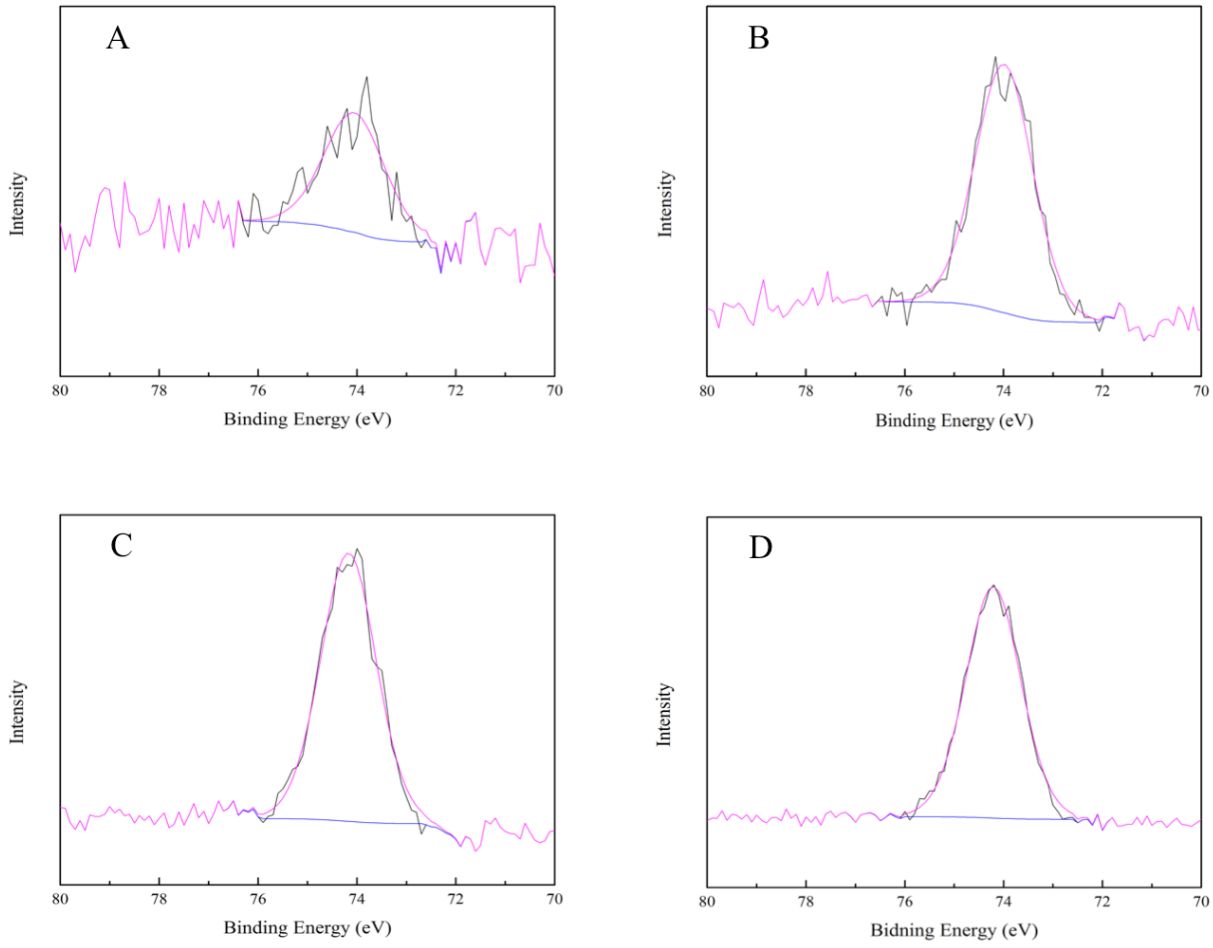


Figure 17. High resolution Al 2p spectra of: (A) Polished, (B) TO, (C) $H_2O_2$ and (D) Mixed samples.

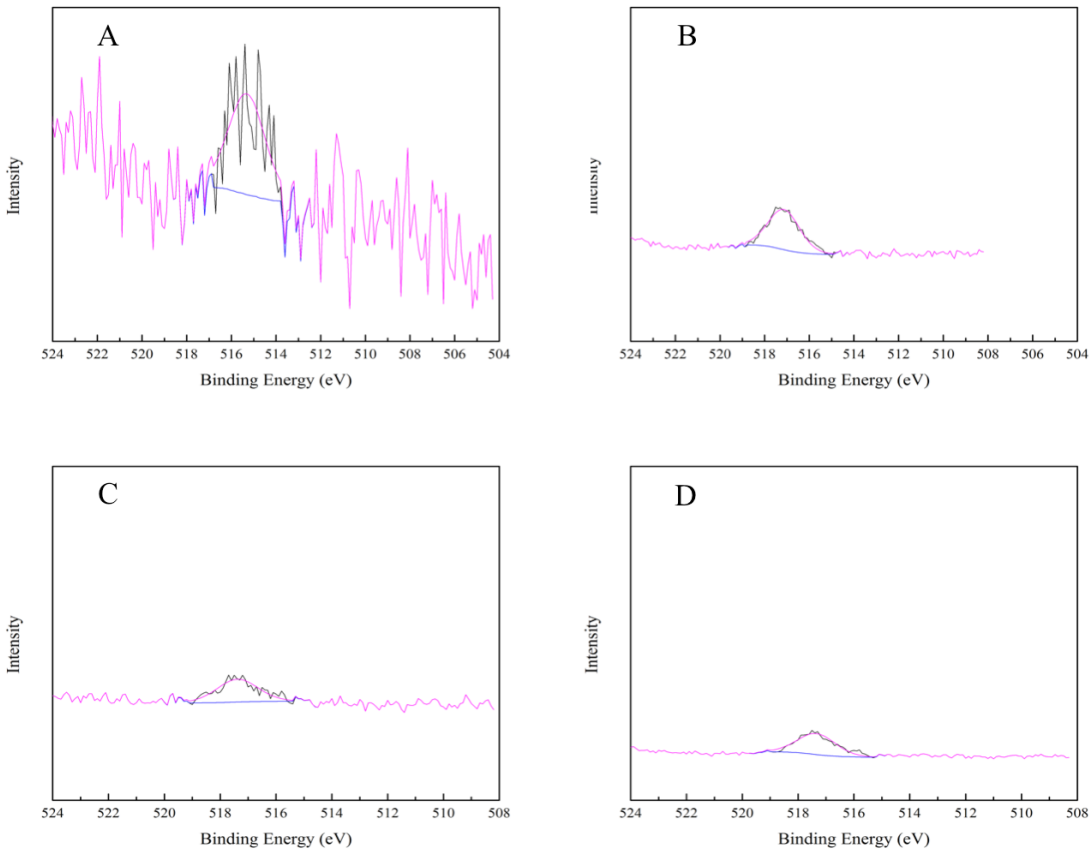


Figure 18. High resolution V 2p spectra of: (A) Polished, (B) TO, (C) $H_2O_2$ and (D) Mixed samples.

The chemical state of Al and V were also determined. The Al spectra indicate major peaks at 74.2-74.7 eV, which can be attributed to the $Al^{3+}$ in $Al_2O_3$ (Figure 17). The V spectrum of polished sample shows a major peak at the binding energy of 515.1 eV, which can be assigned to metallic V in Ti-6Al-4V alloy (Figure 18). An electron binding energy at about 517.2 eV appeared in the modified samples, which can be assigned to $V^{5+}$ in $V_2O_5$.

### 4.2.4 Surface Elemental Composition

Table 3 is a report on the atomic concentration of Ti, Al and V from Ti-6Al-4V samples after different treatments. C, N and O are not included because X-ray photoelectron spectrometry is used mainly as a qualitative analysis technique for light elements. Compared with polished Ti-6Al-4V, all the oxidized samples experienced a significant shift of the atomic concentration of Ti and Al. Meanwhile, the increased Al/Ti ratio in the oxidized Ti-6Al-4V samples clearly indicates that Al is thermodynamically more favorable than Ti. With consideration of the Al content, which has been previously reported to influence protein conformation by potentially exposing cellular binding domains and thus facilitating cell attachment in the oxide layers [163-165], it can therefore be inferred that the TO and Mixed sample groups are more favorable for further studies.

Table 3 Atomic composition of Ti-6Al-4V samples after different treatments.

| | Ti (%) | Al (%) | V (%) | Al/Ti | V/Ti |
|---|---|---|---|---|---|
| P | 78.75 | 19.92 | 1.33 | 0.25 | 0.02 |
| TO | 21.56 | 77.2 | 1.25 | 3.87 | 0.10 |
| $H_2O_2$ | 44.73 | 54.11 | 1.16 | 1.21 | 0.03 |
| Mixed | 20.23 | 78.35 | 1.42 | 3.53 | 0.07 |

### 4.2.5 Surface Hydroxyl Group Concentration

Surface hydroxyl groups are very important in the adsorption of proteins and adherence of polymers [54, 166]. However, the hydroxyl group that directly read from O 1s spectra has been found inaccurate since it contains the oxygen-containing components from C-O and O-C=O in the outmost layer [159]. The oxygen double bond in the carboxyl group yields an O 1s peak around 531 eV, which is close to the OH peak in the O 1s spectra (529.9-530.8 eV in current study). The single oxygen bond in the ester groups or carboxyl groups yields an O 1s peak at about 533 eV, which is at the approximate location of the chemisorbed $H_2O$ peak in O 1s (533.3-533.7 eV in this study). The measured intensity of the OH subpeak (I(OH)meas) thus contains the contribution from oxygen in C-O and O-C=O groups that reside in the organic carbon contamination layer. The contribution from C-O is given by [159, 167]:

$$I(C-O) = x(C-O)\left(\frac{atom\%\ C}{atom\%\ O}\right) I(OH)meas$$

where x(C-O) is the atomic fraction of the C-O group in the C 1s spectrum,

$$x(C-O) = \frac{I(C-O)}{I(C-H) + I(C-O) + I(O-C=O)}$$

$I(C-H)$, $I\ (C-O)$ and $I\ (O-C=O)$ can be directly read from deconvoluted C peaks. Similarly, the portion of $O-C=O$ in the O 1s peak is,

$$I(O-C=O) = x(O-C=O)\left(\frac{atom\%\ C}{atom\%\ O}\right) I(OH)meas$$

where

$$x(O-C=O) = \frac{I(0-C=O)}{I(C-H) + I(C-O)\ + I(O-C=O)}$$

Then, the corrected intensity of OH peak is

$$I(OH) = I(OH)meas - I(C-O) - I(O-C=O)$$

Finally, the relative surface hydroxyl concentration can be obtained by multiplying the corrected OH intensity with the O atomic concentration. As shown in Figure 19, the sample treated by TO yields the highest surface hydroxyl group concentration, followed by that of the $H_2O_2$, Mixed and polished samples. Interestingly, this is almost the same rank as the surface wettability shown in Section 4.2.2. This result further reveals that TO, $H_2O_2$ and Mixed treatment can improve the surface wettability of polished Ti-6Al-4V by producing higher concentration of surface hydroxyl groups, which have been demonstrated to enhance protein adsorption and cell adhesion [54]. Therefore, the TO sample is favored over $H_2O_2$ and Mixed samples.

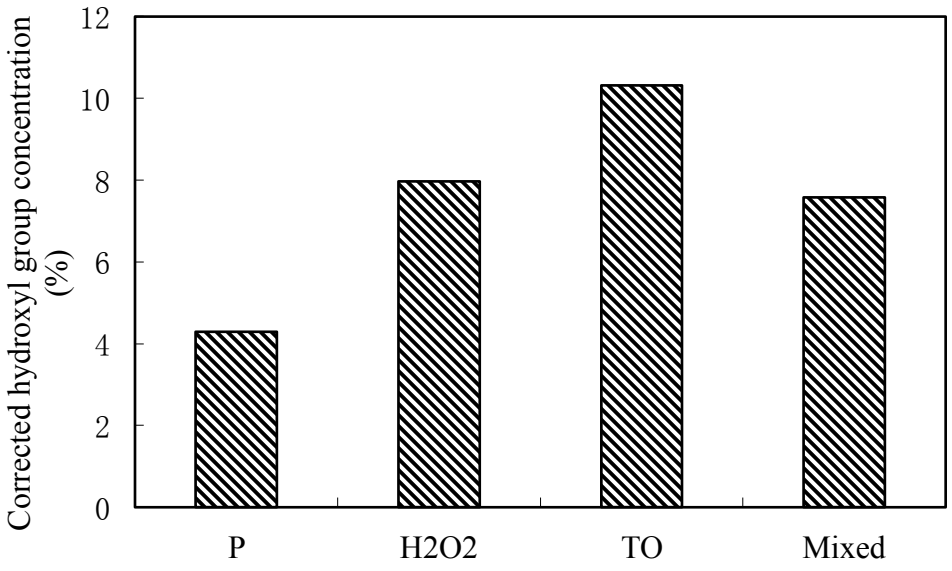


Figure 19. Corrected surface hydroxyl group concentration of Ti-6Al-4V samples after different treatments.

### 4.2.6 Summary

Both TO and $H_2O_2$ treatment can induce striking features onto a Ti-6Al-4V surface. The scanning electron and atomic force microscopy characterizations reveal that the TO sample exhibits the greatest surface roughness and oxide layer thickness by the formation of nano- and micron- scale oxide particles; $H_2O_2$ treatment produces a porous surface that exhibits lowest oxide layer thickness and surface roughness; the Mixed treatment on Ti-6Al-4V results in sharp crests and pits on the surface, which contribute to moderate roughness and oxide layer thickness. The X-ray photoelectron spectroscopy analysis shows that the Ti-6Al-4V surface is mainly composed of $TiO_2$, $Al_2O_3$ and minor $V_2O_5$. Meanwhile, higher hydroxyl group concentration are formed on the TO sample, followed by the $H_2O_2$, Mixed and polished samples. The water contact angle test shows a similar trend of wettability as that of hydroxyl group concentration. Taken together, it can be concluded that the thermally oxidized Ti-6Al-4V has the most promising surface properties as it exhibits the roughest surface with a compact and thick oxide layer, favorable elemental composition, highest surface hydroxyl group concentration and wettability. Therefore, the thermally oxidized Ti-6Al-4V sample is selected for the construction of alginate/chitosan LBL films.

## 4.3 Construction of Ultrathin Film on Rough Ti-6Al-4V Surface for Enhanced Osseointegration and Antibacterial Capability

### 4.3.1 Characterization of the Alginate/Chitosan LBL Film Construction Process

This part reports the construction process of alginate/chitosan LBL film on the thermally oxidized Ti-6Al-4V sample. The water contact angle measurement was first carried out to monitor the variation of wettability during the alginate/chitosan LBL film construction process (Figure 20). An alternative change in the water contact angle was observed after the assembly of each alginate and chitosan single layer. This phenomenon is consistent with previous study and indicates that the samples had been fully covered by alginate/chitosan as the outmost layer [168]. Interestingly, J. Park et al. observed and speculated that the incomplete coverage of chitosan, PGA and PLL monolayers on titanium surface is due to the 0.15 M NaCl used to dissolve these polyelectrolytes, which results in the preferential attachment of $Na^+$ onto the negatively charged Ti surface [169]. However, this phenomenon is not observed in this study. It can be attributed to the mussel-inspired dopamine used prior to alginate/chitosan LBL self-assembly. The strong adhesive properties of the PDA precursor ensured the uniform deposition of first alginate layer, which subsequently results in a compact and even build-up of alginate/chitosan LBL films.

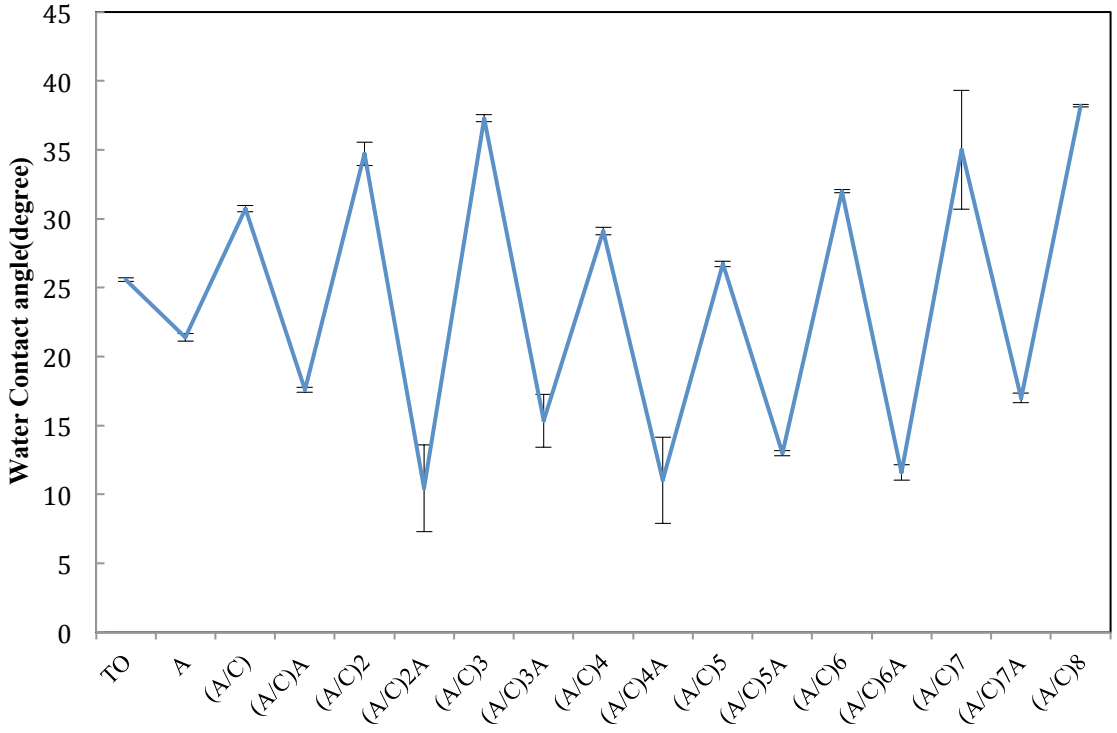


Figure 20. Water contact angle measurement during the alginate/chitosan LBL film construction process (A: alginate; C: chitosan).

A XPS was used to investigate the surface chemistry change during the alginate/chitosan LBL assembly process. All of the spectra obtained indicate the major elements of Ti, Al, Na, Cl, C, N and O (Figure 21). The presence of Na and Cl can be attributed to the 0.14 M NaCl solution used during the preparation of chitosan and alginate polyelectrolytes. The intensity of Ti 2p and Al 2p decreased as the numbers of alginate/chitosan pair increased. The N 1s high resolution spectra (Figure 22) demonstrated the presence of amide and protonated amine groups at binding energies about 398.1 and 401.3 eV, with respect to the use of chitosan [168]. Meanwhile, the gradual increase in the intensity of protonated amine group implies that there was a sustained deposition of alginate/chitosan pairs onto the TO sample. Taken together, the X-ray spectrometry analysis further confirms the layerwise buildup of alginate/chitosan onto the thermally oxidized Ti-6Al-4V surface.

AFM was employed to monitor the surface roughness and topography changes during the alginate/chitosan LBL film construction process. Figure 23 shows that the initial layerwise build-up does not alter the surface topography produced by TO. However, the original oxide particles became larger in TO/$(A/C)_6$ to TO/$(A/C)_{10}$ samples. This phenomenon clearly indicates that the surface topography induced by TO has been altered after six pairs of alginate/chitosan LBL assembly. The topography change was further quantified by roughness measurement. As shown in Figure 24, in TO/(A/C) to

TO/$(A/C)_6$ samples, the roughness values appear to be stable around 80 nm. However, the surface roughness increased to 120.03 ± 22.21 nm on TO/$(A/C)_6$ sample, and finally reaches a value of 211.50 ± 22.95 nm on TO/$(A/C)_{10}$ sample. It is possible that the agglomerated oxide particles were preferentially attacked and encapsulated by alginate/chitosan films, which lead to the increment of the oxide particles' volume. Consequently, the average distance between peaks and valleys were raised, thus giving rise to the larger roughness values.

Accordingly, it is demonstrated that the five pairs of alginate/chitosan are able to fully cover the thermally oxidized Ti-6Al-4V surface, but not significantly alter its surface roughness and topography. Further studies are, therefore, centered on the TO/$(A/C)_5$ sample. In addition, polished, TO and P/$(A/C)_5$ samples were also fabricated and set as control groups to test the hypothesis that the topography produced by TO and the surface chemistry derived from alginate/chitosan LBL film can synergically enhance BMSCs activities. For example, the *in vitro* effect of surface chemistry can be investigated through comparison between P and P/$(A/C)_5$, TO and TO/$(A/C)_5$, which exhibit identical surface topography. In contrast, the effect of surface topography can be evaluated through comparison between the P/$(A/C)_5$ and TO/$(A/C)_5$. Meanwhile, the P and TO samples were not employed to study the effect of surface topography because they exhibit both the different surface chemistry and topography.

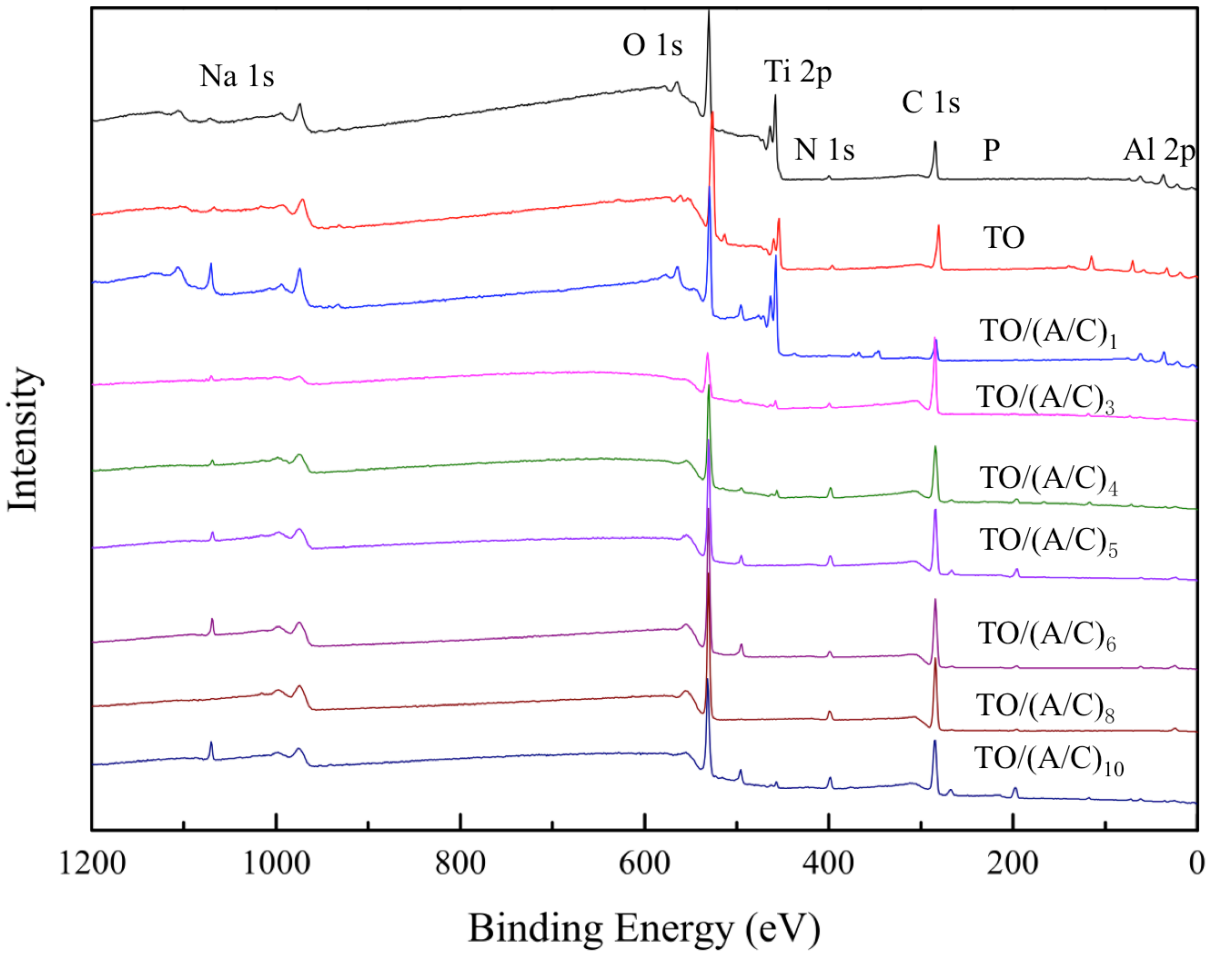


Figure 21. XPS wide scan of Ti-6Al-4V samples after different treatments (A: alginate; C: chitosan).

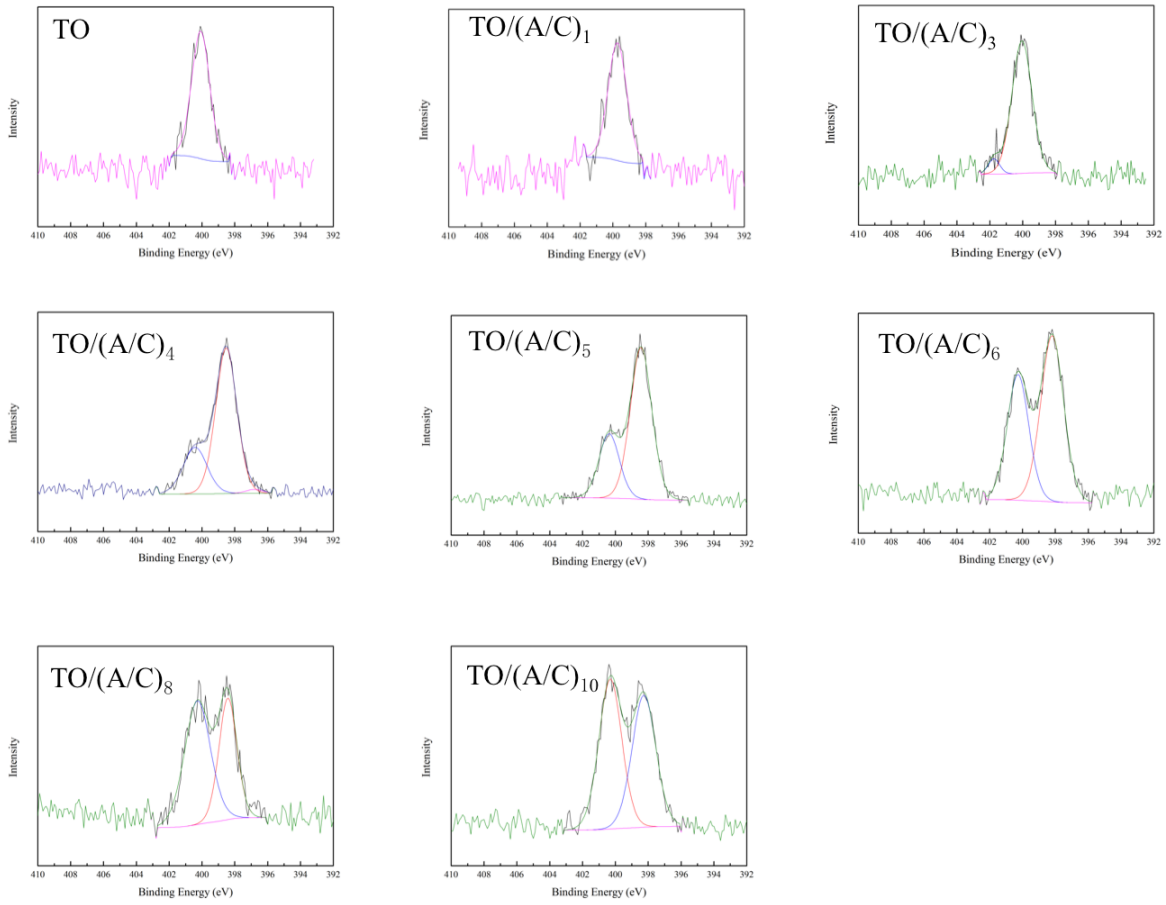


Figure 22. N 1s high resolution scans of Ti-6Al-4V samples after different treatments (A: alginate; C: chitosan).

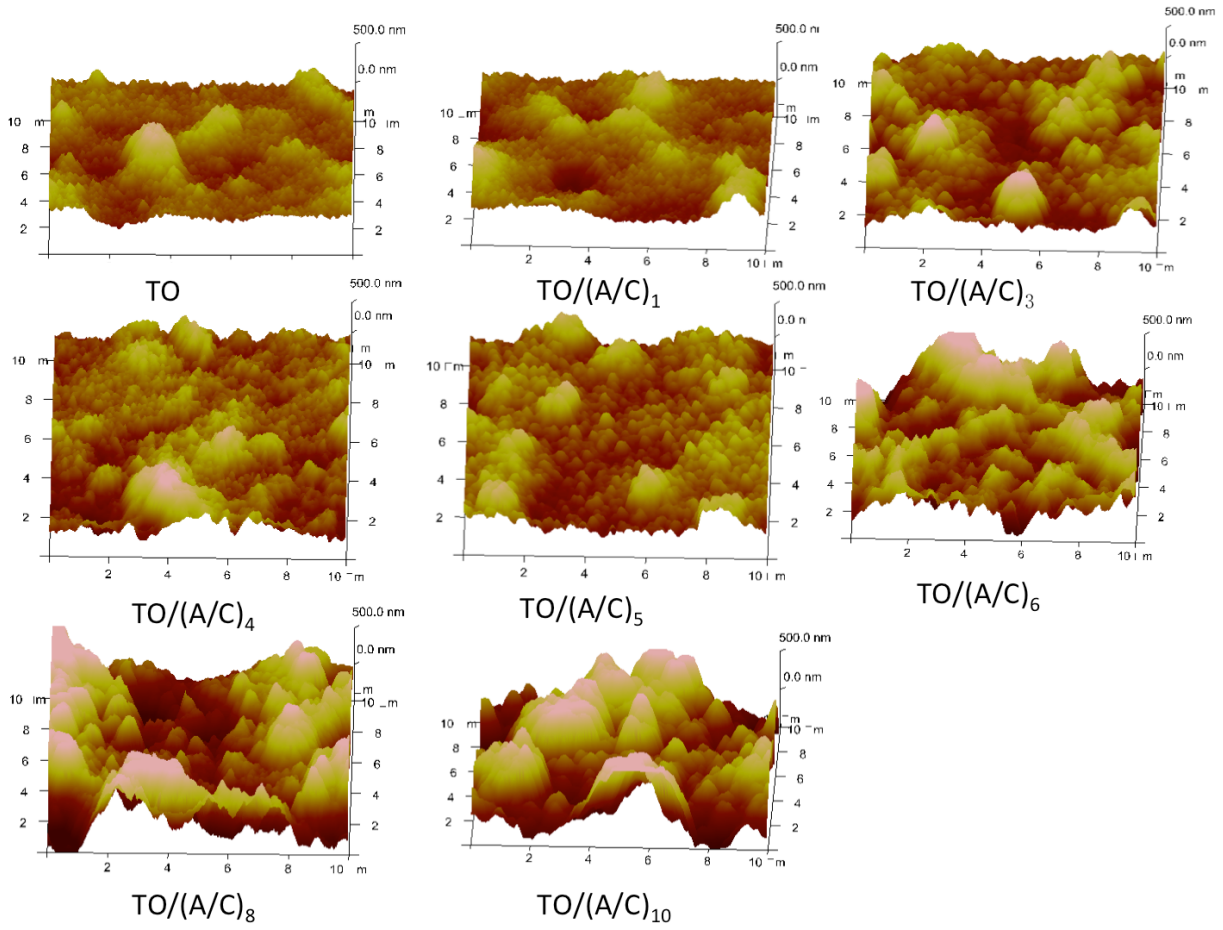


Figure 23. Surface topography change of thermally oxidized Ti-6Al-4V samples during alginate/chitosan LBL film build-up process (A: alginate; C: chitosan. AFM scan area: 10 x 10 $\mu m^2$, z-axis height: 500 nm).

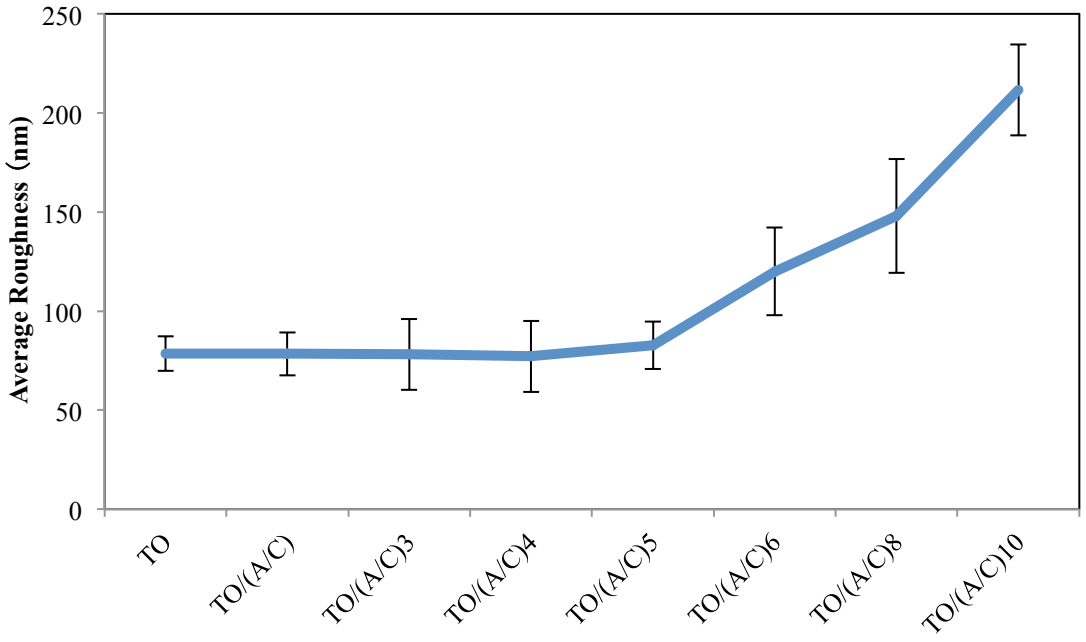


Figure 24. Surface roughness measurement of thermally oxidized Ti-6Al-4V samples with different number of alginate/chitosan pairs (A: alginate; C: chitosan).

### 4.3.2 Characterization of LBL-modified Ti-6Al-4V Surfaces

In this section, SEM and EDS were employed to confirm that whether nano-silver is successfully incorporated into the TO/$(A/C)_5$ sample. Meanwhile, characterizations of surface topography and roughness on the P, TO, P/$(A/C)_5$, TO/$(A/C)_5$ and TO/$(A/C)_5$/Ag samples are also presented as a prerequisite for investigating the role of surface topography and chemistry *in vitro*.

Scanning electron and atomic force microscopy techniques were used to observe the topography and roughness of the modified Ti-6Al-4V samples (Figure 25). The polished and P/$(A/C)_5$ samples were comparatively flat, accompanied by some polishing scratches (Figure 25A&C). The sample treated by TO is covered with single and agglomerated oxide particles (Figure 25B). The TO/$(A/C)_5$ sample is comparable to the TO sample (Figure 25D). On the TO/$(A/C)_5$/Ag sample, additional nano-scale shinny particles can be observed (Figure 25E). The EDS examination demonstrates these white shiny particles appear to be Ag (Figure 26). Roughness measurement by AFM further revealed that the polished and P/$(A/C)_5$ samples showed roughness values of 1.94 and 2.32 nm. The TO, TO/$(A/C)_5$ and TO/$(A/C)_5$/Ag samples exhibited similar roughness values of 78.55, 82.56 and 83.64 nm.

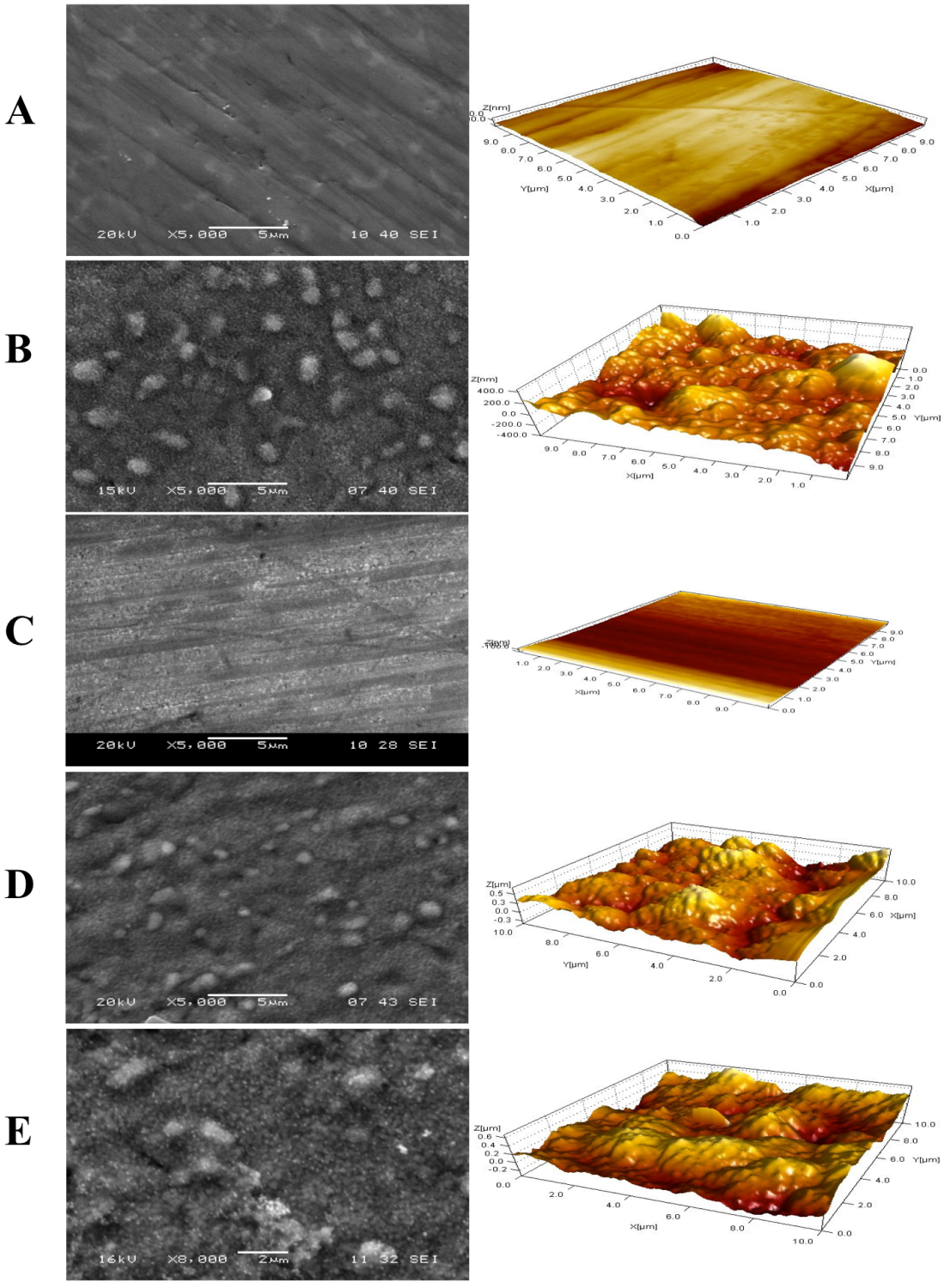


Figure 25. Surface topography of Ti-6Al-4V samples modified by: (A) P, (B) TO, (C) $P/(A/C)_5$, (D) $TO/(A/C)_5$, (E) $TO/(A/C)_5/Ag$ (AFM scan area: 10 x 10 $\mu m^2$).

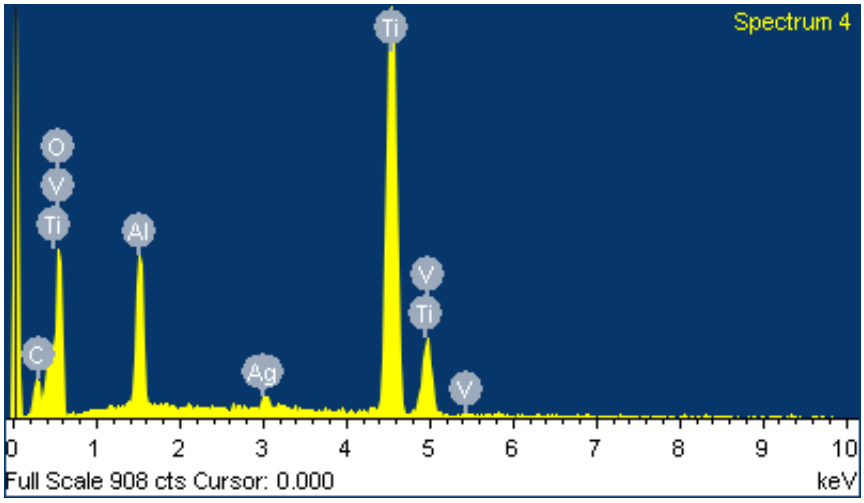


Figure 26. Energy-dispersive spectroscopy analysis of TO/$(A/C)_5$/Ag sample.

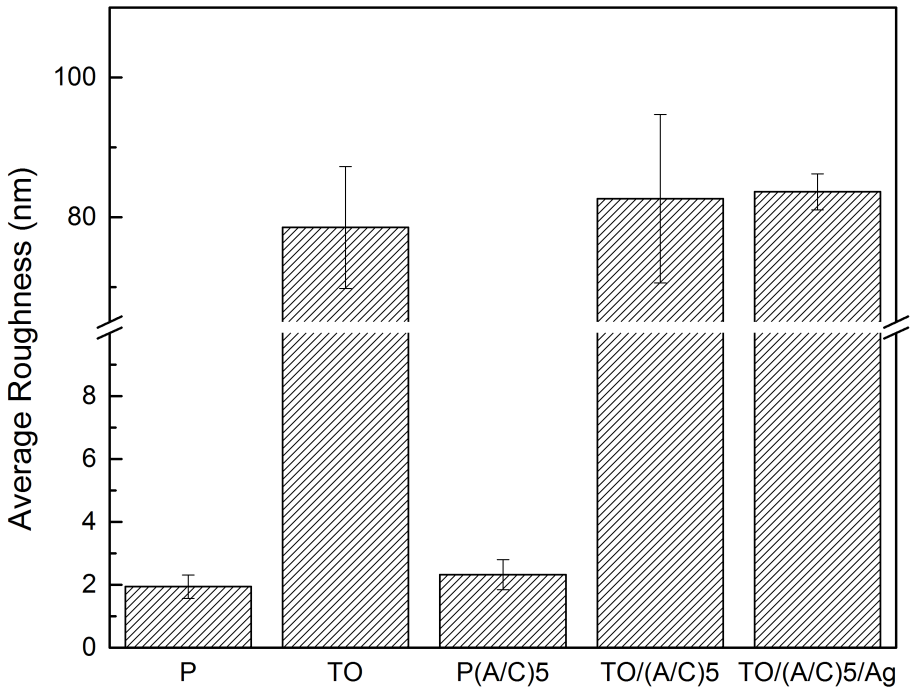


Figure 27. Surface roughness measurement of Ti-6Al-4V samples after different treatments.

### 4.3.3 *In Vitro* Evaluation

#### 4.3.3.1 *In Vitro* Stability of Alginate/Chitosan LBL Film

To test the in vitro stability of the LBLed Ti-6Al-4V samples, the P/$(A/C)_5$, TO/$(A/C)_5$ and TO/$(A/C)_5$/Ag samples were immersed into a PBS for 0, 2, 4 and 8 days. The wettability changes were tested at each time interval. As shown in Figure 28, the water contact angle measurement shows the wettability of all samples was slightly increased on day 2, and then remained almost constant until day 8. The increment on day 2 was possibly caused by the partial hydration of chitosan when these samples were initially immersed into the PBS. Taken together, these data indicate that the LBL films constructed onto the TO samples are physiologically stable.

#### 4.3.3.2 Antibacterial Test

An agar diffusion test was conducted on *E. coli* and *S. aureus* to test the antibacterial ability of the modified Ti-6Al-4V samples (Figure 29). No zone of inhibition can be observed around the polished, TO, P/$(A/C)_5$ and TO/$(A/C)_5$ samples, which indicates their susceptibility to infection. However, the TO/$(A/C)_5$/Ag sample can significantly inhibit *E. coli* and *S. aureus* activities, thus demonstrating the successful releasing of nano-silver from the TO/$(A/C)_5$/Ag sample.

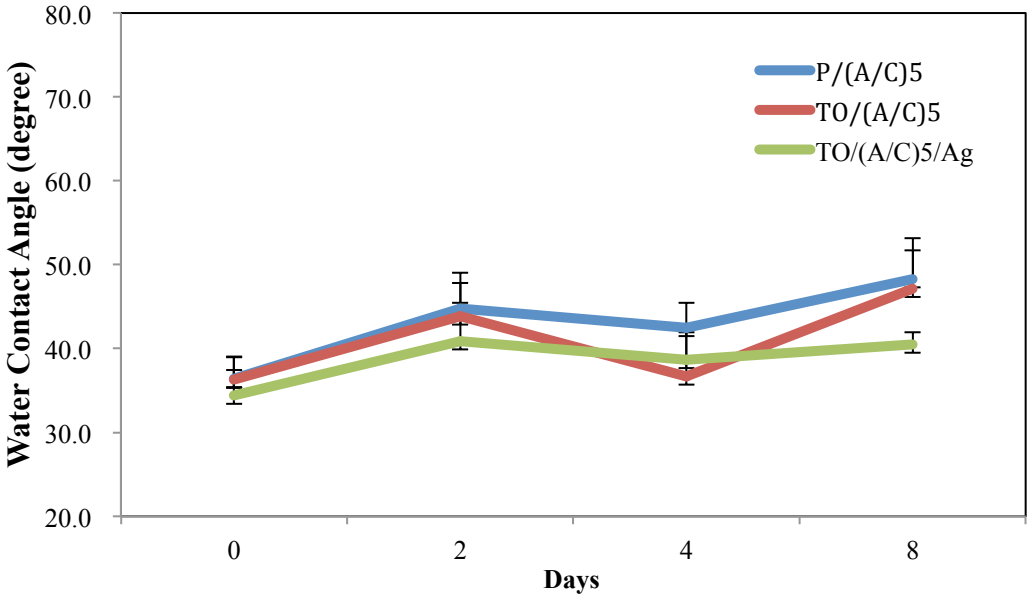


Figure 28. Stability of LBLed Ti-6Al-4V samples under PBS.

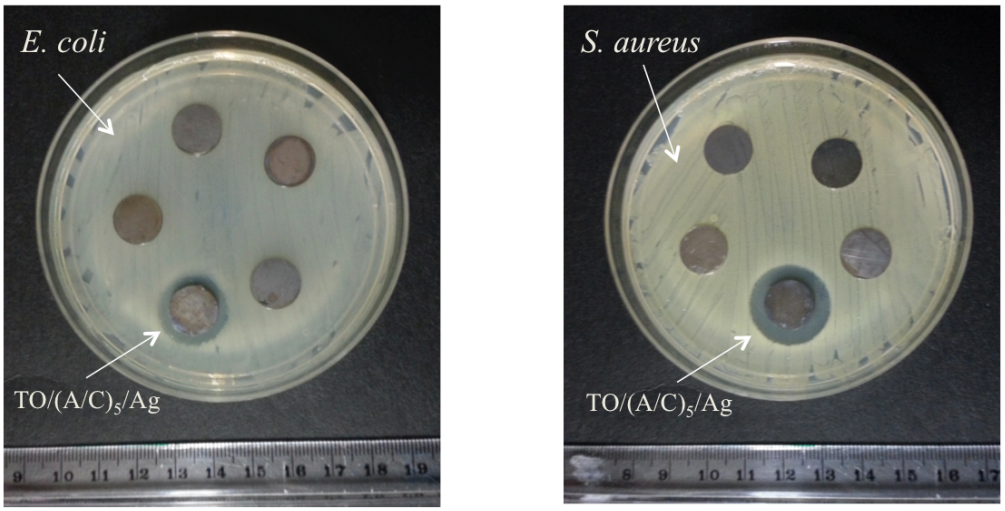


Figure 29. Antibacterial test of Ti-6Al-4V samples after different treatments. (Left: *E. coli*, and right: *S. aureus*).

#### 4.3.3.3 Cell Viability and Morphology

Figure 30 shows the florescent and scanning electron microscopies images of BMSCs adhered onto different Ti-6Al-4V samples. The BMSCs exhibited significant percentage of live cells (green) than dead cells (red) and early phase of adhesion on both the five samples. This phenomenon demonstrates that all the samples are safe and suitable for the growth of BMSCs. Meanwhile, BMSCs exhibited higher cell numbers and more stretched morphologies on TO/$(A/C)_5$ and TO/$(A/C)_5$/Ag samples than that of P, TO and P/$(A/C)_5$ samples. This result indicates that the combination of TO and alginate/chitosan LBL film on Ti-6Al-4V surface contributes to the growth and attachment of BMSC. Meanwhile, the BMSCs cultured on TO/$(A/C)_5$/Ag sample showed less favorable viability and morphology than those cultured on TO/$(A/C)_5$ sample. This phenomenon implies that nano-silver may exhibit slight cytotoxicity. However, this result is acceptable since the BMSCs seeded on the TO/$(A/C)_5$/Ag sample also showed superior viability and morphology than those on P, TO, and P/$(A/C)_5$ samples.

To further understand the derivation the robust BMSC behavior on TO/$(A/C)_5$ and TO/$(A/C)_5$/Ag samples, the role of implant surface chemistry and topography was separately investigated. The role of surface chemistry was studied through comparisons between the samples of P/$(A/C)_5$ and P, TO/$(A/C)_5$ and TO. BMSCs cultured on the P/$(A/C)_5$ and TO/$(A/C)_5$ surfaces showed higher cell numbers and stretched

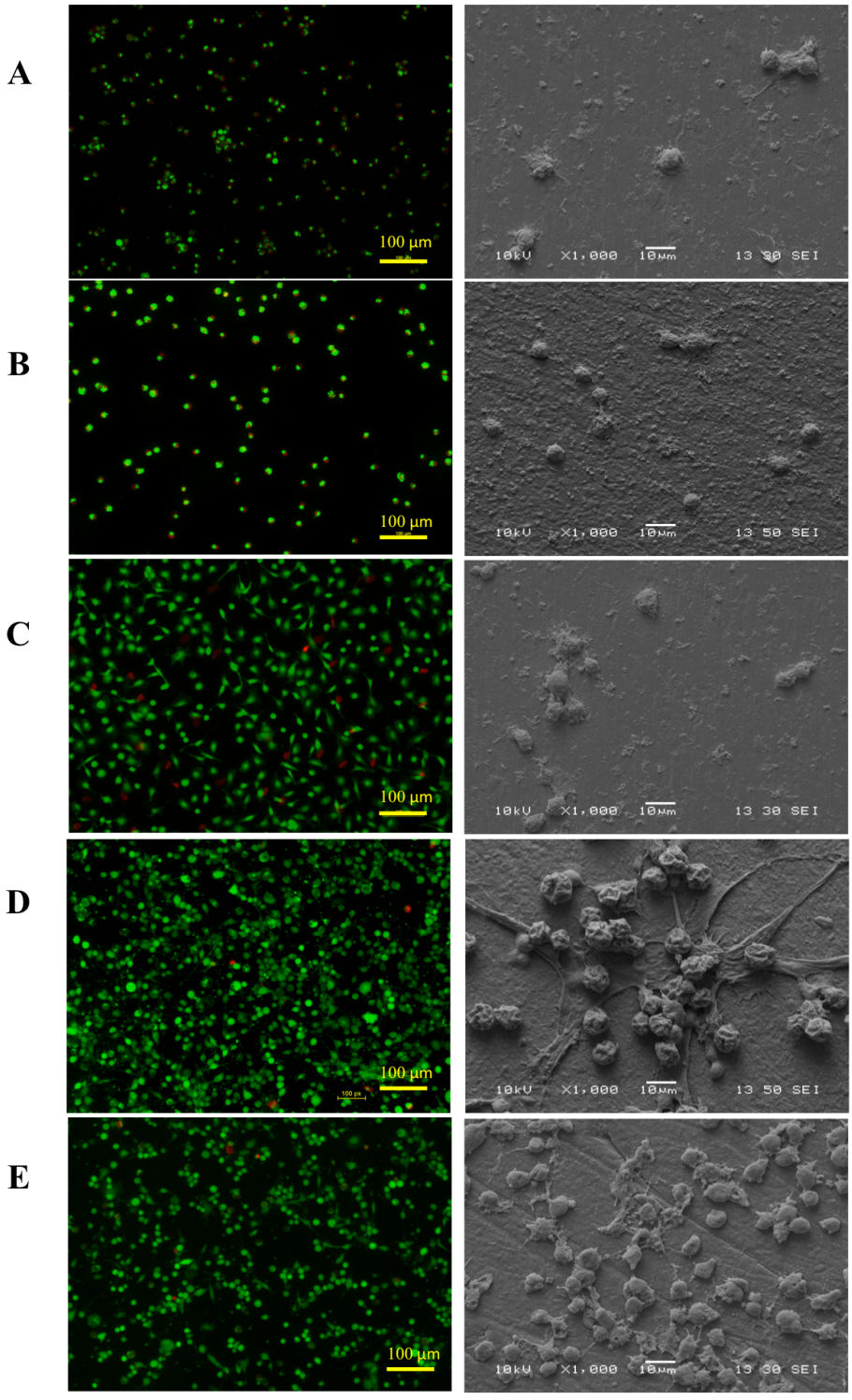


Figure 30. Live & dead fluorescence and SEM images of BMSCs adhered on (A) P, (B) TO, (C) P/$(A/C)_5$, (D) TO/$(A/C)_5$ and (E) TO/$(A/C)_5$/Ag samples, respectively.

morphologies, while BMSCs cultured on P and TO samples were the opposite. This result indicates that the alginate/chitosan film can provide a robust extracellular microenvironment for the growth and attachment of BMSC. In view of the surface topography, BMSCs behaviors on the P/$(A/C)_5$ and TO/$(A/C)_5$ samples were compared. BMSCs cultured on the TO/$(A/C)_5$ sample exhibited greater cell numbers and stretched morphologies, thus demonstrating surface topography is also a key factor for BMSC viability and morphology. Taken together, it can be demonstrated that the high viability and advanced morphology of BMSCs seeded on TO/$(A/C)_5$ sample is derived from the synergy of TO and alginate/chitosan LBL film.

#### 4.3.3.4 Cell Proliferation

An MTT assay was conducted to evaluate the proliferation levels of BMSCs that seeded on different Ti-6Al-4V samples (Figure 31). BMSCs seeded on TO/$(A/C)_5$ and TO/$(A/C)_5$/Ag samples exhibited significantly higher levels of proliferation than those on P, TO and P/$(A/C)_5$ samples at both 3 and 7 days of culturing ($p<0.05$). This result indicates that the combination of TO and alginate/chitosan LBL film build-up on Ti-6Al-4V surface can significantly improve the levels of BMSC proliferation. Meanwhile, it is worth noting that BMSCs seeded on TO/$(A/C)_5$/Ag sample showed comparable levels of proliferation to TO/$(A/C)_5$ sample at days 3 and 7. This phenomenon implies that the nano-silver particles do not jeopardize the improved BMSC

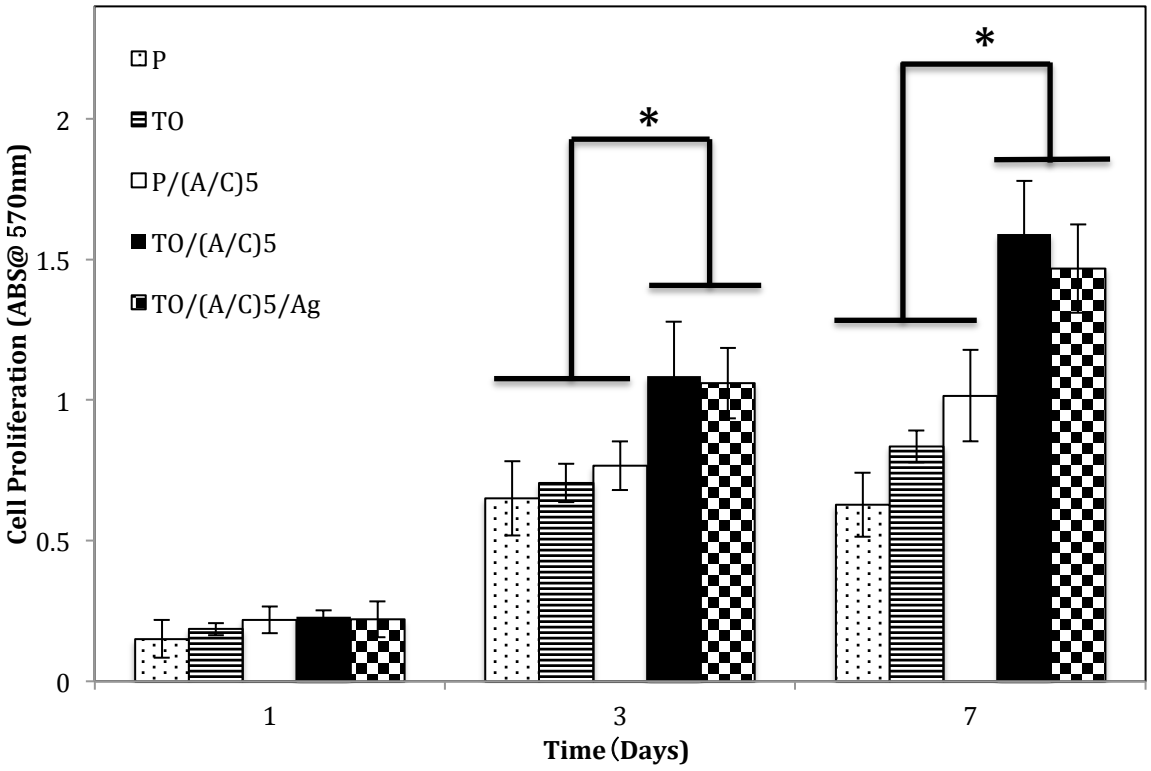


Figure 31. MTT assay. Formosan absorbance expressed as a measure of cell proliferation from BMSCs cultured on different samples (n=4).

proliferation induced by TO and the LBL approach. The slightly lower levels of BMSC proliferation on TO/$(A/C)_5$/Ag as opposed to TO/$(A/C)_5$ sample can be attributed to the potential cytotoxicity of nano-silver.

The role of surface chemistry and topography on BMSC proliferation was further studied. In terms of surface chemistry, BMSCs seeded on P$(A/C)_5$ sample showed significantly higher levels of proliferation than those on P sample at days 3 and 7 ($p<0.05$); same result has also been found between TO/$(A/C)_5$ and TO samples. This phenomenon indicates that alginate/chitosan LBL film is able to provide a robust extracellular microenvironment for BMSC proliferation. In case of surface topography, BMSCs cultured on TO/$(A/C)_5$ sample exhibited consistently higher levels of proliferation than P/$(A/C)_5$ sample at 3 and 7 days of culturing, respectively. Significant differences can be observed at day 3 and day 7 ($p<0.05$). Since surface topography is the only difference between P/$(A/C)_5$ and TO/$(A/C)_5$ samples, it can be therefore postulated that the sub-micron topography produced by TO is able to promote BMSC proliferation. This is consistent with previous studies, which also emphasized the importance of sub-micron topography on cell proliferation [17, 76]. However, these studies only considered the different topography between thermally oxidized and polished titanium, but neglected their differences in surface composition and wettability. Therefore, the present study yields a more convincing demonstration of the effect of sub-micron topography on

BMSC proliferation.

#### 4.3.3.5 Cell Differentiation

The mRNA expressions of BMSCs-related genes on TO/$(A/C)_5$/Ag sample were tested to investigate cell differentiation at the molecular level (Figure 32). The ALP, COL I, OPN and BSP were characterized by q-RT-PCR analysis at 2 and 7 days of BMSCs culturing. ALP, an early marker of differentiated BMSCs, was significantly increased at 7 days' culturing. COL I, the main content of bone ECM, was up-regulated at 2 days (4.29-fold) and 7 days (5.33-fold) of culturing. The other significant component of the bone ECM, BSP, was also up-regulated 1.4-fold and 4.03-fold at 2 and 7 days of culturing, respectively. However, the expression of OPN, a non-collagenous protein that binds to hydroxyapatite in ECM, decreased at 7 days of culturing (3.66-fold) when compared with that at 2 days (4.42-fold). In summary, the up-regulated expressions of ALP, COL I and BSP demonstrate that the TO/$(A/C)_5$/Ag sample is capable of inducing the osteogenic differentiation of BMSC.

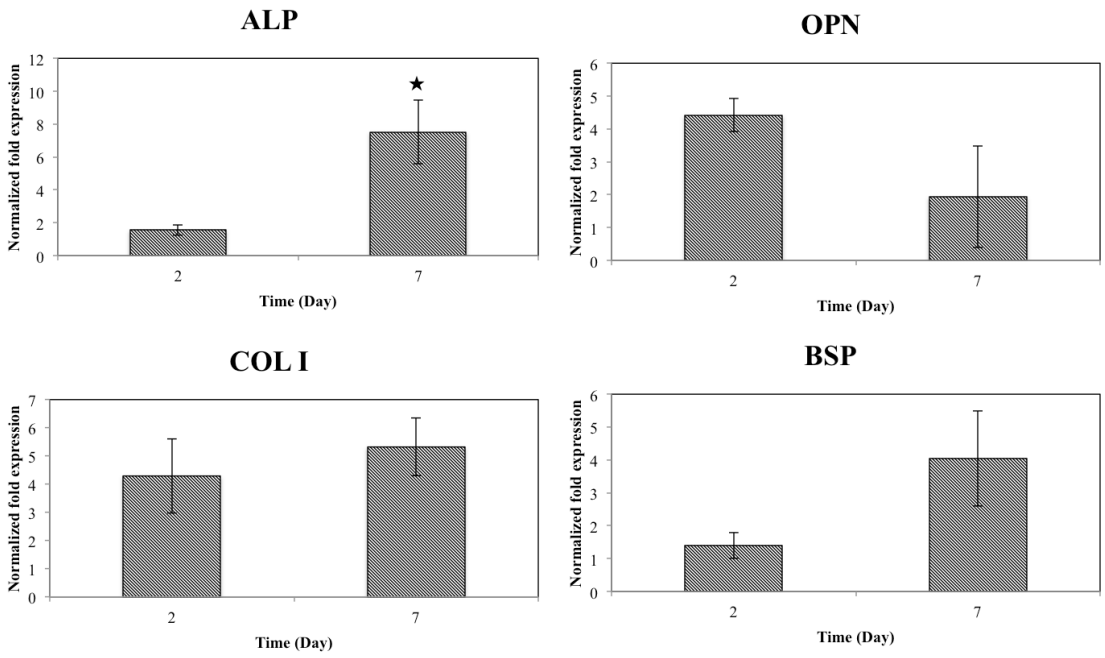


Figure 32. Relative mRNA expressions on TO/(A/C)5/Ag samples (n=3): (A) ALP, (B) BSP, (C) COL I, and (D) OPN.

### 4.3.4 Summary

In this project, the alginate/chitosan LBL films that incorporate nano-silver particles were successfully constructed on thermally oxidized Ti-6Al-4V surface. The alginate/chitosan LBL film completely altered the surface chemistry of Ti-6Al-4V surface while the sub-micron topography induced by TO did not change. Improvements in the BMSC viability, morphology, proliferation and demonstrated antibacterial capability have been observed *in vitro*. Increased ALP, Col I and BSP expression levels on TO/$(A/C)_5$/Ag samples indicate that BMSC differentiation is also positively stimulated by this architectural hybrid system. In summary, the hybrid structure is very effective to improve the osseointegration and anti-infection capability of thermally oxidized Ti-6Al-4V.

# Chapter 5

## Summary and Conclusions

The major findings and conclusions in this dissertation are summarized as follows,

1. TO can induce better surface roughness, thicker oxide layer, better wettability and higher surface hydroxyl group density on Ti-6Al-4V alloy than treatment with $H_2O_2$ and a mix of TO & $H_2O_2$.

2. An alternative change of water contact angle can be observed upon the deposition of alginate and chitosan on the thermally oxidized Ti-6Al-4V surfaces. This phenomenon is consistent with previous study and demonstrates the alginate/chitosan LBL self-assembly is successful on the thermally oxidized Ti-6Al-4V surfaces.

3. Alginate/chitosan LBL film does not alter the surface topography and roughness induced by TO until six alginate/chitosan pairs are deposited.

4. XPS spectra indicate a gradual increase of N 1s intensity during the alginate/chitosan LBL film construction process. High resolution scans indicate the increased N 1s intensity relates to the protoned amine group from chitosan.

5. The TO/$(A/C)_5$ sample can significantly improve the BMSC viability and

proliferation when compared with TO after 3 and 7 days of culturing. Careful analysis reveals that the increased BMSC activities are derived from the synergy of sub-micron topography induced by TO and amine groups from the outmost chitosan layer.

6. The BMSC differentiation test on TO/$(A/C)_5$/Ag sample indicates that the levels of ALP, COL I and BSP expressions were up-regulated after 2 and 7 days of osteogenic induction. The ALP expression also shows significant difference from 0 day of osteogenic induction. Taken together, these results indicate the proposed TO/$(A/C)_5$/Ag surface is able to induce osteogenic differentiation of BMSC.

7. Additional nano-silver particles reduced by dopamine can induce antibacterial capability on TO/$(A/C)_5$ sample without jeopardizing its capability to enhance the viability and proliferation of BMSC.

8. The slight differences of BMSC viability, morphology and proliferation on TO/$(A/C)_5$ and TO/$(A/C)_5$/Ag samples are possibly due to the cytotoxic nature of heavy metals. Therefore, extraordinary attention should be paid when using nano-silver bactericide.

9. Overall, the hybrid structure made of alginate/chitosan LBL film and nano-silver, developed in this work, improves the existing inadequate osseointegration and

poor anti-infection capability of thermally oxidized Ti-6Al-4V, which has not been previously reported.

# Chapter 6

## Suggestions for Future Work

1. In order to further evaluate the biological performance of the proposed architectural hybrid Ti-6Al-4V system, it is suggested to further study its osseointegration and antibacterial capability *in vivo*.

2. The characteristics of the proposed hybrid Ti-6Al-4V system, such as LBL self-assembled alginate/chitosan film thickness and surface potential should be further revealed. This will provide a deeper insight for the surface modification of titanium and its alloys.

# References

[1] Rack HJ, Qazi JI. Titanium alloys for biomedical applications. Materials Science and Engineering: C. 2006;26:1269-77.

[2] Arys A, Philippart C, Dourov N, He Y, Le Q, Pireaux J-J. Analysis of titanium dental implants after failure of osseointegration: Combined histological, electron microscopy, and X−ray photoelectron spectroscopy approach. Journal of biomedical materials research. 1998;43:300-12.

[3] Cai K, Rechtenbach A, Hao J, Bossert J, Jandt KD. Polysaccharide-protein surface modification of titanium via a layer-by-layer technique: characterization and cell behaviour aspects. Biomaterials. 2005;26:5960-71.

[4] Choi J, Konno T, Matsuno R, Takai M, Ishihara K. Surface immobilization of biocompatible phospholipid polymer multilayered hydrogel on titanium alloy. Colloids and surfaces B, Biointerfaces. 2008;67:216-23.

[5] Daw AE, Kazi HA, Colombo JS, Rowe WG, Williams DW, Waddington RJ, et al. Differential cellular and microbial responses to nano-/micron-scale titanium surface roughness induced by hydrogen peroxide treatment. Journal of biomaterials applications. 2013;28:144-60.

[6] Hu Y, Cai K, Luo Z, Zhang R, Yang L, Deng L, et al. Surface mediated in situ differentiation of mesenchymal stem cells on gene-functionalized titanium films fabricated by layer-by-layer technique. Biomaterials. 2009;30:3626-35.

[7] Kumar S, Narayanan TSNS, Raman SGS, Seshadri SK. Thermal oxidation of CP-Ti: Evaluation of characteristics and corrosion resistance as a function of treatment time. Materials Science and Engineering: C. 2009;29:1942-9.

[8] Park JH, Olivares-Navarrete R, Wasilewski CE, Boyan BD, Tannenbaum R, Schwartz Z. Use of polyelectrolyte thin films to modulate osteoblast response to microstructured titanium surfaces. Biomaterials. 2012;33:5267-77.

[9] Yan SG, Zhang J, Tu QS, Ye JH, Luo E, Schuler M, et al. Enhanced osseointegration of titanium implant through the local delivery of transcription factor SATB2. Biomaterials. 2011;32:8676-83.

[10] Le Guehennec L, Soueidan A, Layrolle P, Amouriq Y. Surface treatments of titanium dental implants for rapid osseointegration. Dental materials : official publication

of the Academy of Dental Materials. 2007;23:844-54.

[11] Hu Y, Cai K, Luo Z, Zhang Y, Li L, Lai M, et al. Regulation of the differentiation of mesenchymal stem cells in vitro and osteogenesis in vivo by microenvironmental modification of titanium alloy surfaces. Biomaterials. 2012;33:3515-28.

[12] Phillips JE, Petrie TA, Creighton FP, Garcia AJ. Human mesenchymal stem cell differentiation on self-assembled monolayers presenting different surface chemistries. Acta biomaterialia. 2010;6:12-20.

[13] Hillberg AL, Tabrizian M. Biorecognition through layer-by-layer polyelectrolyte assembly: in-situ hybridization on living cells. Biomacromolecules. 2006;7:2742-50.

[14] Dash M, Chiellini F, Ottenbrite RM, Chiellini E. Chitosan—A versatile semi-synthetic polymer in biomedical applications. Progress in Polymer Science. 2011;36:981-1014.

[15] Lee KY, Mooney DJ. Alginate: properties and biomedical applications. Progress in polymer science. 2012;37:106-26.

[16] Neoh KG, Hu X, Zheng D, Kang ET. Balancing osteoblast functions and bacterial adhesion on functionalized titanium surfaces. Biomaterials. 2012;33:2813-22.

[17] Saldana L, Vilaboa N, Valles G, Gonzalez-Cabrero J, Munuera L. Osteoblast response to thermally oxidized Ti6Al4V alloy. Journal of biomedical materials research Part A. 2005;73:97-107.

[18] Ueno T, Tsukimura N, Yamada M, Ogawa T. Enhanced bone-integration capability of alkali- and heat-treated nanopolymorphic titanium in micro-to-nanoscale hierarchy. Biomaterials. 2011;32:7297-308.

[19] Kumar S, Narayanan T, Raman S, Seshadri S. Thermal oxidation of CP-Ti: Evaluation of characteristics and corrosion resistance as a function of treatment time. Materials Science and Engineering: C. 2009;29:1942-9.

[20] Nagassa M, Daw A, Rowe W, Carley A, Thomas D, Moseley R. Optimisation of the hydrogen peroxide pre−treatment of titanium: surface characterisation and protein adsorption. Clinical oral implants research. 2008;19:1317-26.

[21] Trisi P, Perfetti G, Baldoni E, Berardi D, Colagiovanni M, Scogna G. Implant micromotion is related to peak insertion torque and bone density. Clinical oral implants research. 2009;20:467-71.

[22] Franchi M, Bacchelli B, Martini D, Pasquale VD, Orsini E, Ottani V, et al. Early detachment of titanium particles from various different surfaces of endosseous dental implants. Biomaterials. 2004;25:2239-46.

[23] Schierholz J, Beuth J. Implant infections: a haven for opportunistic bacteria. Journal of Hospital Infection. 2001;49:87-93.

[24] Fisher L, McBride O, Termine J, Young M. Human bone sialoprotein. Deduced protein sequence and chromosomal localization. Journal of Biological Chemistry. 1990;265:2347-51.

[25] Riggs BL, Parfitt AM. Drugs used to treat osteoporosis: the critical need for a uniform nomenclature based on their action on bone remodeling. Journal of bone and mineral research. 2005;20:177-84.

[26] Branemark P-I. Vital microscopy of bone marrow in rabbit. Scandinavian journal of clinical and laboratory investigation. 1959;11:1.

[27] Adell R, Eriksson B, Lekholm U, Brånemark P, Jemt T. A Long-Term Follow-up Study of Osseointegrated Implants in the Treatment of Totally Edentulous Jaws. The International journal of oral & maxillofacial implants. 1990;5:347-59.

[28] Schwartz Z, Boyan B. Underlying mechanisms at the bone–biomaterial interface. Journal of cellular biochemistry. 1994;56:340-7.

[29] Schenk R, Bluser D. Osseointegration:a reality. Periodontology. 2000;17:22-35.

[30] Mendonca G, Mendonca DB, Aragao FJ, Cooper LF. Advancing dental implant surface technology--from micron- to nanotopography. Biomaterials. 2008;29:3822-35.

[31] Laine P, Salo A, Kontio R, Ylijoki S, Lindqvist C, Suuronen R. Failed dental implants - clinical, radiological and bacteriological findings in 17 patients. Journal of cranio-maxillo-facial surgery : official publication of the European Association for Cranio-Maxillo-Facial Surgery. 2005;33:212-7.

[32] Pye AD, Lockhart DE, Dawson MP, Murray CA, Smith AJ. A review of dental implants and infection. The Journal of hospital infection. 2009;72:104-10.

[33] Esposito M, Hirsch J, Lekholm U, Thomsen P. Biological factors contributing to failures of osseointegrated oral implants (II). Etiopathogenesis. European Journal of Oral Sciences 1998;106:721-64.

[34] Damsky C. Extracellular matrix–integrin interactions in osteoblast function and tissue remodeling. Bone. 1999;25:95-6.

[35] Hartgerink JD, Beniash E, Stupp SI. Self-assembly and mineralization of peptide-amphiphile nanofibers. Science. 2001;294:1684-8.

[36] Buser D, Schenk R, Steinemann S, Fiorellini J, Fox C, Stich H. Influence of surface characteristics on bone integration of titanium implants. A histomorphometric study in miniature pigs. Journal of biomedical materials research. 1991;25:889-902.

[37] Hansson S, Norton M. The relation between surface roughness and interfacial shear strength for bone-anchored implants. A mathematical model. Journal of biomechanics. 1999;32:829-36.

[38] F Grizon F, Aguado E, Hure G, Basle M, Chappard D. Enhanced bone integration of implants with increased surface roughness: a long term study in the sheep. Journal of Dentistry. 2002;30:195-203.

[39] Burger EH, KLEIN-NULEND J. Mechanotransduction in bone—role of the lacuno-canalicular network. The FASEB Journal. 1999;13:S101-S2.

[40] Albrektsson T, Wennerberg A. Oral implant surfaces: Part 1--review focusing on topographic and chemical properties of different surfaces and in vivo responses to them. International Journal of Prosthodontics. 2004;17:536-43.

[41] Albrektsson T, Wennerberg A. Oral implant surfaces: Part 2--review focusing on clinical knowledge of different surfaces. International Journal of Prosthodontics. 2004;17:544-64.

[42] Park J, Gemmell C, JE. D. Platelet interactions with titanium: modulation of platelet activity by surface topography. Biomaterials. 2001;22:2671–82.

[43] Lange R, Lüthen F, Beck U, Rychly J, Baumann A, Nebe B. Cell-extracellular matrix interaction and physico-chemical characteristics of titanium surfaces depend on the roughness of the material. Biomolecular engineering. 2002;19:255-61.

[44] Kieswetter K, Schwartz Z, Hummert T, Cochran D, Simpson J, Dean D, et al. Surface roughness modulates the local production of growth factors and cytokines by osteoblast-like MG-63 cells. Journal of Biomedical Materials Research. 1996;32:55-63.

[45] Dike L, Chen C, Mrksich M, Tien J, Whitesides G, Ingber D. Geometric control of switching between growth, apoptosis, and differentiation during angiogenesis using

micropatterned substrates. In Vitro Cellular & Developmental Biology-Animal. 1999;35:441-8.

[46] Webster TJ, Ergun C, Doremus RH, Siegel RW, Bizios R. Specific proteins mediate enhanced osteoblast adhesion on nanophase ceramics. Journal of biomedical materials research. 2000;51:475-83.

[47] Webster TJ, Schadler LS, Siegel RW, Bizios R. Mechanisms of enhanced osteoblast adhesion on nanophase alumina involve vitronectin. Tissue engineering. 2001;7:291-301.

[48] Lim JY, Hansen JC, Siedlecki CA, Runt J, Donahue HJ. Human foetal osteoblastic cell response to polymer-demixed nanotopographic interfaces. Journal of the Royal Society, Interface / the Royal Society. 2005;2:97-108.

[49] Teixeira AI, Abrams GA, Bertics PJ, Murphy CJ, Nealey PF. Epithelial contact guidance on well-defined micro- and nanostructured substrates. J Cell Sci. 2003;116:1881-92.

[50] Kanchanawong P, Shtengel G, Pasapera AM, Ramko EB, Davidson MW, Hess HF, et al. Nanoscale architecture of integrin-based cell adhesions. Nature. 2010;468:580-4.

[51] Klymov A, Prodanov L, Lamers E, Jansen JA, Walboomers XF. Understanding the role of nano-topography on the surface of a bone-implant. Biomaterials Science. 2013;1:135-51.

[52] Siebers M, Ter Brugge P, Walboomers X, Jansen J. Integrins as linker proteins between osteoblasts and bone replacing materials. A critical review. Biomaterials. 2005;26:137-46.

[53] Wang JH, Thampatty BP, Lin JS, Im HJ. Mechanoregulation of gene expression in fibroblasts. Gene. 2007;391:1-15.

[54] Arima Y, Iwata H. Effect of wettability and surface functional groups on protein adsorption and cell adhesion using well-defined mixed self-assembled monolayers. Biomaterials. 2007;28:3074-82.

[55] Benoit DS, Schwartz MP, Durney AR, Anseth KS. Small functional groups for controlled differentiation of hydrogel-encapsulated human mesenchymal stem cells. Nature materials. 2008;7:816-23.

[56] Ivirico J, Salmerón−Sánchez M, Ribelles J, Pradas MM, Soria JM, Gomes ME, et al. Proliferation and differentiation of goat bone marrow stromal cells in 3D scaffolds with

tunable hydrophilicity. Journal of Biomedical Materials Research Part B: Applied Biomaterials. 2009;91:277-86.

[57] Friedenstein A, Piatetzky-Shapiro I, Petrakova K. Osteogenesis in transplants of bone marrow cells. Journal of embryology and experimental morphology. 1966;16:381-90.

[58] Bianco P, Riminucci M, Gronthos S, Robey PG. Bone marrow stromal stem cells: nature, biology, and potential applications. Stem cells. 2001;19:180-92.

[59] Pittenger M, Mackay A, Beck S, Jaiswal R, Douglas R, Mosca J, et al. Multilineage potential of adult human mesenchymal stem cells. Science. 1999;284:143-7.

[60] Martin I, Muraglia A, Campanile G, Cancedda R, Quarto R. Fibroblast growth factor-2 supports ex vivo expansion and maintenance of osteogenic precursors from human bone marrow. Endocrinology. 1997;138:4456-62.

[61] Bruder S, Kraus K, Goldberg V, Kadiyala S. The effect of implants loaded with autologous mesenchymal stem cells on the healing of canine segmental bone defects. The Journal of Bone & Joint Surgery 1998;80:985-96.

[62] Le Blanc K, Gotherstrom C, Ringden O, Hassan M, McMahon R, Horwitz E, et al. Fetal Mesenchymal Stem-Cell Engraftment in Bone after In Utero Transplantation in a Patient with Severe Osteogenesis Imperfecta. Transplantation. 2005;79:1607-14.

[63] Granero-Molto F, Weis JA, Miga MI, Landis B, Myers TJ, O'Rear L, et al. Regenerative effects of transplanted mesenchymal stem cells in fracture healing. Stem cells. 2009;27:1887-98.

[64] Liu Y, Ming L, Luo H, Liu W, Zhang Y, Liu H, et al. Integration of a calcined bovine bone and BMSC-sheet 3D scaffold and the promotion of bone regeneration in large defects. Biomaterials. 2013;34:9998-10006.

[65] Costa-Pinto AR, Correlo VM, Sol PC, Bhattacharya M, Charbord P, Delorme B, et al. Osteogenic differentiation of human bone marrow mesenchymal stem cells seeded on melt based chitosan scaffolds for bone tissue engineering applications. Biomacromolecules. 2009;10:2067-73.

[66] Engh C, Bobyn J, Glassman A. Porous-coated hip replacement. The factors governing bone ingrowth, stress shielding, and clinical results. Journal of Bone & Joint Surgery, British Volume. 1987;69:45-55.

[67] Smith P. Artifical knee joint. A Level Physics Notes: Medical Physics. http://www.astarmathsandphysics.com: A Star Maths and Physics.

[68] Liu X, Chu PK, Ding C. Surface modification of titanium, titanium alloys, and related materials for biomedical applications. Materials Science and Engineering: R: Reports. 2004;47:49-121.

[69] Brunette DM. Titanium in medicine: material science, surface science, engineering, biological responses, and medical applications: Springer; 2001.

[70] Bothe R, Beaton L, Davenport H. Reaction of bone to multiple metallic implants. Surg Gynecol Obstet. 1940;71:598-602.

[71] Wang K. The use of titanium for medical applications in the USA. MaterialsScienceand Engineering A. 1996;213:134-7.

[72] Nico CG, R.L. J, E.A. M, M. R, Jeffcoat M. Influence of Implant Geometry and Surface Characteristics on Progressive Osseointegration. The International Journal of Oral & Maxillofacial Implants. 2002;17:811-5.

[73] Cheng GJ, Pirzada D, Cai M, Mohanty P, Bandyopadhyay A. Bioceramic coating of hydroxyapatite on titanium substrate with Nd-YAG laser. Materials Science and Engineering: C. 2005;25:541-7.

[74] Radin S, Ducheyne P. Plasma spraying induced changes of calcium phosphate ceramic characteristics and the effect on in vitro stability. Journal of materials science: Materials in medicine. 1992;3:33-42.

[75] Ha S-W, Mayer J, Koch B, Wintermantel E. Plasma-sprayed hydroxylapatite coating on carbon fibre reinforced thermoplastic composite materials. Journal of materials science: Materials in medicine. 1994;5:481-4.

[76] Guleryuz H, Cimenoglu H. Surface modification of a Ti–6Al–4V alloy by thermal oxidation. Surface and Coatings Technology. 2005;192:164-70.

[77] Guleryuz H, Cimenoglu H. Effect of thermal oxidation on corrosion and corrosion-wear behaviour of a Ti-6Al-4V alloy. Biomaterials. 2004;25:3325-33.

[78] MacDonald DE, Rapuano BE, Deo N, Stranick M, Somasundaran P, Boskey AL. Thermal and chemical modification of titanium-aluminum-vanadium implant materials: effects on surface properties, glycoprotein adsorption, and MG63 cell attachment. Biomaterials. 2004;25:3135-46.

[79] Kofstad P, Etherington DM, Boucher B. High temperature corrosion: Elsevier applied science New York; 1988.

[80] Alonso M, Saldana L, Valles G, González-Carrasco JL, Gonzalez-Cabrero J, Martınez M, et al. In vitro corrosion behaviour and osteoblast response of thermally oxidised Ti6Al4V alloy. Biomaterials. 2003;24:19-26.

[81] Nishiguchi S, Kato H, Fujita H, Oka M, Kim H, Kokubo T, et al. Titanium metals form direct bonding to bone after alkali and heat treatments. Biomaterials. 2001;22:2525-33.

[82] Bagno A, Bello C. Surface treatments and roughness properties of Ti-based biomaterials. Journal of Materials Science: Materials in Medicine. 2004;15:935-49.

[83] Mustafa K, Wroblewski J, Lopez BS, Wennerberg A, Hultenby K, Arvidson K. Determining optimal surface roughness of TiO2 blasted titanium implant material for attachment, proliferation and differentiation of cells derived from human mandibular alveolar bone. Clinical Oral Implants Research. 2001;12:515-25.

[84] Schneider GB, Perinpanayagam H, Clegg M, Zaharias R, Seabold D, Keller J, et al. Implant Surface Roughness Affects Osteoblast Gene Expression. Journal of Dental Research. 2003;82:372-6.

[85] Ronold H, Ellingsen J. Effect of micro-roughness produced by TiO2 blasting—tensile testing of bone attachment by using coin-shaped implants. Biomaterials. 2002;23:4211-9.

[86] Wennerberg A, Albrektsson T, Johansson C, Andersson B. Experimental study of turned and grit-blasted screw-shaped implants with special emphasis on effects of blasting material and surface topography. Biomaterials. 1996;17:15-22.

[87] Nanci A, Wuest J, Peru L, Brunet P, Sharma V, Zalzal S, et al. Chemical modification of titanium surfaces for covalent attachment of biological molecules. Journal of Biomedical Materials Research. 1998;40:324-35.

[88] Morra M, Cassinelli C, Cascardo G, Cahalan P, Cahalan L, Fini M, et al. Surface engineering of titanium by collagen immobilization. Surface characterization and in vitro and in vivo studies. Biomaterials. 2003;24:4639-54.

[89] Bierbaum S, Beutner R, Hanke T, Scharnweber D, Hempel U, Worch H. Modification of Ti6Al4V surfaces using collagen I, III, and fibronectin. I. Biochemical and morphological characteristics of the adsorbed matrix. Journal of Biomedical

Materials Research Part A. 2003;67:421-30.

[90] Bierbaum S, Hempel U, Geissler U, Hanke T, Scharnweber D, Wenzel K, et al. Modification of Ti6Al4V surfaces using collagen I, III, and fibronectin. II. Influence on osteoblast responses. Journal of Biomedical Materials Research Part A. 2003;67:431-8.

[91] U. G, Hempel U, Wolf C, Scharnweber D, Worch H, Wenzel K. Collagen type I-coating of Ti6Al4V promotes adhesion of osteoblasts. Journal of Biomedical Materials Research. 2000;51:752-60.

[92] Kinsella C, Cray J, Durham E, Burrows A, Vecchione L, Smith D, et al. Recombinant human bone morphogenetic protein induces boneformation. Proceedings of the National Academy of Sciences. 2011;1327:1173-81.

[93] Nielsen H, Andreassen T, Ledet T, Oxlund H. Local injection of TGF-O increases the strength of tibial fractures in the rat. Acta Orthopaedica. 1994;65:37-41.

[94] Shah A, Lazatin J, Sinha R, Lennox T, Hickok N, Tuan R. Mechanism of BMP-2 stimulated adhesion of osteoblastic cells to titanium alloy. Biology of the Cell. 1999;91:131-42.

[95] Becker J, Kirsch A, Schwarz F, Chatzinikolaidou M, Rothamel D, Lekovic V, et al. Bone apposition to titanium implants biocoated with recombinant human bone morphogenetic protein-2 (rhBMP-2). A pilot study in dogs. Clinical oral investigations. 2006;10:217-24.

[96] Vehof J, Haus M, De Ruijter A, Spauwen P, Jansen J. Bone formation in transforming growth factor beta-I-loaded titanium fiber mesh implants. Clinical Oral Implants Research. 2002;13:94-102.

[97] Lind M, Overgaard S, K. S, Nguyen T, Ongpipattanakul B, Bünger C. Transforming growth factor-beta 1 enhances bone healing to unloaded tricalcium phosphate coated implants: an experimental study in dogs. Journal of Orthopaedic Research. 1996;14:345-50.

[98] Liu Y, Enggist L, Kuffer AF, Buser D, Hunziker EB. The influence of BMP-2 and its mode of delivery on the osteoconductivity of implant surfaces during the early phase of osseointegration. Biomaterials. 2007;28:2677-86.

[99] Lee DW, Yun YP, Park K, Kim SE. Gentamicin and bone morphogenic protein-2 (BMP-2)-delivering heparinized-titanium implant with enhanced antibacterial activity and osteointegration. Bone. 2012;50:974-82.

[100] Yang B, Uchida M, Kim H-M, Zhang X, Kokubo T. Preparation of bioactive titanium metal via anodic oxidation treatment. Biomaterials. 2004;25:1003-10.

[101] Le Guéhennec L, Soueidan A, Layrolle P, Amouriq Y. Surface treatments of titanium dental implants for rapid osseointegration. Dental materials. 2007;23:844-54.

[102] Li L-H, Kong Y-M, Kim H-W, Kim Y-W, Kim H-E, Heo S-J, et al. Improved biological performance of Ti implants due to surface modification by micro-arc oxidation. Biomaterials. 2004;25:2867-75.

[103] Schüpbach P, Glauser R, Rocci A, Martignoni M, Sennerby L, Lundgren A, et al. The human bone-oxidized titanium implant interface: A light microscopic, scanning electron microscopic, back-scatter scanning electron microscopic, and energy-dispersive x-ray study of clinically retrieved dental implants. Clinical implant dentistry and related research. 2005;7:36-43.

[104] Kim H, Miyaji F, Kokubo T, Nakamura T. Effect of heat treatment on apatite-forming ability of Ti metal induced by alkali treatment. Journal of Materials Science: Materials in Medicine. 1997;8:341-7.

[105] Kokubo T, Kim H-M, Kawashita M. Novel bioactive materials with different mechanical properties. Biomaterials. 2003;24:2161-75.

[106] Kim H, Miyaji F, Kokubo T, Nakamura T. Preparation of bioactive Ti and its alloys via simple chemical surface treatment. Journal of Biomedical Materials Research. 1996;32:409-17.

[107] Nishio K, M. N, Akiyama H, Nishiguchi S, Kim H, Kokubo T, et al. The effect of alkali- and heat-treated titanium and apatite-formed titanium on osteoblastic differentiation of bone marrow cells. Journal of Biomedical Materials Research. 2000;52:652-61.

[108] Nishiguchi S, Nakamura T, Kobayashi M, Kim H, Miyaji F, Kokubo T. The effect of heat treatment on bone-bonding ability of alkali-treated titanium. Biomaterials. 1999;20:491-500.

[109] Oh SH, Finones RR, Daraio C, Chen LH, Jin S. Growth of nano-scale hydroxyapatite using chemically treated titanium oxide nanotubes. Biomaterials. 2005;26:4938-43.

[110] Oh S, Jin S. Titanium oxide nanotubes with controlled morphology for enhanced bone growth. Materials Science and Engineering: C. 2006;26:1301-6.

[111] Park J, Davies J. Red blood cell and platelet interactions with titanium implant surfaces. Clinical Oral Implants Research. 2000;11:530-9.

[112] Trisi P, Lazzara R, Rebaudi A, Rao W, Testori T, Porter S. Bone-implant contact on machined and dual acid-etched surfaces after 2 months of healing in the human maxilla. Journal of Periodontology. 2003;74:945-56.

[113] Trisi P, Lazzara R, Rao W, Rebaudi A. Bone-implant contact and bone quality: evaluation of expected and actual bone contact on machined and osseotite implant surfaces. International Journal of Periodontics & Restorative Dentistry. 2002;22:535-45.

[114] Mante FK, Little K, Mante MO, Rawle C, Baran GR. Oxidation of Titanium, RGD Peptide Attachment, and Matrix Mineralization of Rat Bone Marrow Stromal Cells. Journal of Oral Implantology. 2004;30:343-9.

[115] Orsini G, Assenze B, Scarano A, Piattelli M, Piattelli A. Surface analysis of machined versus sandblasted and acid-etched titanium implants. International Journal of Oral & Maxillofacial Implants. 2000;15:779-84.

[116] Novaes AB, Papalexiou V, Grisi MFM, Souza SSLS, Taba M, Kajiwara JK. Influence of implant microstructure on the osseointegration of immediate implants placed in periodontally infected sites. A histomorphometric study in dogs. Clinical Oral Implants Research. 2004;15:34-43.

[117] Yang G-l, He F-m, Zhao S-s, Wang X-x, Zhao S-f. Effect of H2O2/HCl Heat Treatment of Implants on In Vivo Peri-implant Bone Formation. International Journal of Oral & Maxillofacial Implants. 2008;23.

[118] Nagaoka A, Yokoyama Ki, Sakai Ji. Evaluation of hydrogen absorption behaviour during acid etching for surface modification of commercial pure Ti, Ti–6Al–4V and Ni–Ti superelastic alloys. Corrosion Science. 2010;52:1130-8.

[119] Weiner S, Wagner H. The material bone: structure-mechanical function relations. Annual Review of Materials Science. 1998;28:271-98.

[120] Palin E, Liu H, Webster TJ. Mimicking the nanofeatures of bone increases bone-forming cell adhesion and proliferation. Nanotechnology. 2005;16:1828.

[121] Ngiam M, Liao S, Patil AJ, Cheng Z, Chan CK, Ramakrishna S. The fabrication of nano-hydroxyapatite on PLGA and PLGA/collagen nanofibrous composite scaffolds and their effects in osteoblastic behavior for bone tissue engineering. Bone. 2009;45:4-16.

[122] Kuboki Y, Jin Q, Kikuchi M, Mamood J, Takita H. Geometry of artificial ECM: sizes of pores controlling phenotype expression in BMP-induced osteogenesis and chondrogenesis. Connective tissue research. 2002;43:529-34.

[123] Lamers E, Walboomers XF, Domanski M, te Riet J, van Delft FC, Luttge R, et al. The influence of nanoscale grooved substrates on osteoblast behavior and extracellular matrix deposition. Biomaterials. 2010;31:3307-16.

[124] Fiedler J, Ozdemir B, Bartholoma J, Plettl A, Brenner RE, Ziemann P. The effect of substrate surface nanotopography on the behavior of multipotnent mesenchymal stromal cells and osteoblasts. Biomaterials. 2013;34:8851-9.

[125] Lim J, Hansen J, Siedlecki C, Hengstebeck R, Cheng J, Winograd N, et al. Osteoblast adhesion on poly(L-lactic acid)/polystyrene demixed thin film blends: effect of nanotopography, surface chemistry, and wettability. Biomacromolecules. 2005;6:3319-27.

[126] You MH, Kwak M, Kim D, Kim K, Levchenko A, Kim D, et al. Synergistically enhanced osteogenic differentiation of human mesenchymal stem cells by culture on nanostructured surfaces with induction media. Biomacromolecules. 2010;11:1856-62.

[127] de Villiers MM, Otto DP, Strydom SJ, Lvov YM. Introduction to nanocoatings produced by layer-by-layer (LbL) self-assembly. Advanced drug delivery reviews. 2011;63:701-15.

[128] Gribova V, Auzely-Velty R, Picart C. Polyelectrolyte Multilayer Assemblies on Materials Surfaces: From Cell Adhesion to Tissue Engineering. Chemistry of Materials. 2012;24:854-69.

[129] Van Oss C, Good R, Chaudhury M. The role of van der Waals forces and hydrogen bonds in “hydrophobic interactions” between biopolymers and low energy surfaces. Journal of Colloid and Interface Science. 1986;111:378-90.

[130] Kim B-S, Park SW, Hammond PT. Hydrogen-bonding layer-by-layer-assembled biodegradable polymeric micelles as drug delivery vehicles from surfaces. Acs Nano. 2008;2:386-92.

[131] Wang L, Fu Y, Wang Z, Fan Y, Zhang X. Investigation into an alternating multilayer film of poly (4-vinylpyridine) and poly (acrylic acid) based on hydrogen bonding. Langmuir. 1999;15:1360-3.

[132] Kim B, Park S, Hammond P. Hydrogen-bonding layer-by-layer-assembled

biodegradable polymeric micelles as drug delivery vehicles from surfaces. Acs Nano. 2008;2:386-92.

[133] Jiang C, Markutsya S, Tsukruk VV. Compliant, robust, and truly nanoscale free−standing multilayer films fabricated using spin−assisted layer−by−layer assembly. Advanced Materials. 2004;16:157-61.

[134] Li Y, Wang X, Sun J. Layer-by-layer assembly for rapid fabrication of thick polymeric films. Chemical Society Reviews. 2012;41:5998-6009.

[135] Decher G. Fuzzy nanoassemblies: toward layered polymeric multicomposites. Science. 1997;277:1232-7.

[136] Hellstrom S. Basic Models of Spin Coating. Physics 210, Stanford University. http://large.stanford.edu/: Stanford University; 2007.

[137] U Lindahl MH. Glycosaminoglycans and their binding to biological macromolecules. Annual Review of Biochemistry. 1978;47.

[138] Costa-Pinto AR, Reis RL, Neves NM. Scaffolds based bone tissue engineering: the role of chitosan. Tissue engineering Part B, Reviews. 2011;17:331-47.

[139] Lahiji A, Sohrabi A, Hungerford D, Frondoza C. Chitosan supports the expression of ECM proteins in human osteoblasts and chondrocytes. Journal of biomedical materials research. 2000;51:586-95.

[140] Smidsrød O. Alginate as immobilization matrix for cells. Trends in biotechnology. 1990;8:71-8.

[141] Aggarwal N, HogenEsch H, Guo P, North A, Suckow M, Mittal SK. Biodegradable alginate microspheres as a delivery system for naked DNA. Canadian journal of veterinary research. 1999;63:148.

[142] Gombotz WR, Wee SF. Protein release from alginate matrices. Advanced drug delivery reviews. 2012;64:194-205.

[143] Ravi Kumar MN. A review of chitin and chitosan applications. Reactive and functional polymers. 2000;46:1-27.

[144] Wu MY, Ning C, Liu LK, Hua Y, Li QL, Chen SH. Chitosan/Alginate Multilayer Scaffold Encapsulating Bone Marrow Stromal Cells In Situ on Titanium. Journal of Bioactive and Compatible Polymers. 2009;24:301-15.

[145] Li Z, Ramay HR, Hauch KD, Xiao D, Zhang M. Chitosan-alginate hybrid scaffolds for bone tissue engineering. Biomaterials. 2005;26:3919-28.

[146] Yang Y, He Q, Duan L, Cui Y, Li J. Assembled alginate/chitosan nanotubes for biological application. Biomaterials. 2007;28:3083-90.

[147] Xie HG, Zheng JN, Li XX, Liu XD, Zhu J, Wang F, et al. Effect of surface morphology and charge on the amount and conformation of fibrinogen adsorbed onto alginate/chitosan microcapsules. Langmuir. 2009;26:5587-94.

[148] Schwartz-Arad D, Laviv A, Levin L. Failure causes, timing, and cluster behavior: an 8-year study of dental implants. Implant dentistry. 2008;17:200-7.

[149] Rubin LG, Shih S, Shende A, Karayalcin G, Lanzkowsky P. Cure of Implantable Venous Port—Associated Bloodstream Infections in Pediatric Hematology-Oncology Patients without Catheter Removal. Clinical infectious diseases. 1999;29:102-5.

[150] Marambio-Jones C, Hoek EMV. A review of the antibacterial effects of silver nanomaterials and potential implications for human health and the environment. Journal of Nanoparticle Research. 2010;12:1531-51.

[151] Wijnhoven SWP, Peijnenburg WJGM, Herberts CA, Hagens WI, Oomen AG, Heugens EHW, et al. Nano-silver – a review of available data and knowledge gaps in human and environmental risk assessment. Nanotoxicology. 2009;3:109-38.

[152] Jagadeesh BH, Prabha TN, Srinivasan K. Activities of β-hexosaminidase and α-mannosidase during development and ripening of bell capsicum (Capsicum annuum var. variata). Plant Science. 2004;167:1263-71.

[153] Collera-Zúñiga O, García Jiménez F, Meléndez Gordillo R. Comparative study of carotenoid composition in three mexican varieties of Capsicum annuum L. Food Chemistry. 2005;90:109-14.

[154] Sharma VK, Yngard RA, Lin Y. Silver nanoparticles: green synthesis and their antimicrobial activities. Advances in colloid and interface science. 2009;145:83-96.

[155] Yuan W, Ji J, Fu J, Shen J. A facile method to construct hybrid multilayered films as a strong and multifunctional antibacterial coating. Journal of Biomedical Materials Research Part B: Applied Biomaterials. 2008;85:556-63.

[156] Qu J, Lu X, Li D, Ding Y, Leng Y, Weng J, et al. Silver/hydroxyapatite composite coatings on porous titanium surfaces by sol-gel method. Journal of biomedical materials

research Part B, Applied biomaterials. 2011;97:40-8.

[157] Saravanan S, Nethala S, Pattnaik S, Tripathi A, Moorthi A, Selvamurugan N. Preparation, characterization and antimicrobial activity of a bio-composite scaffold containing chitosan/nano-hydroxyapatite/nano-silver for bone tissue engineering. International journal of biological macromolecules. 2011;49:188-93.

[158] Faure E, Falentin-Daudré C, Jérôme C, Lyskawa J, Fournier D, Woisel P, et al. Catechols as versatile platforms in polymer chemistry. Progress in polymer science. 2013;38:236-70.

[159] McCafferty E, Wightman J. Determination of the concentration of surface hydroxyl groups on metal oxide films by a quantitative XPS method. Surface and Interface Analysis. 1998;26:549-64.

[160] Kang B-S, Sul Y-T, Oh S-J, Lee H-J, Albrektsson T. XPS, AES and SEM analysis of recent dental implants. Acta biomaterialia. 2009;5:2222-9.

[161] Khalifa ZS, Lin H, Ismat Shah S. Structural and electrochromic properties of TiO2 thin films prepared by metallorganic chemical vapor deposition. Thin Solid Films. 2010;518:5457-62.

[162] Ola O, Mercedes Maroto-Valer M. Role of catalyst carriers in CO2 photoreduction over nanocrystalline nickel loaded TiO2-based photocatalysts. Journal of Catalysis. 2014;309:300-8.

[163] Anselme K, Linez P, Bigerelle M, Le Maguer D, Le Maguer A, Hardouin P, et al. The relative influence of the topography and chemistry of TiAl6V4 surfaces on osteoblastic cell behaviour. Biomaterials. 2000;21:1567-77.

[164] Zreiqat H, Howlett CR. Titanium substrata composition influences osteoblastic phenotype: In vitro study. Journal of biomedical materials research. 1999;47:360-6.

[165] MacDonald D, Rapuano B, Deo N, Stranick M, Somasundaran P, Boskey A. Thermal and chemical modification of titanium–aluminum–vanadium implant materials: effects on surface properties, glycoprotein adsorption, and MG63 cell attachment. Biomaterials. 2004;25:3135-46.

[166] Tanaka Y, Saito H, Tsutsumi Y, Doi H, Imai H, Hanawa T. Active hydroxyl groups on surface oxide film of titanium, 316L stainless steel, and cobalt-chromium-molybdenum alloy and its effect on the immobilization of poly (ethylene glycol). Materials transactions. 2008;49:805-11.

[167] Lu X, Wang Y, Yang X, Zhang Q, Zhao Z, Weng LT, et al. Spectroscopic analysis of titanium surface functional groups under various surface modification and their behaviors in vitro and in vivo. Journal of Biomedical Materials Research Part A. 2008;84:523-34.

[168] Lawrie G, Keen I, Drew B, Chandler-Temple A, Rintoul L, Fredericks P, et al. Interactions between alginate and chitosan biopolymers characterized using FTIR and XPS. Biomacromolecules. 2007;8:2533-41.

[169] Park JH, Schwartz Z, Olivares-Navarrete R, Boyan BD, Tannenbaum R. Enhancement of surface wettability via the modification of microtextured titanium implant surfaces with polyelectrolytes. Langmuir : the ACS journal of surfaces and colloids. 2011;27:5976-85.